SAND79-8181
Unlimited Release

Preliminary Design Report
New Ideas for Heliostat Reflector Cleaning Systems

J. Schumacher, J. Hansen, J. Nevenzel

Prepared by Sandia Laboratories, Albuquerque, New Mexico 87115
and Livermore, California 94550 for the United States Department
of Energy under Contract DE-AC04-76DP00789.

Printed December 1979

Sandia Laboratories
energy report

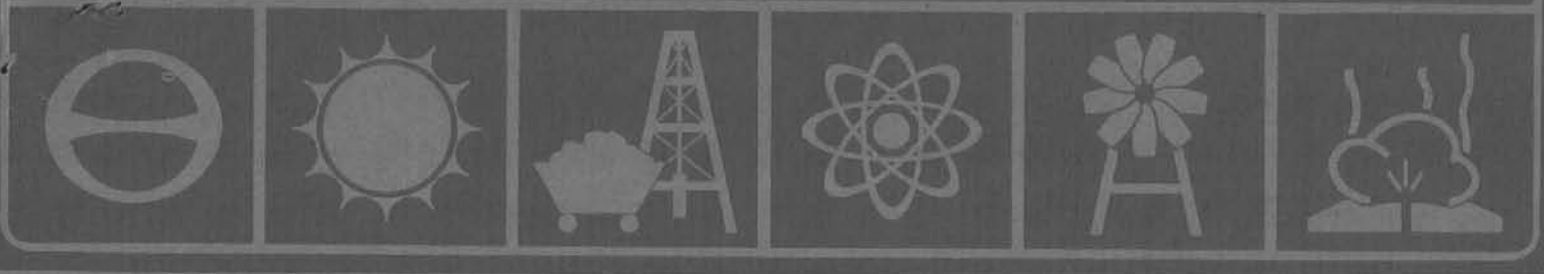

Issued by Sandia Laboratories, operated for the United States Department of Energy by Sandia Corporation.

NOTICE

Printed in the United States of America
Available from
National Technical Information Service
U. S. Department of Commerce
5285 Port Royal Road
Springfield, VA 22161
Price: Printed Copy $7.25 ; Microfiche $3.00

SAND79-8181
Unlimited Release
Printed December 1979

PRELIMINARY DESIGN REPORT

NEW IDEAS FOR HELIOSTAT REFLECTOR CLEANING SYSTEMS

J. Schumacher
J. Hansen
J. Nevenzel
Schumacher and Associates, Inc.

Prepared for Sandia Laboratories
by
Schumacher and Associates, Inc.
under
Contract 83-0035K

Report finished August 31, 1979

Acknowledgment

The authors wish to express appreciation for the technical contributions of Consultants R.K. Steele and F.E. Luffman. Also appreciated are the helpful discussions with R.B. Pettit and Dr. E.P. Roth of Sandia, Albuquerque on the subjects of reflectometer and wind tunnel design. Assistance on report preparation from G.D. Aldrich and S.C. Burghdorf is also recognized.

TABLE OF CONTENTS

1.0 INTRODUCTION

This report summarizes an investigation of new methods of cleaning heliostat reflectors. The initial stimulus to undertake this effort was a SANDIA request for proposal on "New Ideas, Collector Subsystem for Solar Central Receiver" (Reference 1). Schumacher and Associates, Inc. responded with a proposal (Reference 2) for "New Ideas for Heliostat Reflector Cleaning Systems." Work on this portion of the total effort was authorized by a SANDIA contract dated March 12, 1979 (Reference 3). The total contract effort was performed in the period March 15 to August 31, 1979.

The importance of an efficient cleaning system is demonstrated by a recent study by Eason (Reference 4) which reports that for a 100 MW plant 4M$ of otherwise lost energy can be recovered by washing 26 times per year while the annual cost of washing is only 0.7M$. The goal of the effort being reported here has been to find an alternate system to provide adequate cleaning at no more than, and hopefully less than, the above cost on a life cycle basis. Specifically, a method was sought in which the dirt removal would be by non-physical contact, i.e., by primarily through the movement of air. Any form of washing presents some disadvantage from the standpoint of having to recover water and chemicals for environmental reasons.

The adhesion of dust to a mirror surface is a complex process involving several force mechanisms. Zimon (Reference 5) categorizes the adhesive forces in a gaseous medium into four components; molecular, electric, Coulomb and capillary. The molecular component is a function of particle size as well as true contact area and surface roughness. Electrical forces depend on the potential difference between the particles and the surface and are proportional to the two-thirds power of particle size. Coulomb forces are the result of the interaction between charged particles and the surface

and are inversely proportional to the square of the particle size. The presence of moisture in the gap between surfaces eliminates the electric forces and reduces Coulomb forces with time. Capillary forces occur in the presence of a liquid meniscus between the particles and the surface and are thus highly dependent on humidity. They are roughly proportional to particle size for small particles. As noted by Berg (Reference 6), capillary forces may be of the order of 10,000 g's whereas the surface energetic forces are more of the order of 100 g's or less. Total adhesion is an unknown combination of these force mechanisms, and varies with environmental conditions and time. Even under steady environmental conditions an aging phenomenon generally occurs, as noted by Zimon (Reference 5), wherein total adhesion reaches a maximum within 30 minutes after dust deposition. Over and above these adhesion forces are chemical reaction bonds of very high magnitude that may develop in time.

Mechanisms by which cleaning takes place in an air flow with and without vibrational forces are discussed by Zimon (Reference 5). In conventional ultrasonic cleaning, using liquids, the main factors responsible for cleaning are cavitation and acoustic streaming (References 7 and 8). The cavitation effect predominates, causing erosion due to impact loading by the implosion of air bubbles. However, a fatigue failure mechanism is also present due to pulsating bubbles which do not implode, but oscillate over a relatively long period of time. In cleaning with air flow alone, the mechanisms are erosion and denudation. Erosion involves the removal of top particles by overcoming the autohesion forces between layers of particles. Denudation is the detachment of the final layer and remaining individual particles by overcoming the adhesion forces between the dust and the

surface. The denudation depends on air flow velocity whereas erosion is a function of both the velocity and the duration of the air flow. Cleaning can be accelerated by increasing air flow velocity, by injection of particles in the air stream (dust, water, etc.) or by the superposition of a vibrational field. Detachment by particle-laden air is due partly by collision forces between airborne and attached particles and partly by virtue of the air velocity. Detachment in the presence of vibrations is analogous to the fatigue failure mechanism observed in ultrasonic cleaning in liquids.

The approach taken in this investigation has been to seek suitable cleaning methods for heliostat mirrors based on the air flow cleaning mechanisms mentioned above, including enhancement with water particle injection or ultrasonic vibrations. The experimental work is divided into two groups. Under Concept No. 1, a variety of air nozzles are investigated. These include vortex generating orifices which have combined rotational and translational motion that imparts a scrubbing action to the air flow. Streamline nozzles that direct flow normal to the surface are also studied with and without water injection. The Concept No. 1 studies are described in Section 5.1 below.

Concept No. 2 transmits ultrasonic energy from an electro-mechanical transducer through air to the surface to be cleaned. It uses a circular plate connected at its center to a mechanical amplifier rod which is in turn connected to a piezoelectric transducer. The transducer is fed by a commercially available ultrasonic power source (5-100 watts) operating in the vicinity of 21 kHz.

The transmission of high power ultrasonics through air has always been difficult to achieve due to the low specific acoustic impedance and the high absorption characteristics

of the air. However, some pioneering work which has continued over a period of years by Gallego-Juarez, et al has resulted in a transducer capable of generating high power levels efficiently in gases (References 9 and 10). This is the type of transducer being investigated as a possible enhancement to an air flow scheme for dust denudation. The Concept No. 2 studies are given in Section 5.2, below.

Another major engineering and fabrication task has been the design and construction of a reflectometer to evaluate the efficiency of the various cleaning devices and processes by measurement of mirror reflectivity after cleaning, after dusting and weathering, and then again after recleaning. Extensive research revealed there is no suitable commercial unit readily available at a reasonable cost. An instrument that measures reflectivity with a precision of 99.9% has been designed and built for less than $850 material cost. This instrument is described in Section 3.1 below.

Still another engineering/fabrication task of considerable scope besides the actual cleaning devices design and testing has been the design and construction of a dust deposition wind tunnel system. The objective here has been to provide a system for uniform deposition of dust while simulating air currents that would be expected at an actual test site. The system is described below in detail in Section 3.2.

2.0 SUMMARY OF RESULTS

The feasibility of two new concepts for cleaning heliostat refectors has been investigated in this program and the results are itemized below. In addition, this phase of the program involved the design and construction of a reflectometer and wind tunnel and the performance of some dust accumulation studies, the results of which are also listed below.

(1) A vortex generator type air nozzle has good cleaning ability but requires very close proximity to the mirror surface (.30 inches for a .10 inch nozzle)

(2) A converging air nozzle with water mist injection has good cleaning ability. Based on tests performed, reflectance recovery ranges from 99% for unaged mirror specimens to 84% for 30-day aged specimens. The polymer coated mirrors (REPCON, Reference 21) allowed reflectance recovery of nearly 99% for 4-day aged mirror specimens and 98% for the 30-day aged specimen tested. The width of the cleaned path for a 2.54 mm diameter nozzle ranges from 1.5 to 2.0 cm with an optimum cleaning height off mirror surface of 10 cm for a nozzle supply pressure of 100 psig. The water usage is minimal with a flow of 2.14 ml/min being used by one nozzle for the test results summarized above.

(3) The presence of "medium" intensity (130+dB) air propagated ultrasound with air blast appears to appreciably increase the cleanability of a mirror when compared to cleaning with the air blast alone. Test results are limited because high power operation in the desired range (160+dB) was not achieved. Operating the ultrasonic radiating plate at 15.4 kHz with 130+dB output sound pressure level resulted in

a mirror surface area of approximately 28 cm^2 with 98% or greater reflectance recovery and an area of ~70 cm^2 with greater than 96% reflectance recovery. For comparison, the air blast without ultrasound produced areas of 5 cm^2 for $\geq$ 98% recovery and 33 cm^2 for $\geq$ 96% recovery. These tests were performed on a 4-day aged mirror specimen with clean and dusty reflectances of 85.1% and 79.7%, respectively. The transducer height off the mirror surface was 41 mm.

(4) A preliminary cost study, based on the vortex generator type system, indicates life cycle costs competitive with MDAC/CAL CHEM washing system costs.

(5) Dust accumulation studies in a natural environment and performed with the low speed wind tunnel have been correlated in terms of equivalent reflectance loss but not in terms of equivalent adhesion properties. Aging greatly affects adhesion forces and more studies are required in this area.

(6) A low cost laboratory reflectometer has been built for use in this program. Based on this experience, a low cost field instrument appears feasible. Approximate estimated costs are $3000 each for quantities greater than 100 and $5000 each for less than 20.

3.0 SPECIAL EQUIPMENT

3.1 S & A Reflectometer

The principal measurements required to evaluate cleaning effectiveness are the reflectances of the mirror surface before and after the cleaning process.

The presence of dust particles on the mirror surface results in optical losses due to absorption and scattering of the incident light beam. (Ref. 6) The remaining portion of light is specularly reflected back from the mirror surface, at a reduced intensity, with the angular profile of the reflected beam essentially the same as that of the incident beam and at an angle off the normal equal to the incident angle. (Ref. 11) Reflectometers are designed to measure the intensity of this reflected beam, over a selected wavelength range, relative to the intensity of the incident beam.

Several reflectometers for measuring bi-directional specular reflectance have been developed, but none were available for use at the S & A facilities during the performance period of this contract. Consequently, the design and fabrication of a reflectometer constituted the first major effort during this contract phase.

3.1.1 Design Parameters

The initial phase of the reflectometer design involved a literature review to gain familiarity with presently operating reflectometers and to obtain insight into desirable characteristics which might be incorporated into this instrument. Sandia personnel were extremely helpful in this regard, providing much information on the current state-of-the-art of reflectometer design. The principal reflectometers reviewed prior to final design of the S & A instrument consisted of a portable field

unit and a laboratory unit, both located at Sandia-Albuquerque (References 12 and 13). In addition, a review was conducted of the Sandia specification for a portable reflectometer under development by Beckman Instruments (Ref. 14). Numerous other references pertaining to optics, reflectance spectroscopy and solar radiation were reviewed (References 15 through 18).

The selection of design parameters for the S & A reflectometer was guided by the fundamental requirement of this study; that being the laboratory measurement of relative reflectance of the test mirror surfaces before dust deposition, after dust deposition and after cleaning, with the ability to then generate percent reflectance recovery due to any given cleaning method. Low cost was also a prime objective. The measurement of absolute reflectance over a wavelength range or solar averaged reflectance was considered a secondary goal, although, as will be shown later, excellent agreement was obtained between measured reflectance values of the McDonnell-Douglas heliostat panel at S & A using this instrument, and "typical" McDonnell-Douglas heliostat panel reflectance data as supplied by Sandia in Reference 19.

The design parameters selected for the S & A reflectometer are summarized in Table 3-1, where they are compared to the equivalent properties of the three reflectometers reviewed. For the purpose of defining the extent of cleaned area of mirror samples during this study, it was found to be desirable to mount the reflectometers on a movable carriage. The S & A reflectometer thus has a base design that permits traversing for 15 cm across the sample without lifting the instrument.

The S & A reflectometer is described in detail in Section 3.1.2 below and procedures for its alignment and use are presented in Sections 3.1.3 and 3.1.4, respectively. Tests performed to characterize and calibrate the instrument are described in Section 3.1.5.

Table 3-1. Comparison of Design Parameters of Four Reflectometers

	Sandia-Lab	Sandia-Portable	Bechman-Portable	S & A - Lab
Optical Parameters				
Source	Tungsten Filamant	Tungsten Filament	Tungsten Filament	Tungsten Filament
Transmitted/Detected Wavelength	400-900 nm Variable Narrow Band	350-750 nm with Corion IRS Filter	450 nm/400-600 nm Manual Selectable	350-1200 nm Corion IRS Filter optional
Incident Angle	Variable	Variable	20 degrees	20 degrees
Collimated Beam Size	6 to 19 mm Variable Iris	5 mm	40 mm square	2 to 15 mm Variable Iris
Source Aperture	.25 mm x 1.5 mm	.25 mm dia.	--	0.20 mm dia.
Source Divergent Angle	1 mrad x 6 mrad	5.0 mrad	17.5 mrad	2.5 mrad
Collection Aperture		12 mm dia.	--	2 mm dia.
Collection Equivalent Divergence Angle	1 to 15 mrad x 36 mrad (Variable width slit)	24 mrad	--	25 mrad
General Parameters				
Self Calibration Possible	Yes	No	Yes	Yes
Readout Type	Digital/Computer Link	Digital	Digital	Digital
Adaptable to Surfaces Other than 2nd Surface Mirrors	Yes	Yes	Yes	Yes

Additional Design Features for S & A Reflectometer

Base design to provide for 15 cm traversing for reflectance profile data

3.1.2 Instrument Description

Figures 3-1 and 3-2 are photographs of the S & A reflectometer in the normal measurement position and in the self-calibration position, respectively. Figures 3-3 and 3-4 show front view and plan view drawings of the reflectometer head assembly. Figure 3-5 is a schematic representation of the reflectometer system. As can be seen from these figures, the reflectometer is basically composed of a light source optics tube and a collection optics tube mounted on a rolling carriage plate with power to the light source and detector monitoring electronics contained in a separate power box.

In the source optics tube, light from the tungsten filament passes through the filter (optional) and then through the focusing lens where the filament image is focused on the circular aperture. This then becomes the "point" source for the collimating lens. This "point" source of .200 mm diameter is placed at the focal point of the collimating lens (F.L. = 80 mm), the resultant divergence angle of the light beam being 2.5 mradians (.20mm/80mm). Before leaving the source optics tube the collimated beam is "stopped down" by a variable iris. This allows the selection of a desired spot size on the mirror surface for reflectance measurement. Currently the light source/receiver/amplifier chain allows the selection of any spot size between 1.2 to 15 mm (.047" to .59").

Upon leaving the iris, the collimated beam passes through the front surface of the glass mirror to the rear surface where it is reflected back through the front surface and to the entrance of the collection optics tube. The incident and reflected angles are 20 degrees off the axis line normal to the mirror surface. The reflected collimated light beam, with its energy somewhat attenuated by the passage through the glass and dust and by its incomplete reflectance from

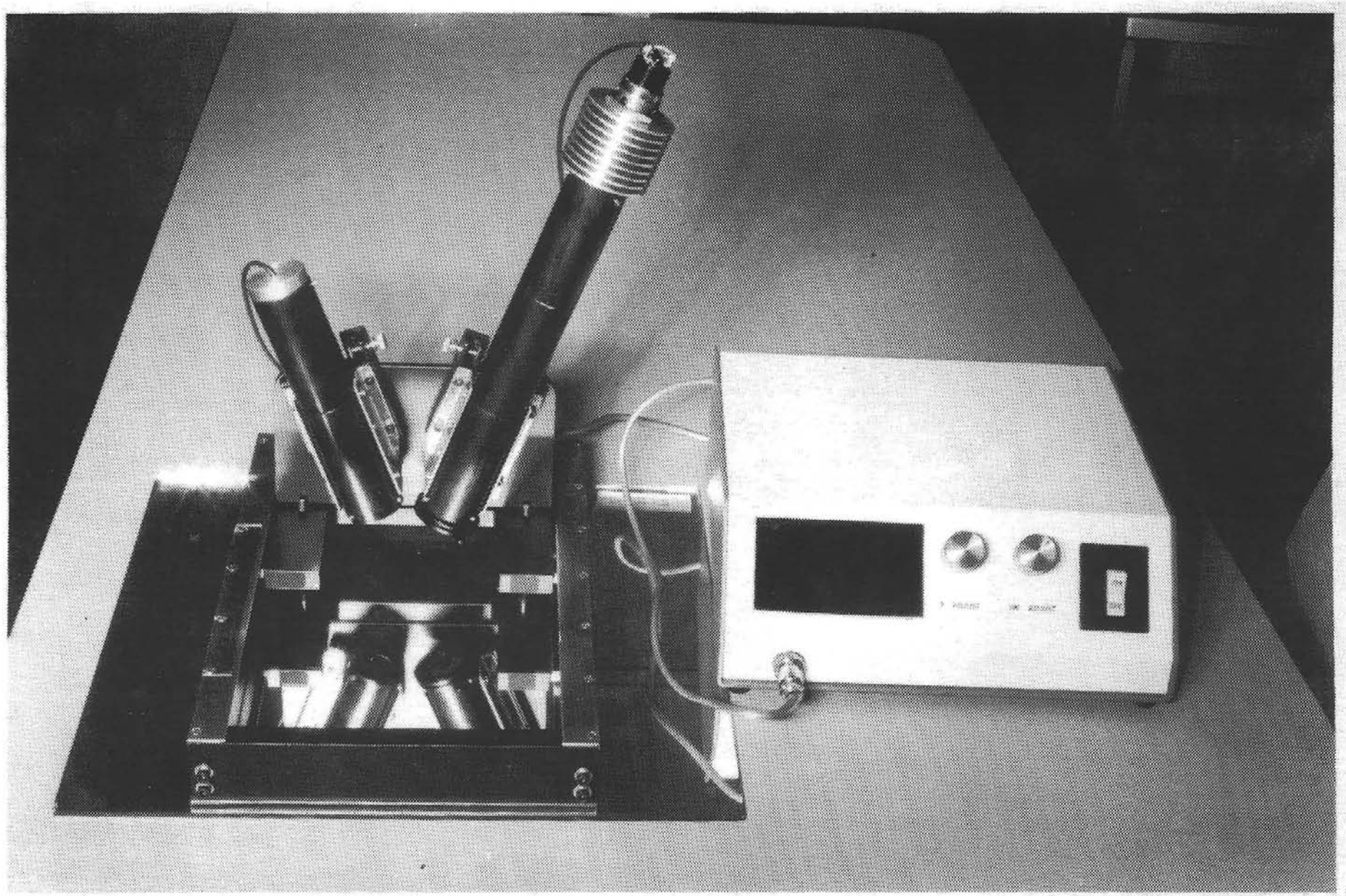

S & A Reflectometer in the Measurement Position

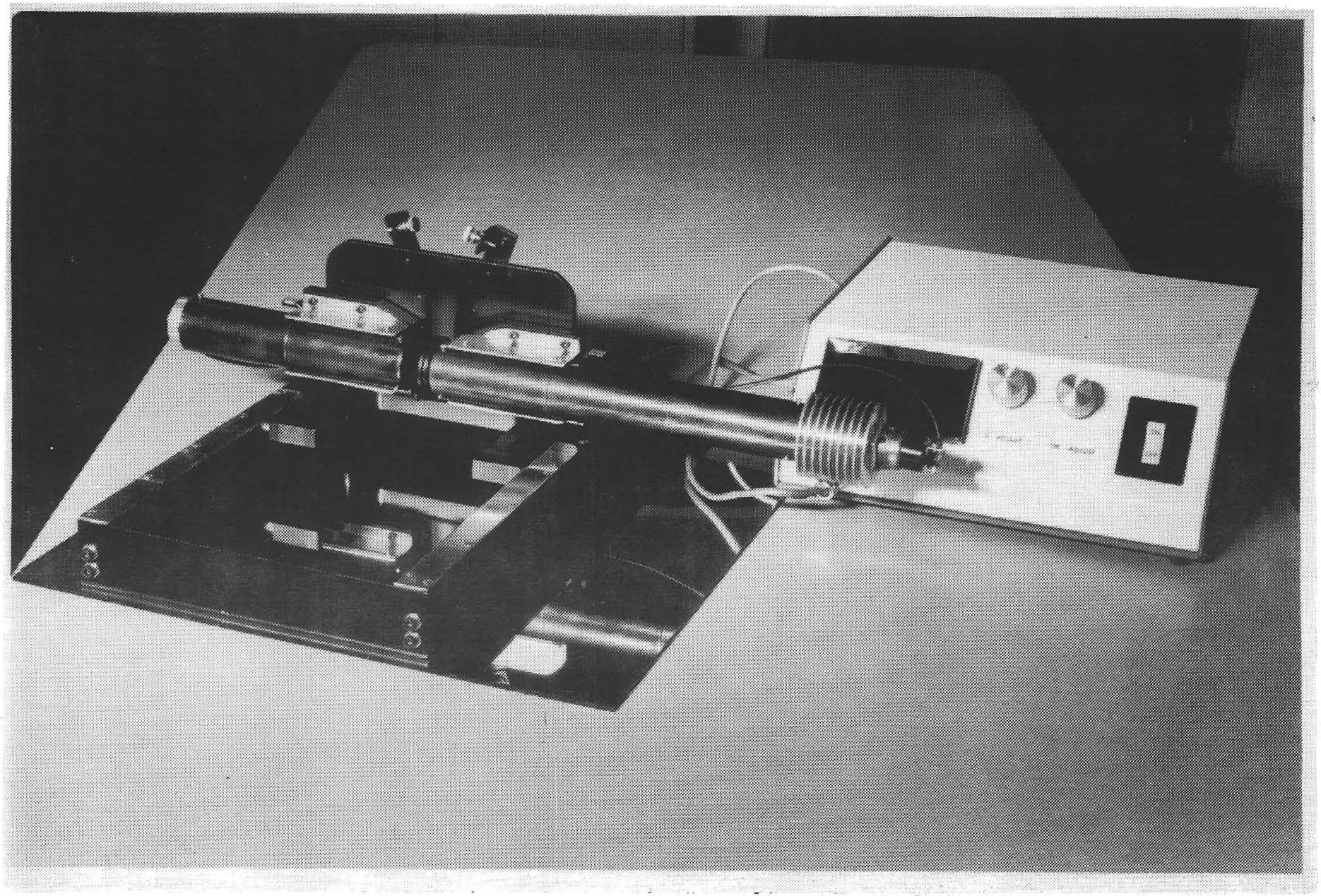

S & A Reflectometer in the Self-Calibration Position

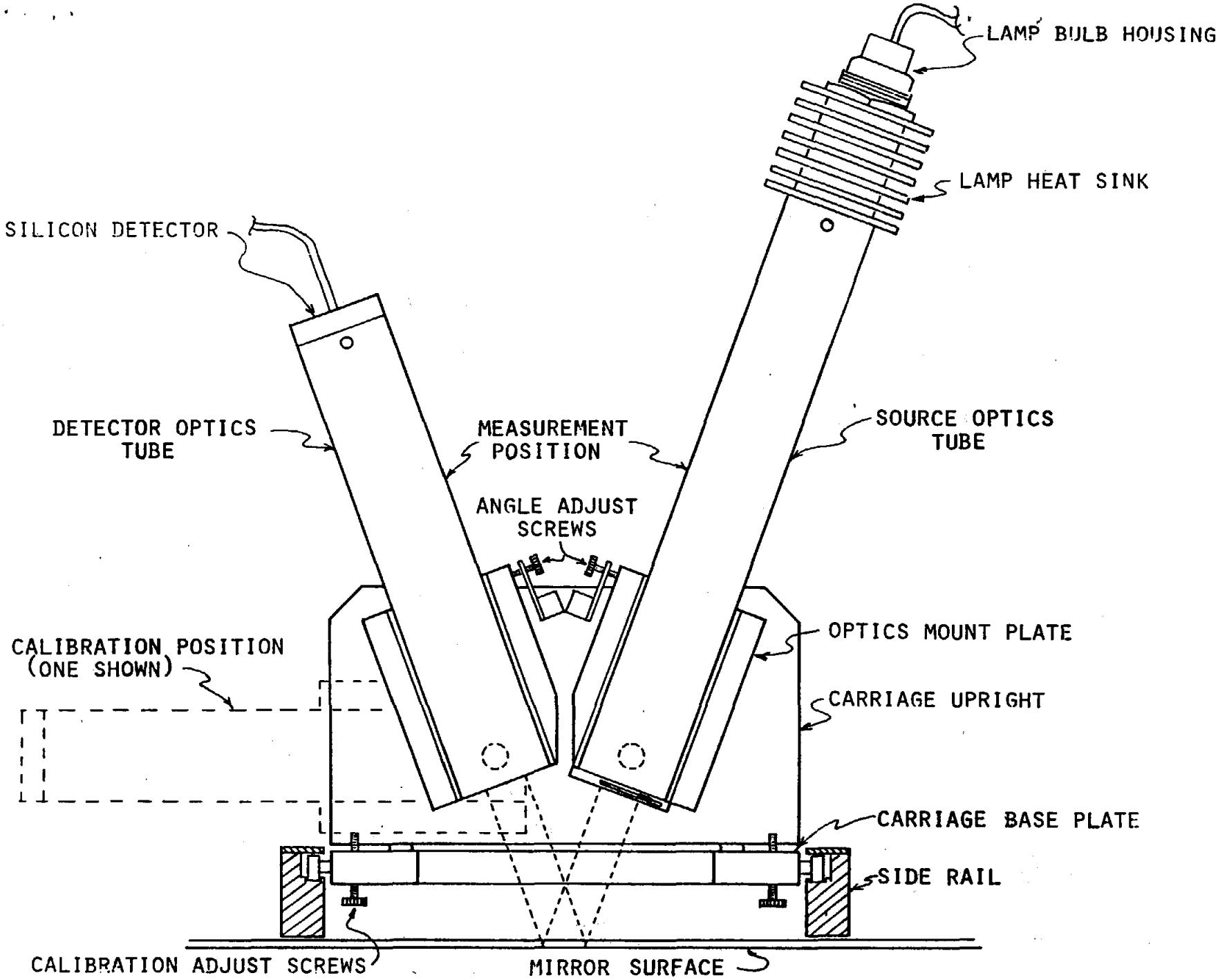

Figure 3-3. S & A Reflectometer - Front View

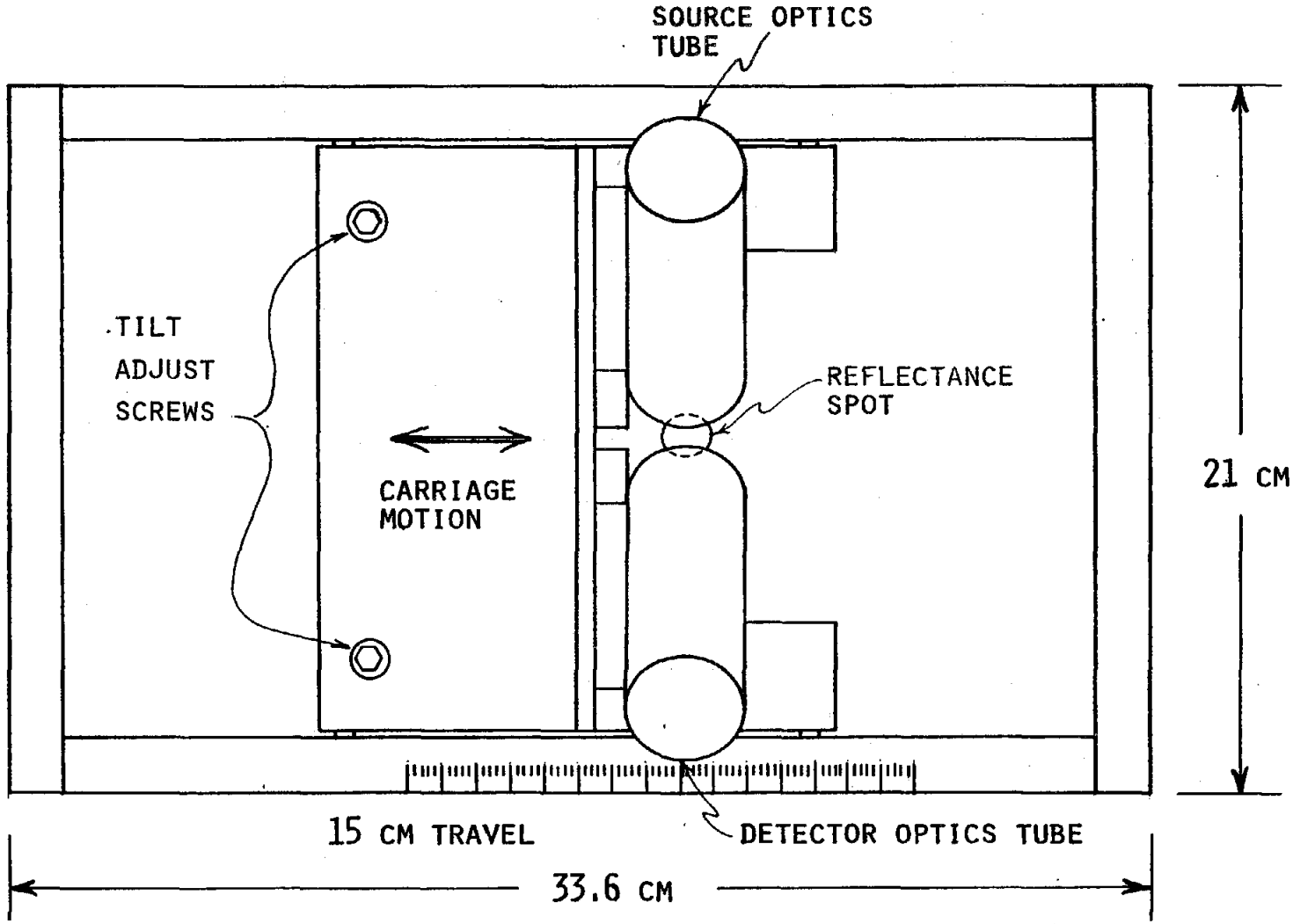

Figure 3-4. S & A Reflectometer - Plan View

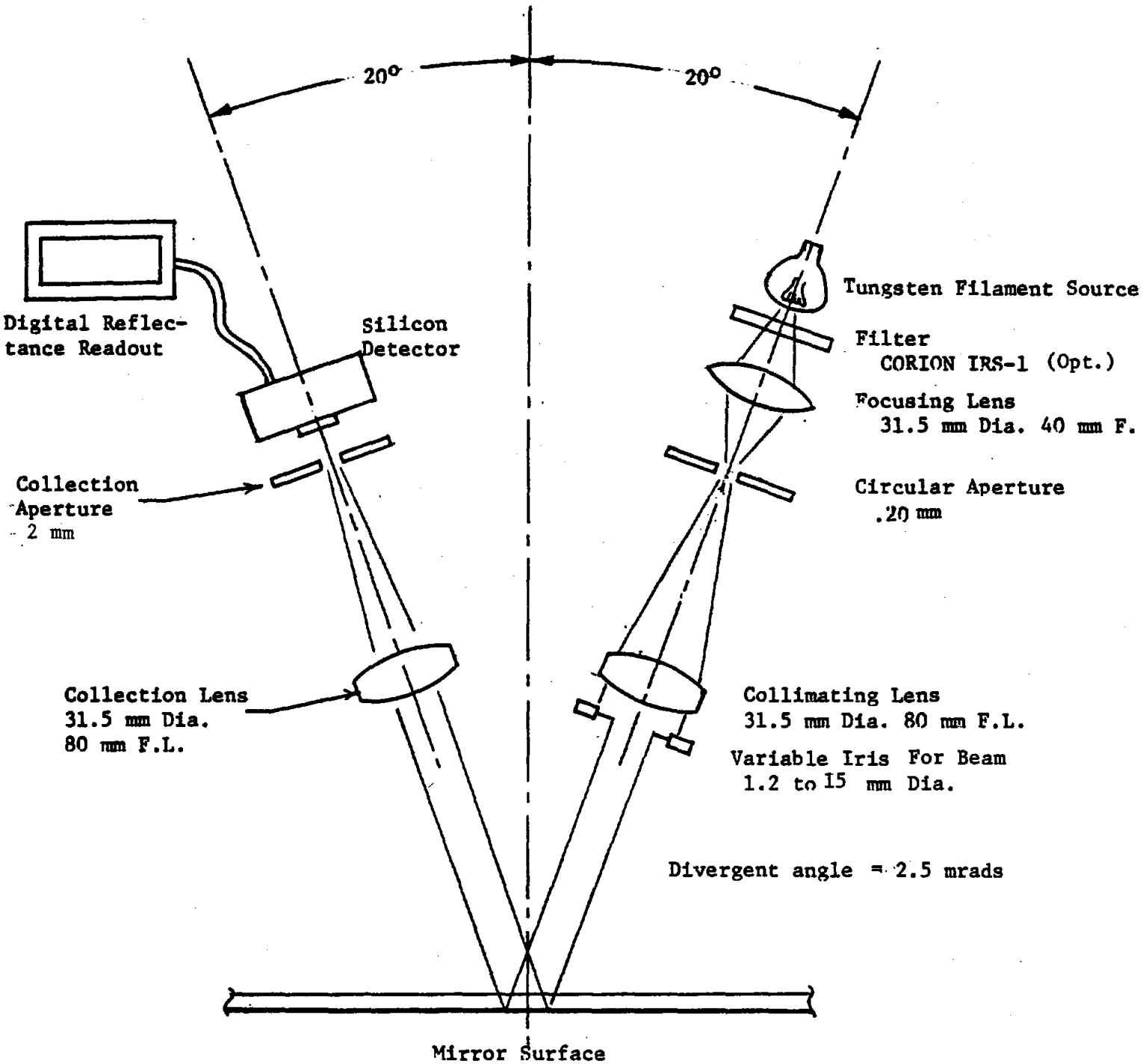

Figure 3-5. Schematic Diagram of S & A Reflectometer

the silvered surface, is then focused by the collection lens (identical to the source collimation lens) onto the collection aperture. At this point, the image of the "point" source provided by the source optics circular aperture has been recovered. Due to scattering effects, the magnitude of which are dependent upon the reflective material being measured, the image at the collection aperture plane will always be larger than that originating from the source aperture (Reference 13). Because of this, and to aid in aperture alignment, a diameter of 2 mm was chosen for the collection aperture. This corresponds to a beam divergence angle of 25 mradians (2mm/80mm). At this point the light intensity of the image is detected by a photovoltaic silicon detector. Electronics required to process this signal, a digital readout meter, and the source power supply are contained in a separate, detachable cabinet.

The source and collection optics tubes are secured to the optics mounting plates which are mounted to the carriage upright plate at ball bearing pivot points. This allows the rotation of each of the optics tubes by 70 degrees such that the source collimated beam may be pointed directly into the collection optics tube thereby providing a measure of the 100 percent light intensity. This then obviates the need for a "calibration standard" mirror for use in conjunction with reflectance measurements.

The carriage upright plate is mounted to the carriage base plate using an adjustment screw system which allows optics tilt adjustment for the purpose of beam alignment. The carriage base plate is provided with miniature ball bearing rollers which run in the rail grooves of the rail base. The rail length provides for a maximum carriage plate movement of 15 cm. It is then possible to make smooth traverses of a cleaned area for the gathering of reflectance profile data. This feature also allows taking 16 reflectance readings, spaced 1 cm apart, for purposes of average reflectance measurement

without movement of the felt backed reflectometer base on the dust mirror surface.

Because of the ability to individually adjust the angles of the source and collection optics tubes, the reflectometer may be aligned for use with second surface mirrors of varying thickness as well as front surface mirrors or other reflective material.

3.1.3 Alignment Procedures

Alignment of the reflectometer falls into two categories: (1) mechanical alignment of the optics and (2) electrical adjustment of the "zero" and "100 percent" amplifier potentiometers. The first alignment is performed one time only for the reflective material being measured while the electrical adjustments are performed as needed during use of the instrument.

Mechanical alignment is accomplished through the adjustment of four basic parameters: (1) tilt adjustment of the carriage upright (which holds the optics tubes) with respect to the carriage base plate (which is parallel to the mirror surface), (2) fine adjustment of the measurement angle adjust screws, (3) fine adjustment of the calibration adjust screw and (4) adjustment of the lamp bulb housing (this adjustment is only performed when the lamp bulb is replaced). These adjustments are first performed with the detector plate removed and are accomplished by visually aligning the filament image in the center of the collection aperture. The calibration adjust screws are trimmed first. Following that, the tilt and angle adjust screws are trimmed together to obtain the same image as presented in the calibration position. Upon completing the visual alignment, the detector plate is reinserted in the optics tube and the unit turned on. The tilt and angle adjustments are repeated to obtain

the maximum reading on the digital readout with the optics in the measurement position. After this, the calibration screws are adjusted to obtain maximum reading in the calibration position. Note that the calibration position must be adjusted last. Once these adjustments have been made, only the angle adjust screws need be trimmed when changing reflective surfaces to be measured.

Electrical adjustment of the "zero" and "100 percent" amplifiers is accomplished by turning the two 10-turn potentiometers on the front of the cabinet. Prior to taking any reflectance readings, the optics tubes are placed in the calibration position and the "100 percent" potentiometer is adjusted to give a reading of 100.0 on the digital readout. The collection optics are then raised to the measurement position and the "zero" potentiometer adjusted to obtain 00.0 on the digital readout. The source optics tube is then raised to the measurement position and the reflectance readings read off the digital readout directly in percent reflectance. Upon completing a measurement traverse across a mirror sample, the zero and 100% readings should be double checked to insure that instrument drift has not occurred. Instrument drift is very minimal, however, as shown in Section 3.1.5.

3.1.4 Measurement Procedures

The reflectometer is designed with the capability of accepting filters in the source and collection optics. However, in the present configuration filters are not installed. This does cause a slight sensitivity to higher ambient light levels. This was investigated in Section 3.1.5 with the conclusion that normal room lighting does not adversely effect reflectance readings. Based on the ambient light sensitivity tests of Reference 12, it is anticipated that the S & A lab reflectometer could easily be made insensitive

to outdoor sunlight exposure with the addition of the filters. However, in its present configuration, the reflectometer should be used in subdued or normal room ambient lighting conditions.

Prior to taking reflectance measurements, the instrument should be permitted to warm for about five minutes to allow the lamp bulb and circuitry to stabilize. After this time, the electronics are adjusted for 0.0 and 100.0 readings as described in the previous section. Reflectance measurements may now be taken. As previously mentioned, consistent with proper measurement procedure, the 0.0 and 100.0 calibrations should be checked and noted at the end of each measurement traverse. If they deviate by more than 0.1 or 0.2 percent reflectance the potentiometers should be readjusted and reflectance measurements retaken.

If measurements are being performed on small mirror samples (e.g. 7" x 7" or 14"x 14") it is necessary to assure that the mirrors are placed on a very even and flat surface. Warping of the mirrors by a slight amount affects the reflected beam and will show up in reflectance measurements.

3.1.5 Characterization and Calibration

A number of checks were made on the reflectometer to determine its characteristics and accuracy. These included:

1) Linearity of the detection cell
2) Tungsten filament source stability time
3) Stray light effect
4) Absolute reflectance calibration
5) Measurement reproducibility

Linearity of the Infra-red Industries detector was assured by the manufacturer over a 2-3 decade range.

To determine the appropriate warmup time for the instrument, startup transient tests were performed. For these tests, the instrument was placed in the calibration position and the system turned on. Intensity readings were taken at various time intervals from time zero to one hour. Figure 3-6 presents a typical data plot and illustrates that the instrument may be used after as short a warmup period as 5 minutes. With typical reflectance measurement traverses taking usually no more than 1 minute, the slight drift of the instrument after short warmup times is not detrimental to accuracy of the measurements.

The effect of ambient room light was first checked by observing the difference in calibration readings with three different lighting levels. A subdued lighting level was used as the basic measurement setting. This was accomplished by turning off overhead lights in the near vicinity of the instrument.

Normal office/lab overhead florescent lighting produced an increase in reading of approximately 0.05. Directing four photofloods (1200 watts) on the ceiling 7 feet overhead produced an increase in reading of 0.3. Some of this increase would be seen also in the measurement position of the optics (could be more or less depending on source angle of ambient light) thereby not necessarily significantly affecting the actual reflectance measurement. To check the ambient light effect on actual reflectance measurement the reflectance of one spot on a 14" test mirror was measured under four different lighting conditions. The results of this test are shown in Table 3-2. The instrument was adjusted to 00.0 and 100.0 in each environment prior to reflectance measurement.

These results indicate that the instrument without filters may be used in normal overhead florescent lighting with

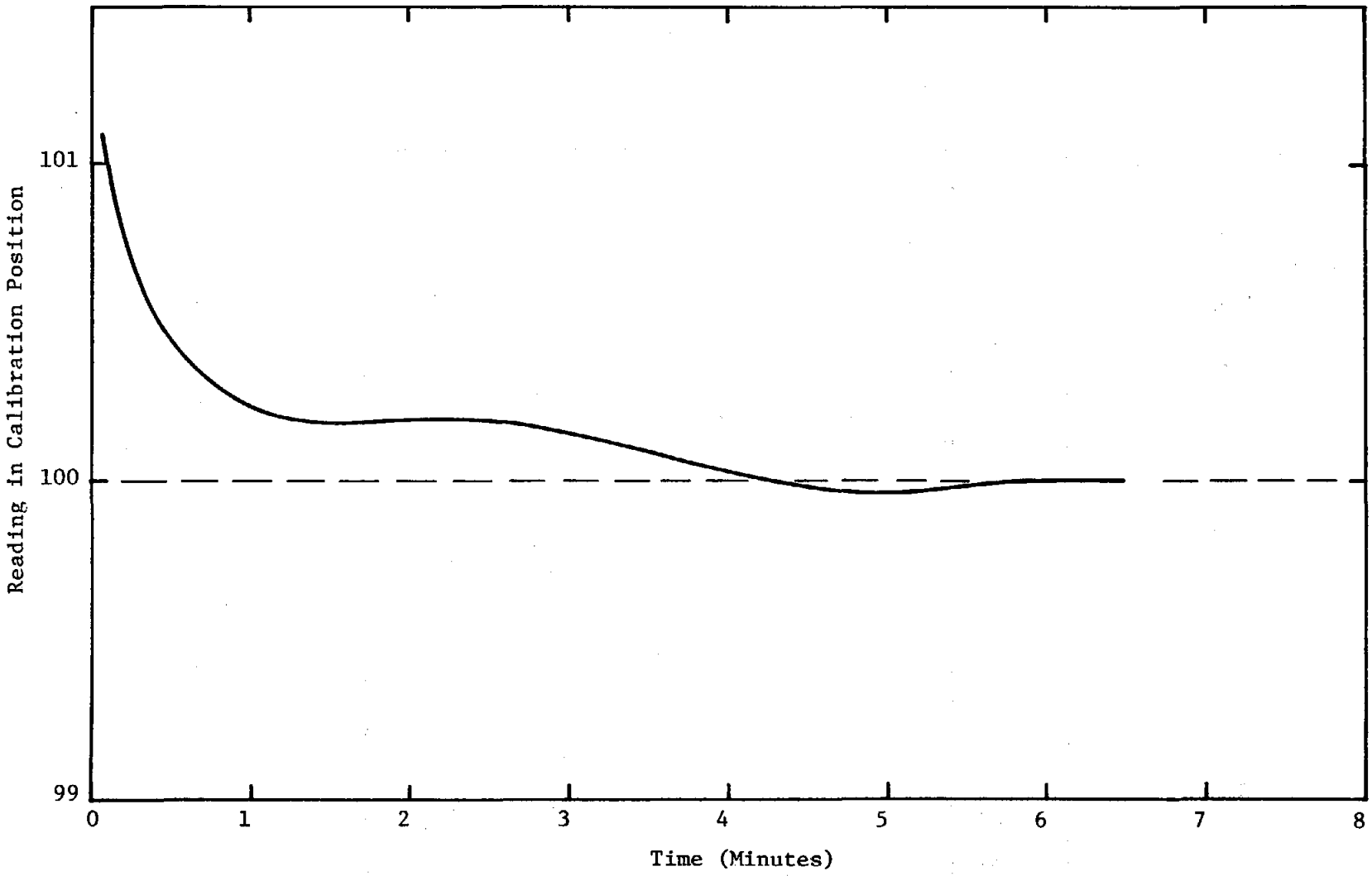

Figure 3-6. Typical Data Plot for Startup Transient Tests of the S & A Reflectometer

Table 3-2. Reflectance Measurements Taken on a Clean 14" x 14" Mirror Under Various Lighting Conditions

Environment	Reflectance
1. Total Darkness	83.6%
2. Subdued room light	83.6%
3. Normal office/lab florescent light	83.6%
4. 1200 Watt Floodlamps on Ceiling	85.3%
5. Outdoors - Direct Sun - 50° off Horizon - Front of instrument facing away from sun	90.5%

Note: Measurements taken without optional filters

adequate results. Usage in higher light areas and outdoors does not produce acceptable results and would require the use of filters.

Absolute reflectance measurement capability was checked by comparing reflectance readings taken with the S & A reflectometer on the on-site McDonnell-Douglas mirror panel to typical reflectance data for the McDonnell-Douglas panels as provided by Sandia-Albuquerque. The Sandia data provided reflectance vs. wavelength from 350 nm to 2500 nm.(Ref. 19). To provide a more valid comparison, the wavelength dependent reflectance data was weighted by the IRI detector response curve to obtain a reflectance value expected to be "seen" by the S & A reflectometer.

Figure 3-7 presents relative radiation and response characteristics, plotted as a function of wavelength, of various parameters pertinent to the reflectometer. Parameter curves are shown all on one plot using a common wavelength scale. Comparing curves to one another should be done with care, however, since the ordinate scale, when used for relative energy, is a scale normalized to 1.0 or 100% representing the maximum value of energy on the given curve. The IRI detector response curve shown in Figure 3-7 is used as a multiplier for the Sandia furnished reflectance data (See Table 3-3) to arrive at the weighted reflectance. To obtain reflectance measurements, the reflectometer was placed in four spots on the McDonnell-Douglas mirror panel and traverses made with reflectance readings taken every 1 cm (16 readings per traverse). Results are presented in Table 3-4. The measured reflectance average value of 88.73% compares very closely with the expected weighted average reflectance of 88.96%.

Measurement reproducibility was investigated by repeatedly taking reflectances of the McDonnell-Douglas mirror panel at various times throughout a one day period. Measurements

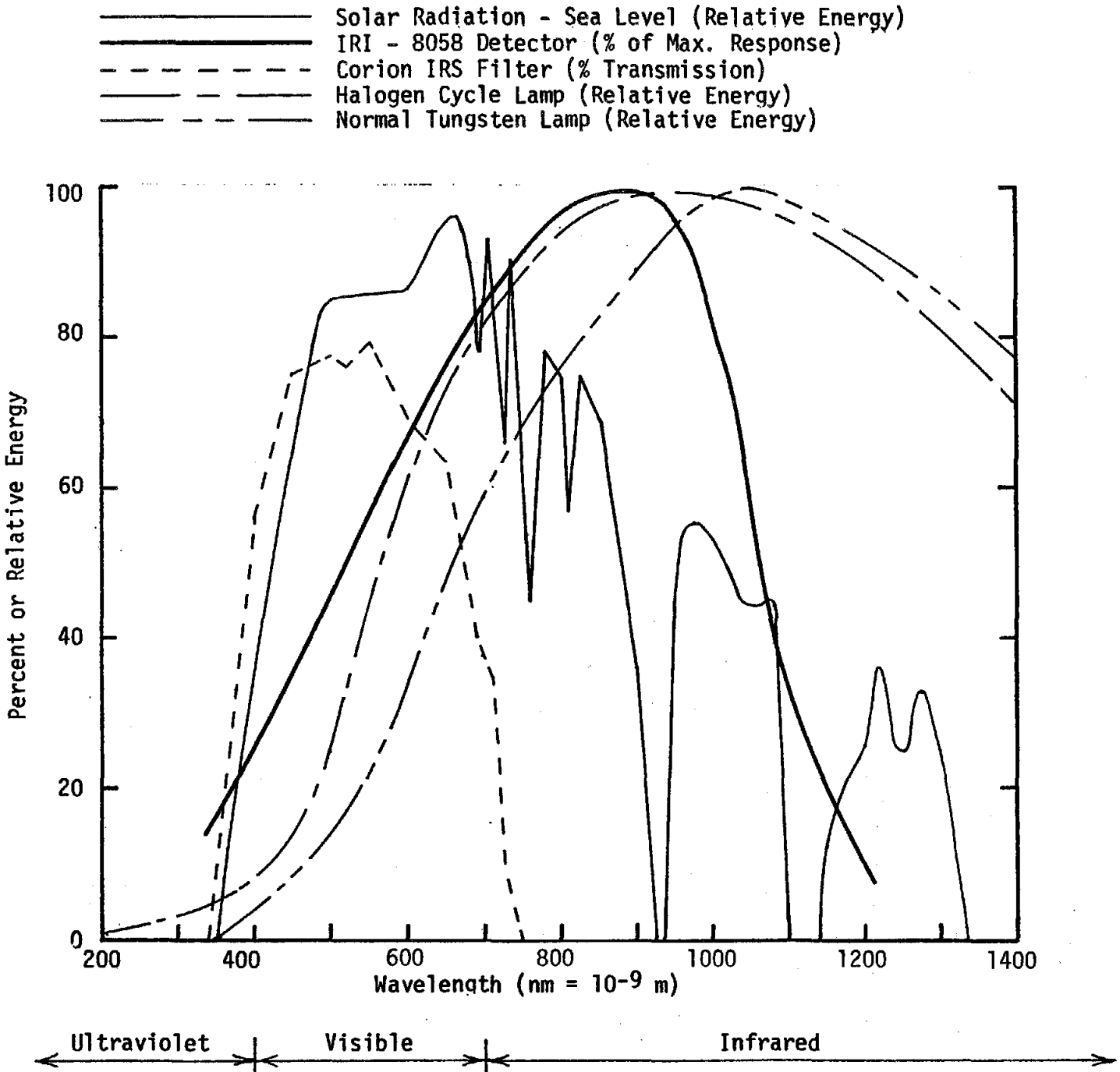

Figure 3-7. Relative Radiation and Response Characteristics vs. Wavelength Relevant to S & A Reflectometer

Table 3-3. Absolute Reflectance of McDonnell-Douglas Panel Weighted by Reflectometer Detector Wavelength Response Curve

Wavelength (nm)	IRI[1] Detector Response	Tabulated[2] Reflectance Data	[3] Weighted Reflectance
350	15.5	.6955	10.78
400	26	.8890	23.11
450	35	.9133	31.97
500	47	.9450	44.42
550	56	.9461	52.98
600	69	.9403	64.88
700	84	.9185	77.15
800	97	.8845	85.80
900	99.5	.8559	85.16
1000	80	.8444	67.55
1100	33	.8407	27.74
1200	9.5	.8446	8.02
	$\Sigma = 651.5$		$\Sigma = 579.56$

$$\text{Weighted Average} = \frac{579.56}{651.5} = .8896 = 88.96\%$$

Notes:

(1) From Figure 3-7 (Infrared Industries - 8058 Detector)

(2) From Reference 19

(3) Taken as Detector Response x Tabulated Reflectance

Table 3-4. S & A Reflectometer Measurements on an MDAC Heliostat Mirror

Traverse Location (cm)	Reflectance (%)			
	Position 1	Position 2	Position 3	Position 4
0	88.8	88.8	88.8	88.7
1	88.8	88.7	88.8	88.6
2	88.8	88.7	88.8	88.5
3	88.8	88.8	88.8	88.5
4	88.9	88.8	88.7	88.5
5	88.9	88.8	88.8	88.5
6	88.8	88.8	88.7	88.6
7	88.8	88.8	88.7	88.6
8	88.8	88.7	88.8	88.6
9	88.8	88.8	88.8	88.6
10	88.9	88.7	88.7	88.6
11	88.8	88.8	88.6	88.5
12	88.8	88.8	88.7	88.6
13	88.7	88.9	88.8	88.7
14	88.7	88.8	88.7	88.7
15	88.7	88.8	88.7	88.7
Data Mean	88.8	88.78	88.74	88.59
Data Standard Deviation	.063	.054	.063	.077

Data for all 64 Readings: Mean 88.73 Standard Deviation = .103

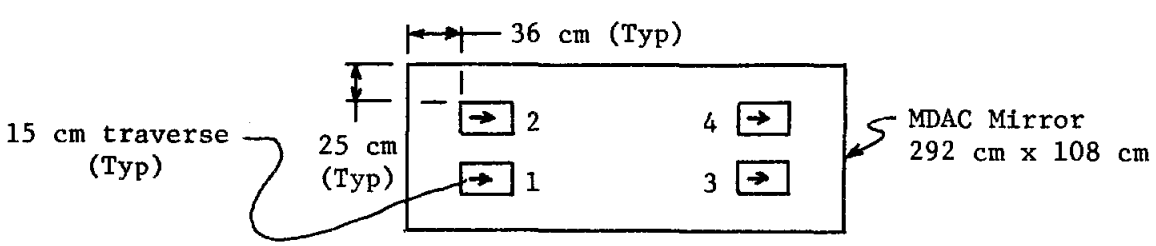

were taken at the same spot each time and 0 and 100 calibrations were performed prior to each measurement. Ten measurements were taken with a mean of 89.34% and reproducible with a standard deviation of .05 % reflectance reading.

Although available time did not permit it during the period of this study, it would be desirable to investigate the reflectometer characteristics in greater depth. Some areas of investigation recommended for further study are:

1. Light filtration - Determine the advantages of light filtration in the source or collection optics or both upon the operating characteristics of the reflectometer.
2. Source/Collection Electronics - In order to use filters, such as the Corion Infra-red Suppressor (IRS), either a greater gain is needed in the amplifier stage of the detector circuit or a more powerful source lamp is needed. This also applies to the usage of small iris settings on the source tube. In the present configuration the lamp detector electronics combination allows a minimum stopped-down light beam of 5.8 mm in diameter. The iris has the capability of reducing the incident beam to a diameter of 1.5 mm. The small beam diameters are helpful for measuring reflectance profiles while the larger diameters facilitate taking average readings of larger areas.
3. Measurement correlation - Further characterization of the instrument spectral response and correlation of measured reflectances with solar-averaged reflectance properties is recommended for future work.
4. Second-generation portable unit - Because of its relatively, low material cost and very favorable operating characteristics, it is recommended that the current unit be examined for adaptation to a portable, low cost field unit.

3.2 S & A LOW SPEED WIND TUNNEL

As part of the total effort under this contract it was necessary to design and construct a system for depositing dust onto mirror samples in a rapid, uniform and repeatable manner. The system built to accomplish this is basically a low velocity wind tunnel with variable speed blower, as described in the following sections.

3.2.1 Design Requirements

The requirements for the design of a dust deposition system were determined from a review of existing Sandia methods (References 6 and 20), and from the consideration of the sizes of test specimens to be used in the cleaning studies. In addition, cost and schedule goals had a significant impact on many of the design decisions.

Upon consultation with Sandia personnel, it was agreed that a horizontal air flow system with velocities of 10 MPH or less was preferred over gravity settlement in calm air, as it more nearly represents field conditions. The smaller size dust particles (<10μ) are the ones that adhere the strongest to glass. It is especially important to have impingement of these particles on the surface of the specimen to get the best dust usage and adhesion. This can be accomplished by inclining the test specimens to the air stream and/or using flaps in the wind tunnel to deflect the air stream down onto the specimen.

The size of the wind tunnel was governed by the size of the mirror test specimens. First of all, Sandia provided S & A with a McDonnell-Douglas heliostat mirror 292 cm x 108 cm (9 feet-7inches x 3 feet-6½ inches). To deposit dust over a significant portion of this mirror, the wind tunnel was designed to have an 8 ft. deposition length and to sit on top of the MDAC mirror. A width of 20 inches was selected to adequately accommodate 14 in. x 14 in. test mirrors as well as 2 adjacent 7 in. x 7 in. mirrors. For portability, light weight and low cost, the wind tunnel was constructed

of wood in three separate sections which are joined with bolts. A detail design description is provided in the following section.

3.2.2 Design Description

A photograph of the wind tunnel is given in Figure 3-8, and details of the three structural sections composing the total assembly are provided in Figures 3-9a, b, and c.

The 30 inch long entry section, 8-foot long main section, and 26 inch long exit section are constructed of plywood and wood framing. For ease of handling and transportation, the sections connect to each other with flanged, bolted joints. For minimal skin friction, the "A" side of the plywood is faced inward. This surface has also been coated with sealant and white paint to improve the visibility through the clear plastic windows, three of which are located along the top wall and three along one side wall.

The air movement is provided by a 1000 rpm blower rated at 865 to 520 CFM at static pressure of 0.3 to 0.7 inch, respectively (Figure 3-9a). To provide variability of "wind" speed in the flow path of given restriction, a five-speed control was added to the blower. The main tunnel cross section was sized at 10 inches by 20 inches inside to achieve realistic wind speeds with this supply system. The blower is bolted to a movable stand at one end and directly to the tunnel entry section at the other. Uniformity of air flow and dust deposition across the width of the tunnel was accomplished by experimentation with various air flow control devices and various dust introduction and dispersal methods. The end result is a Venturi-like restriction in the divergent entry portion of the tunnel with dust injection just downstream of this restricted cross section. A restriction on one side of the blower was also required to achieve uniformity.

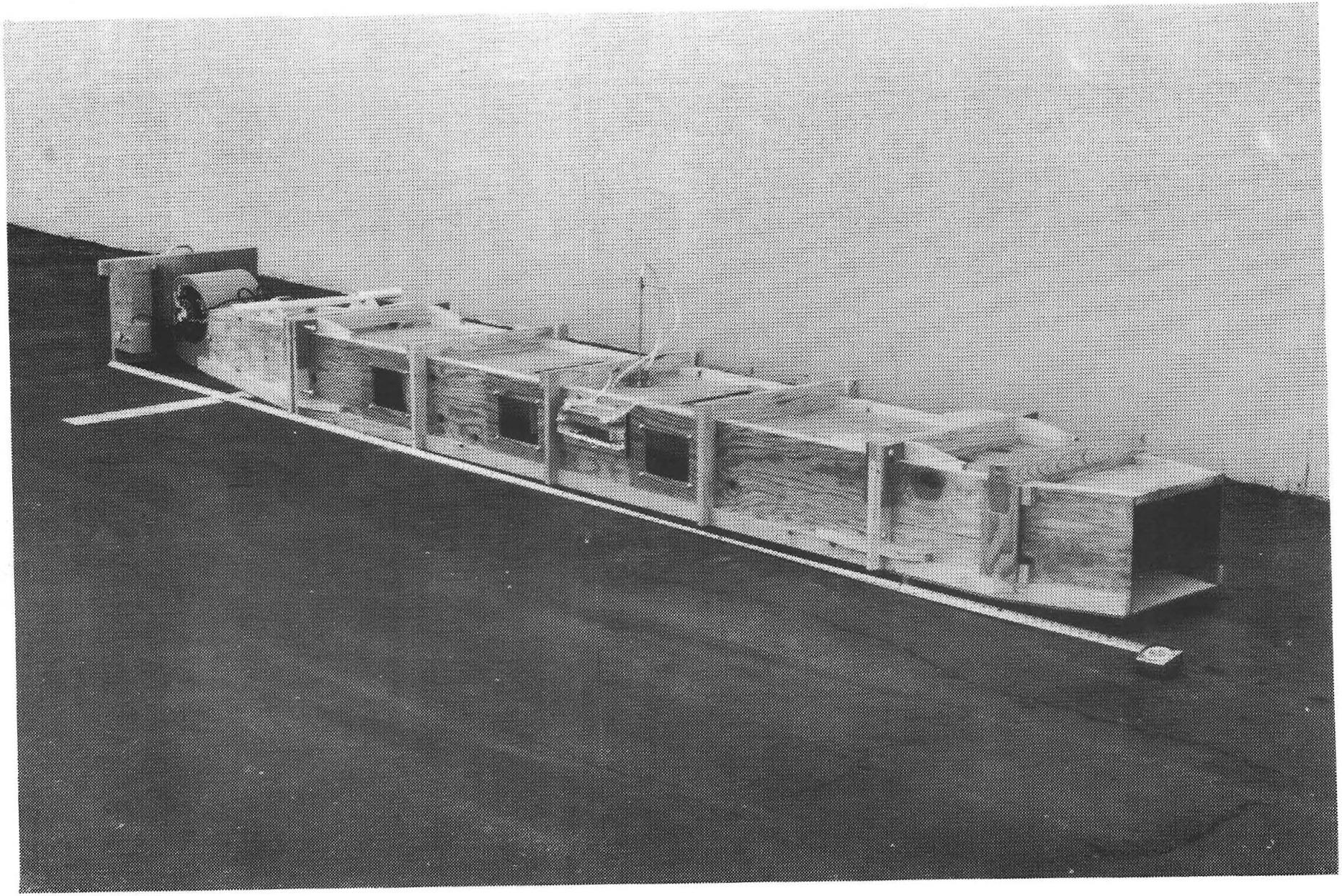

Figure 3-8. S & A Low Speed Dust Deposition Wind Tunnel

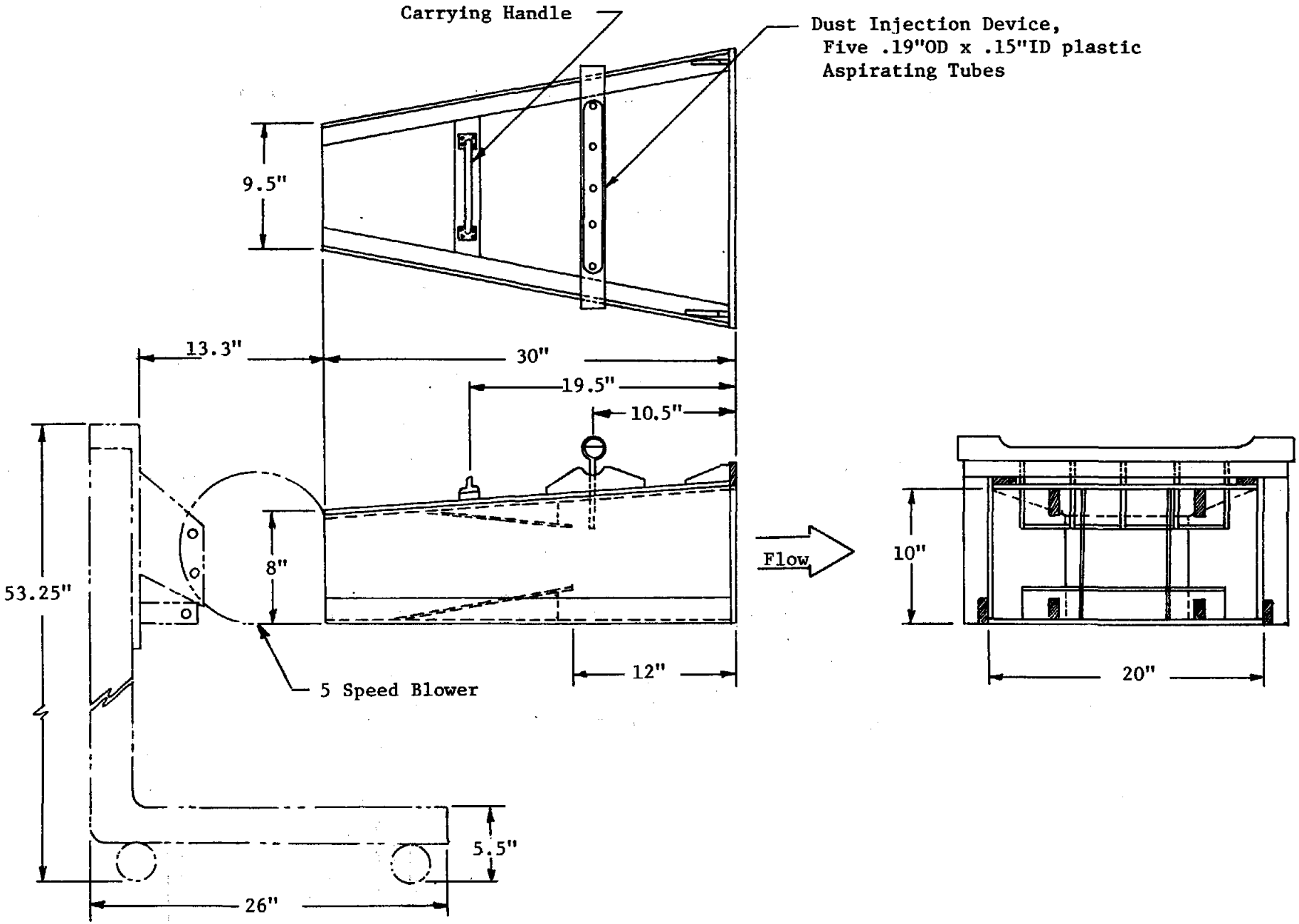

Figure 3-9a. Dust Deposition Wind Tunnel Entry Section

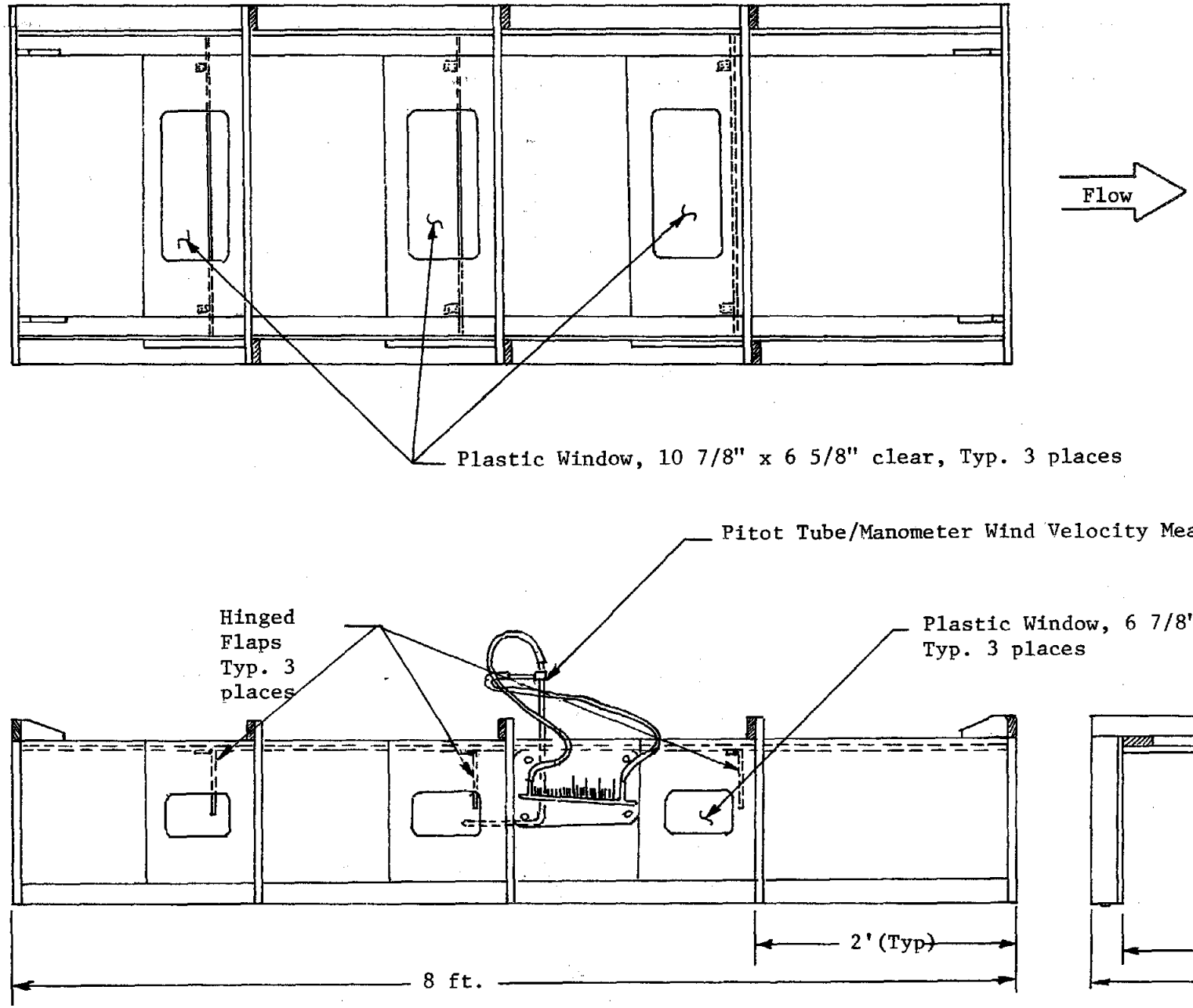

Figure 3-9b. Dust Deposition Wind Tunnel Center Section

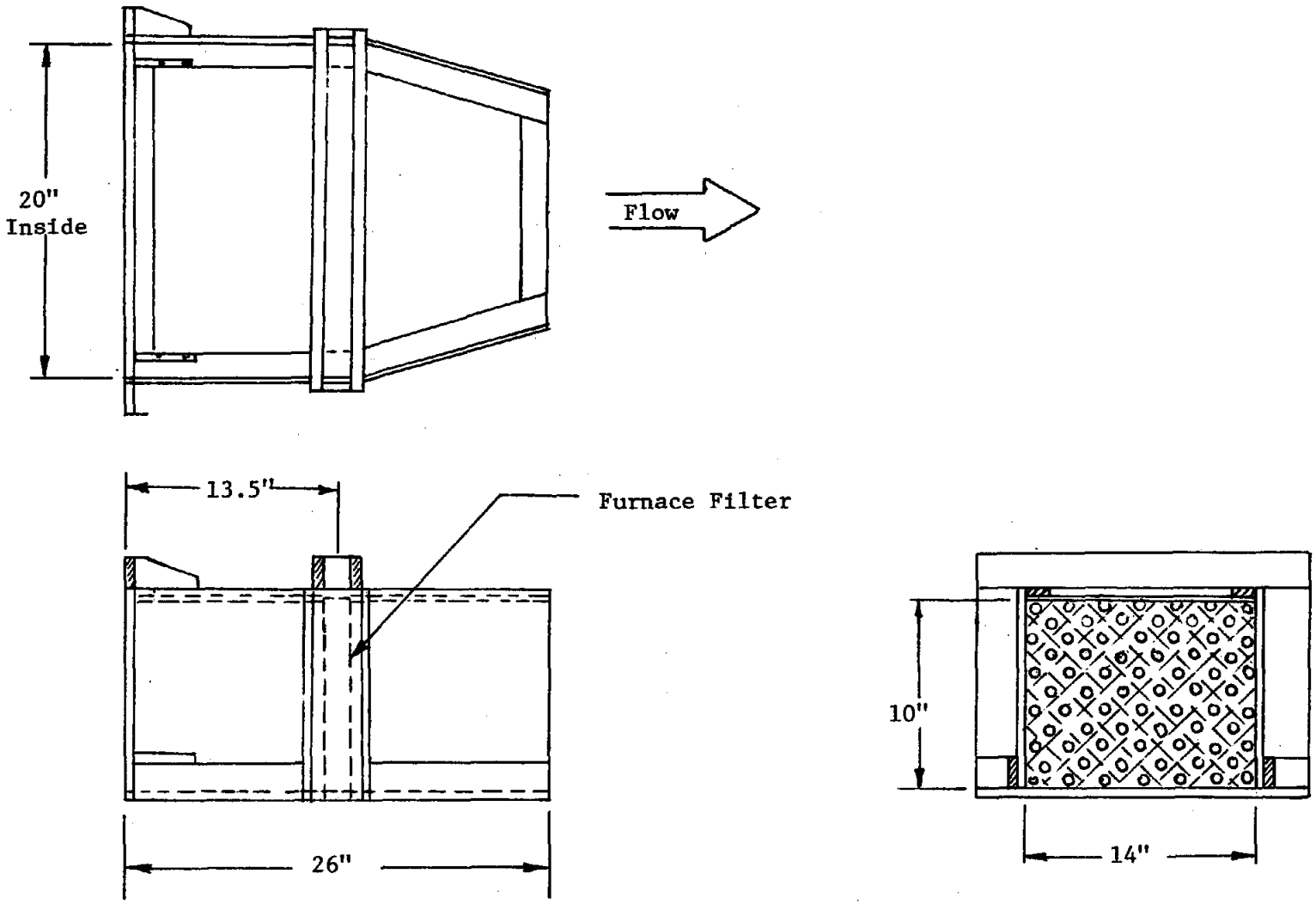

Figure 3-9c. Dust Deposition Wind Tunnel
Exit Section

The injector is an aspirating system with a horizontal hopper made from plastic pipe and located outside of and above the tunnel. Five small vertical plastic injector tubes penetrate the tunnel top wall and the bottom of the hopper to feed dust to the airstream. The dust used, as recommended by SANDIA, is fine Arizona desert dust, AC Spark Plug Division of General Motors part number AC-154-3094. The particle size distribution and chemical composition of this dust are shown in Tables 3-5 and 3-6, respectively.

To improve precipitation and uniform deposition, transverse flaps are suspended from the tunnel top at three approximately equally spaced locations along the tunnel main section length. The convergent exit section of the tunnel also contributes to the flow control. In addition to capturing non-deposited dust, an ordinary furnace filter helps provide back pressure required for the blower. Typical velocities achieved in the wind tunnel are shown in Table 3-7. Besides the five blower speed settings, velocity can be further controlled by varying the back pressure through the use of additional filters in the exit section.

The effect of air blow off on the dusted mirror specimens was also investigated. Four mirror specimens were placed in the tunnel oriented like those of Figure 4-4. Deposit was made using 4 teaspoons of dust in the wind tunnel dust injector. Reflectance losses were checked after deposition, after 1 minute of wind tunnel operation at high fan speed without dust injection and after each mirror was held in the air stream in front of the tunnel fan box section at 2 feet from the exit. Table 3-8 summarizes the results and indicates that the after blow does tend to remove some of the larger particles and reduce the reflectance loss somewhat. For consistency in technique the high speed fan after blow is recommended (Column 2).

Table 3-5. AC Fine Desert Dust
Particle Size Distribution

Particle Size (μ)	Percentage Composition
0 - 5	39 ± 2%
5 - 10	18 ± 3%
10 - 20	16 ± 3%
20 - 40	18 ± 3%
40 - 80	9 ± 3%

Table 3-6. Typical Chemical Analysis of AC
Fine Desert Dust

Constituent	Weight (%)	Constituent	Weight (%)
SiO_2	65 - 76	TiO_2	0.5 - 1.0
Al_2O_3	11 - 17	V_2O_3	0.10
Fe_2O_3	2.5 - 5.0	ZrO	0.10
Na_2O	2 - 4	BaO	0.10
CaO	3 - 6	Loss on Ignition	2 - 4
MgO	0.5 - 1.5		

Table 3-7. Low Speed Wind Tunnel Velocities

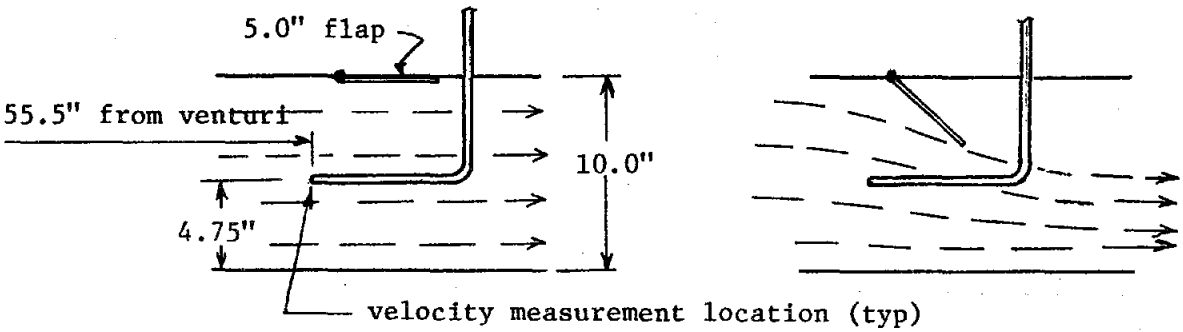

Blower Speed Setting	Air Velocity - Flaps Up			Air Velocity - Flaps Down		
	meters/ sec.	ft/ min.	mph	meters/ sec.	ft/ min.	mph
1	1.5	300	3.4	2.1	410	4.7
2	2.1	410	4.7	2.7	540	6.1
3	2.5	500	5.7	3.0	600	6.8
4	2.9	570	6.5	3.4	665	7.6
5	3.0	600	6.8	3.7	720	8.2

Table 3-8. Effect of After Blow on 14" Square Wind Tunnel Deposited Mirror Samples

Mirror Location	Spectral Reflectance Loss		
	After Deposit	After High Speed Blow (1 Min)	After Placing Perpendicular To Air Stream 2' Away
14-DR-3	.055	.047	.043
14-DU-3 With Repcon	.057	.052	.046
14-DU-3 Without Repcon	.311	.308	.279
14-DU-6	.261	.254	.220
14-DR-4	.056	.051	.390

4.0 DUST ACCUMULATION STUDIES

4.1 Dust Accumulation in the S & A Wind Tunnel

The parameters that affect dust buildup on mirror samples in the wind tunnel are primarily mirror inclination, mirror location relative to the flaps, blower speed and, of course, the quantity of dust introduced. Exploratory tests were performed on these parameters to arrive at a standard procedure for dust deposition. Although time did not permit a thorough investigation of these variables, some general trends can be reported.

A photograph of dust buildup on the MDAC heliostat mirror is given in Figure 4-1. Figure 4-2 shows the dust accumulation along the length of the heliostat mirror achieved using 2 teaspoons of dust in the wind tunnel. The blower was set at the middle position, no. 3, during the deposition period (about 4 minutes) and then set at the highest speed, position no. 5, for about 1 minute to blow off non-adhering particles. The trend is for greater dust accumulation between flaps and towards the aft end of the wind tunnel. Reflectance losses vary from 15 to 30 percent. Transverse distributions of reflectance at 5 stations are shown in Figure 4-3. The overall average reflectance was 0.66 with a standard deviation of 0.055.

Four mirror samples, 14" x 14", were inclined at 3^{o} in the wind tunnel and tested for dust accumulation as a function of quantity of dust injected into the air stream. Results are shown in Figure 4-4. Half of the first specimen was coated with the polymer coating REPCON, (Ref. 21), as was the entire surface of the last specimen. This coating greatly reduces the dust adhesion characteristics of the mirror surface, as can be seen from the reflectance loss plots in Figure 4-4.

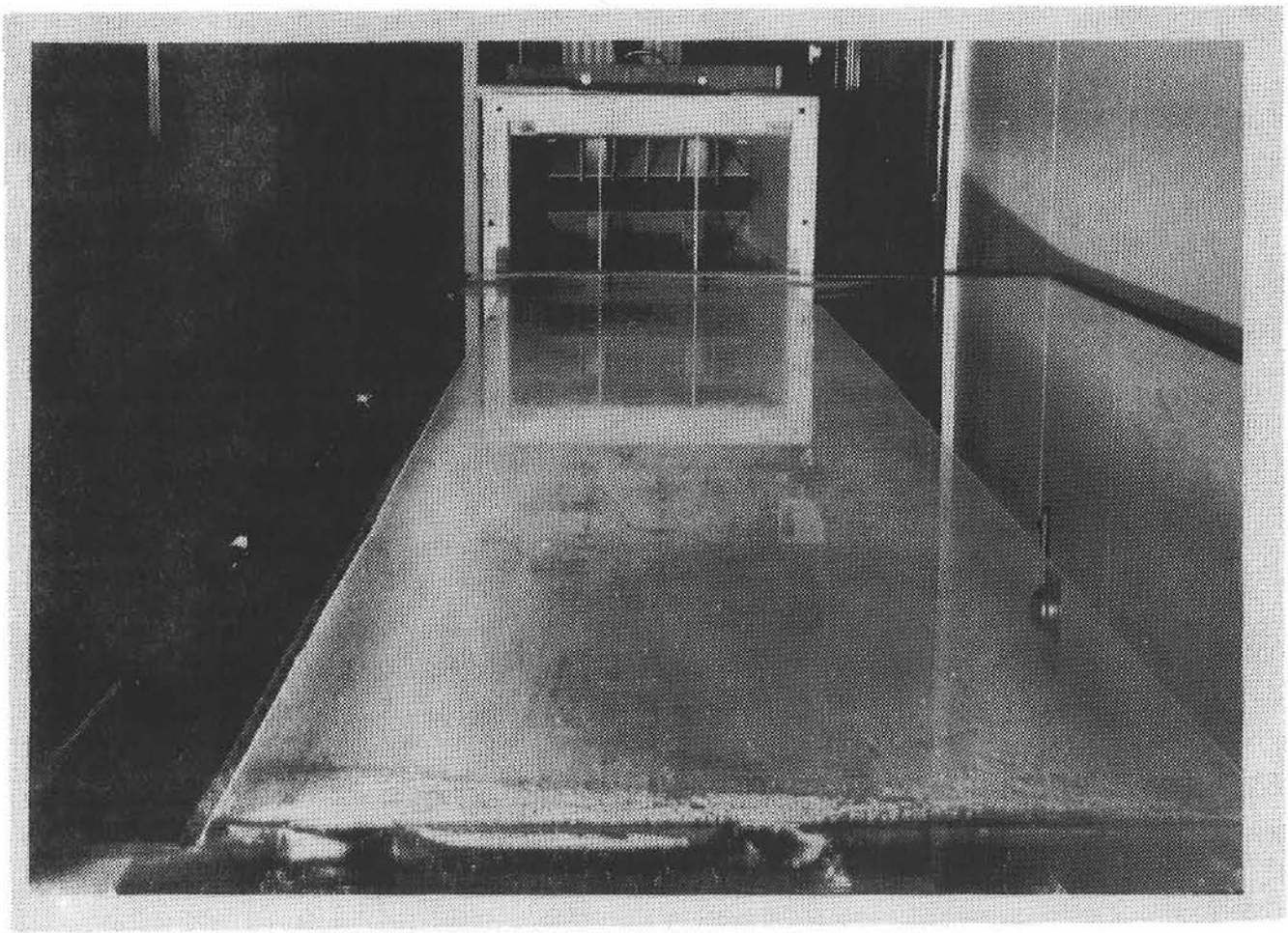

Figure 4-1. Dust Accumulation Test on MDAC Heliostat Mirror using S & A Wind Tunnel

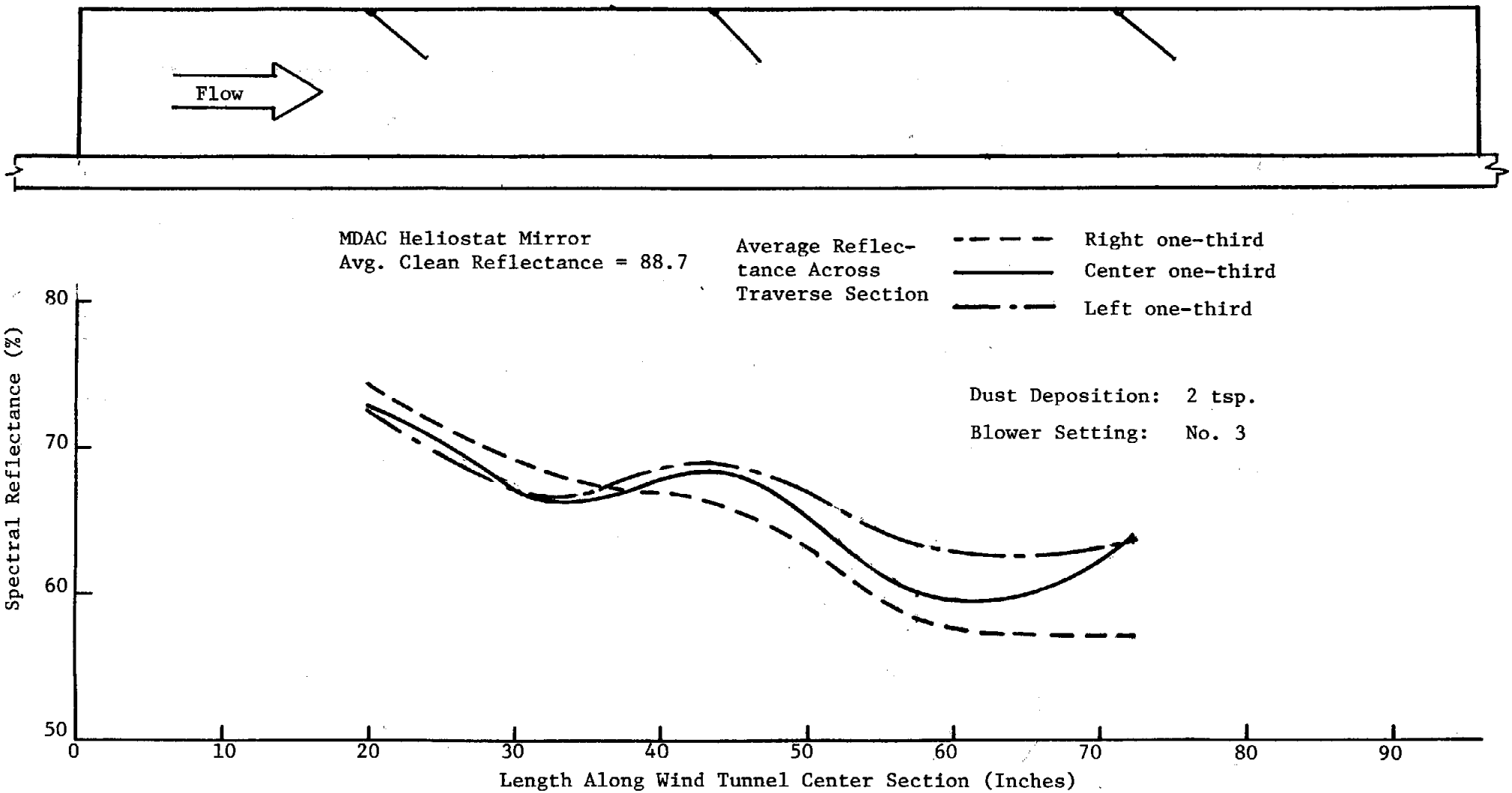

Figure 4-2. Dust Accumulation in Wind Tunnel - Longitudinal Distribution

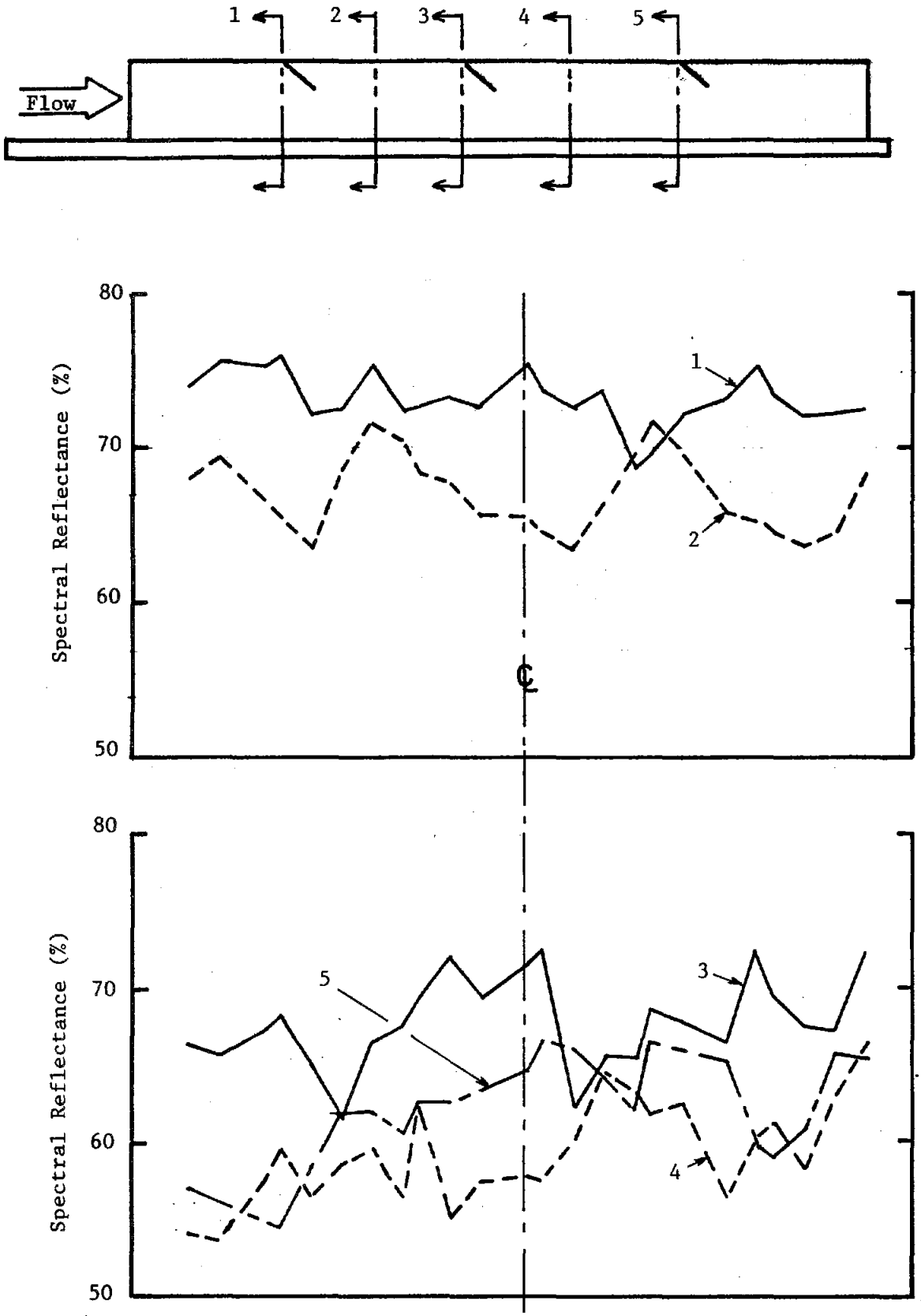

Figure 4-3. Dust Accumulation in Wind Tunnel
Transverse Distributions

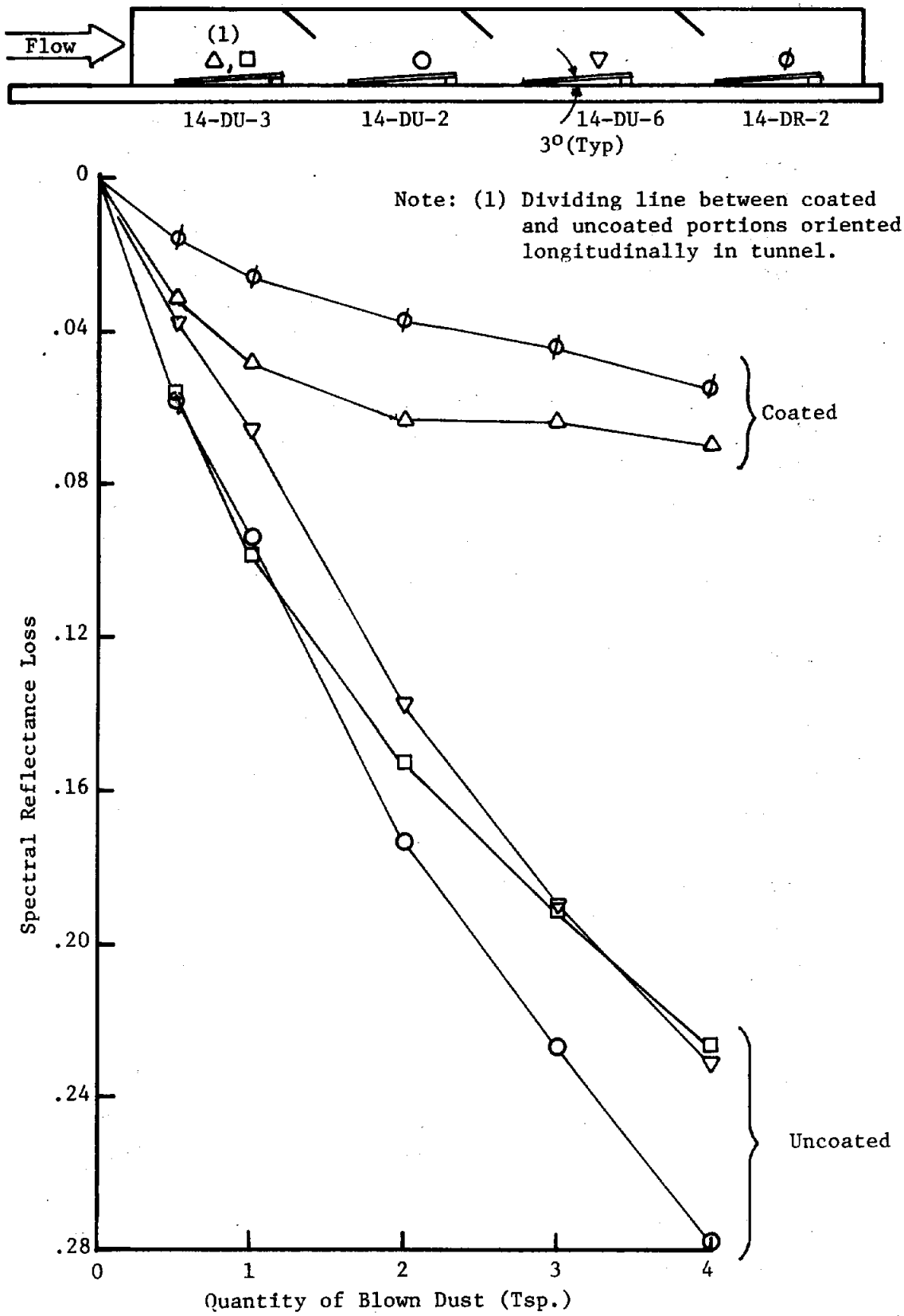

Figure 4-4. Dust Accumulation on 14" x 14" Mirror Samples in S & A Wind Tunnel

4.2 Natural Dust Accumulation

Natural dust accumulation in Sacramento, California was measured over a seven day period, using two 14" x 14" mirror samples on the roof of the S & A office building. One mirror was coated with REPCON polymer coating and the other was uncoated. Both mirrors were inclined 55^{o} from the horizontal and faced south. Reflectance loss was measured daily using the S & A reflectometer. Figure 4-5 presents the results of this study, including humidity and average wind velocity conditions. There was no precipitation in Sacramento during the week of testing (6/25/79 to 7/2/79). As was found in the wind tunnel testing, the coated mirror was noticeably more resistant to dust adhesion, although this didn't show up until after the first two days. Reflectance losses for the week were .056 and .073 reflectance units for the coated and uncoated specimens, respectively. The reflectance loss curves follow the trend of Sandia-Albuquerque test data (Ref. 22) as illustrated in Figure 4-5.

Total natural dust accumulation at three different locations were also measured after one month exposure to the natural environment. Six 7" x 7" mirror samples were distributed as shown in Table 4-1. Photographs of the dirty mirrors are given in Figure 4-6 and reflectance losses are shown in Table 4-1. The Pioneer, CA tests were affected by pine tree pollen and rain spots; no rain occurred at the other location.

The differences between coated and uncoated mirror reflectances was not as pronounced percentagewise after one month exposure as it was for the one week tests. Furthermore, neither of the natural dust buildup tests showed the pronounced effects of the polymer coating exhibited in the wind tunnel tests. Apparently the dust adhesion properties of the

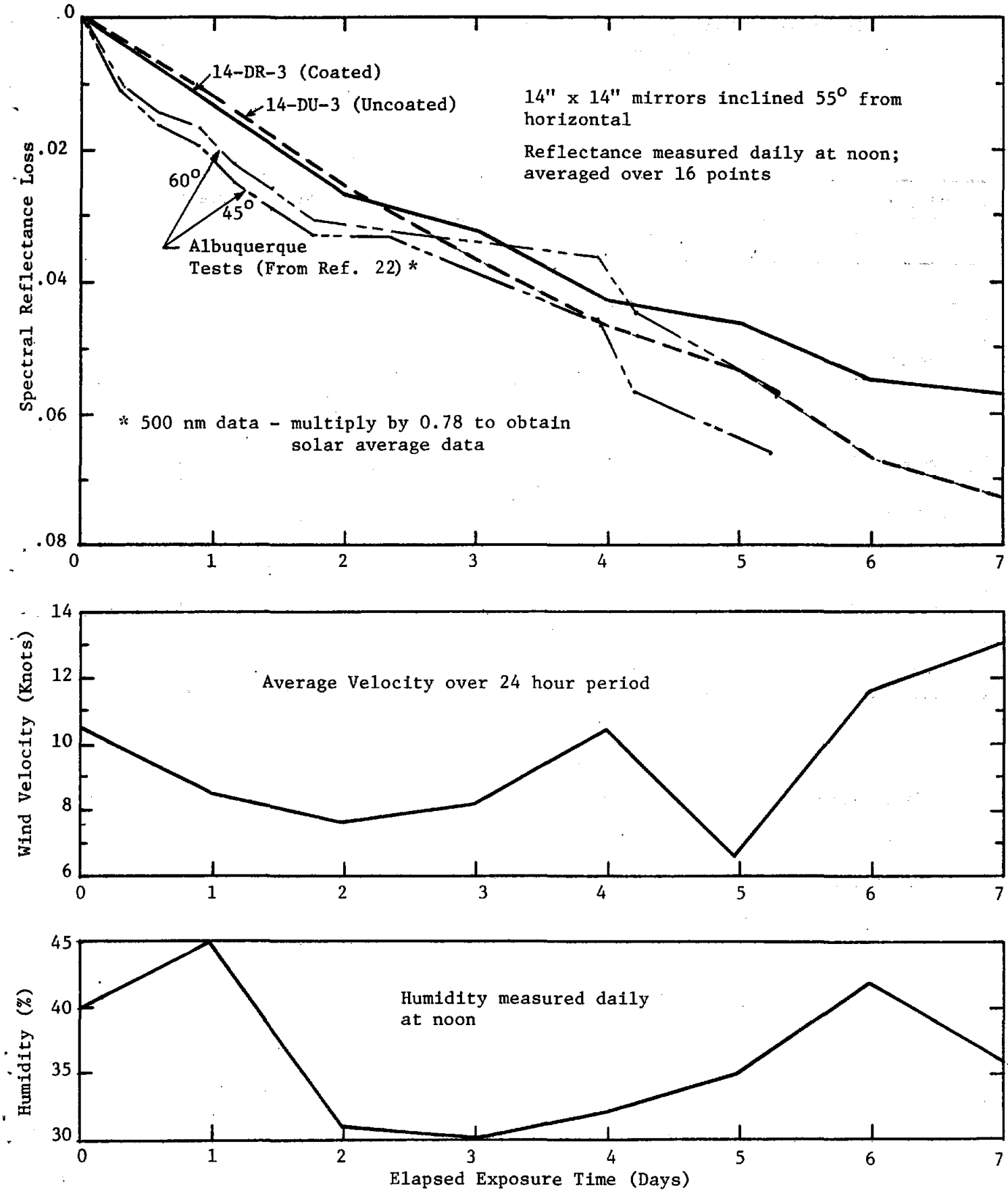

Figure 4-5. Dust Accumulation and Natural Environment in Sacramento, California for the 7-day Period 6/25/79 to 7/2/79 (no precipitation)

Table 4-1. Natural Dust Accumulation of 7" x 7" Mirror Samples After One Month Exposure at 3 Different Locations

Mirror I.D.	Coating	Location	Elevation	Reflectance Loss
7-SCU-1	Uncoated	Sacramento, CA	Sea Level	.29
7-SCR-1	REPCON	Sacramento, CA	Sea Level	.26
7-BCU-1	Uncoated	Bass Lake, CA	1200 Ft.	.19
7-BCR-1	REPCON	Bass Lake, CA	1200 Ft.	.17
7-PCU-1	Uncoated	Pioneer, CA	4200 Ft.	.26
7-PCR-1	REPCON	Pioneer, CA	4200 Ft.	.25

Time period for exposure was 1 month, 5/25/79 to 6/25/79

Mirrors inclined 45° from horizontal facing South

Initial clean reflectance = .77 for all samples

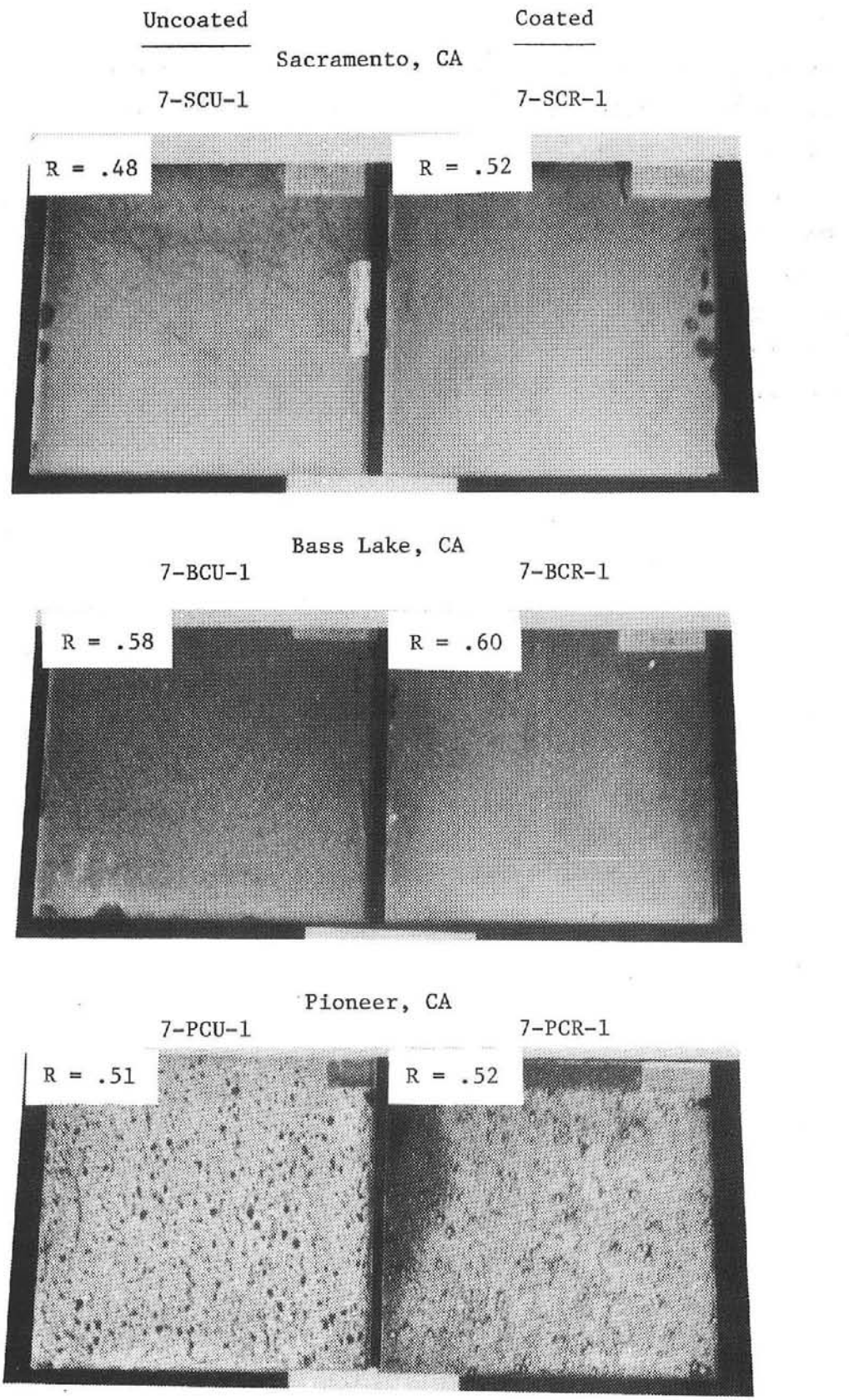

Clean Reflectance = .77 for all samples

Figure 4-6. Natural Dust Accumulation Samples After One Month Exposure

coated surface are significantly influenced by exposure time in a natural environment and further tests are required to evaluate such effects.

For uncoated mirror samples, dust accumulation in the wind tunnel is comparable to natural dust buildup, as illustrated in Figure 4-7. A 4 minute run with 1 teaspoon of dust in the wind tunnel is roughly equivalent to a week of natural exposure in the Sacramento area.

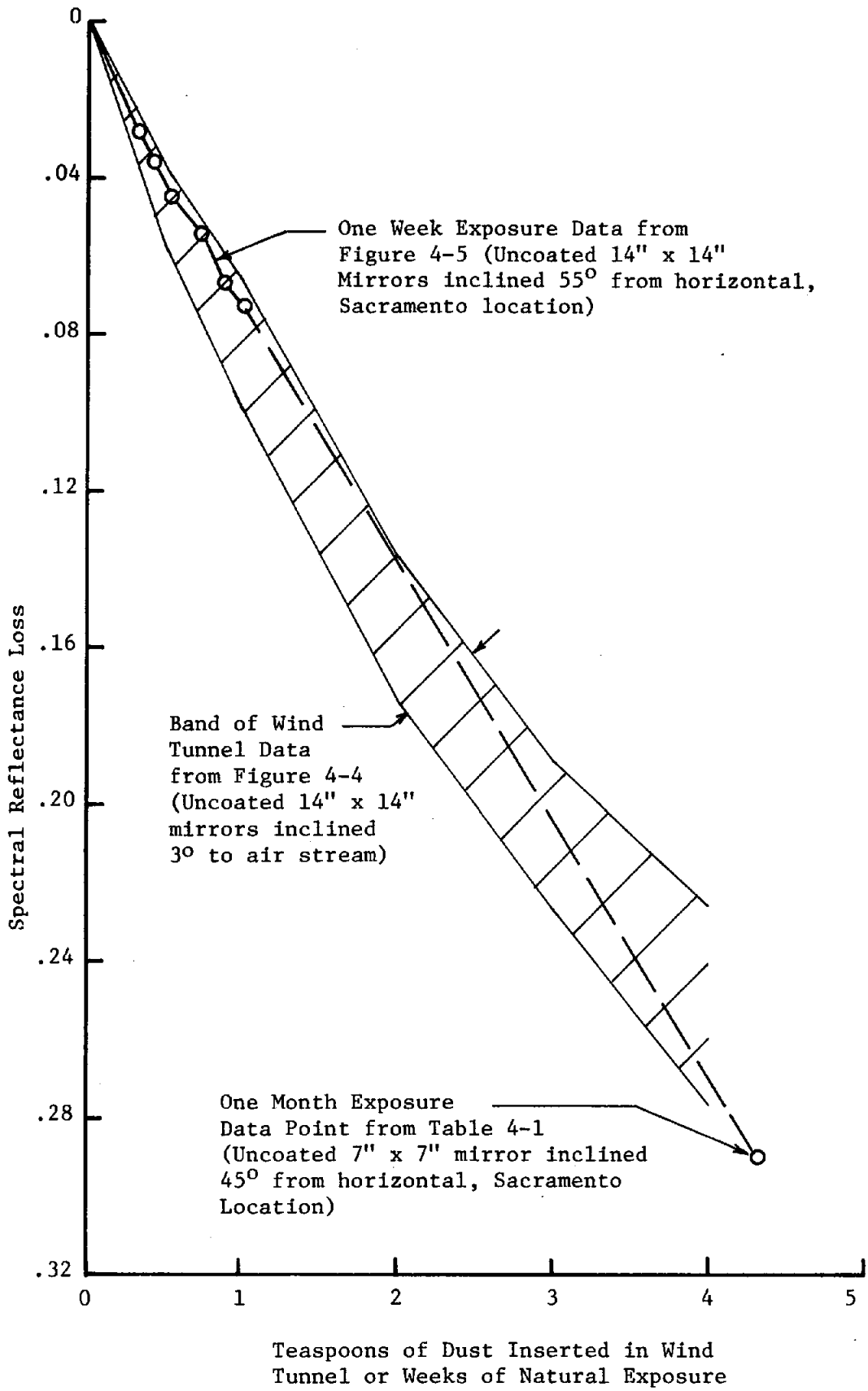

Figure 4-7. Comparison of Natural and Wind Tunnel Dust Accumulation

5.0 CLEANING TEST PROGRAM

The cleaning test program addresses two basic categories of cleaning head design both of which are based on high velocity air flow cleaning mechanisms involving erosion and denudation of the dust coating on the mirror surface. The first category includes air flow alone and air flow enhanced with water particle injection. This category, called Concept 1, involves the testing of a variety of air nozzles both with and without the aid of water particle injection. Further details and experimental results of Concept No. 1 studies are presented in Section 5.1.

Concept No. 2, the second category, involves the weakening or breakage of the dust-to-mirror surface bonds with high intensity air propagated ultrasound. The dust particles, which now are subjected to reduced adhesive forces, are then blown from the mirror surface with high velocity air and collected in a filter. This concept is presented in detail in Section 5.2.

During the experimental work for each of these concepts cleaning effectiveness was investigated with consideration given to two primary affectors of dust adhesion; (1) clean mirror precoating with a commonly available silicone polymer (REPCON, Reference 21) and (2) the age of the dust coating as subjected to the outdoors environment (including sunlight, wind, humidity, temperature, etc.)

Since adhesion may be significantly influenced by exposure duration, the dust accumulated by the wind tunnel deposition method, as described in Section 3.2, may not have the same resistance to cleaning as the same amount of dust naturally deposited over a period of several weeks. Aged cleaning test specimens were therefore prepared for cleaning program use by first depositing dust on them in the wind tunnel

and then setting them outside for a period of one month. Six 7" x 7" mirrors were prepared in this manner and were distributed as shown in Table 5-1. Each pair of specimens was inside a ventilated box with a plastic film window on top so that it was exposed to ambient conditions of temperature, humidity and sunlight while being protected from further dust accumulation and rain. Cleaning tests on these specimens as well as on the same day deposited specimens are described below in Sections 5.1 and 5.2 for Concepts 1 and 2, respectively.

5.1 Concept No. 1 - Air Nozzle Cleaning Heads

5.1.1 Basic Principles of Operation and Test Setup

In Section 1 various mechanisms of removing dust particles from a surface were introduced. These included the detachment of dust in an air flow using high velocity air or using high velocity air with a dense particulate in suspension. The first of these mechanisms, enhanced by a vortex scrubbing action, was the primary cleaning method to be initially investigated for the concept 1 design. Design and testing of this concept led to other air supplied cleaning head configurations which departed from the vortex shedding concept. These later concepts still maintain the high velocity air wash as the fundamental cleaning mechanism but consider enhancements such as additional acoustic energy input or dense particle mist injection into the air stream.

The results of this preliminary study involved, then, five basic cleaning head design variations. Each of these, along with their basic cleaning mechanism, are listed below.

1. Vortex Generator - high velocity air with vortex scrubbing enhancement
2. Converging Nozzle with Acoustic Cavities - high velocity air with additional acoustic energy input

Table 5-1. Distribution of Aging Samples

Mirror I.D.	Coating	Location	Elevation	Reflectance Loss After Wind Tunnel Dust Deposition And Aging*
7-SDU-1	Uncoated	Sacramento, CA	Sea Level	.18
7-SDR-1	Coated	Sacramento, CA	Sea Level	.21
7-BDU-1	Uncoated	Bass Lake, CA	1200 Feet	.27
7-BDR-1	Coated	Bass Lake, CA	1200 Feet	.27
7-PDU-1	Uncoated	Pioneer, CA	4200 Feet	.13
7-PDR-1	Coated	Pioneer, CA	4200 Feet	.33

* Various levels of dust deposition were used in the wind tunnel
Time period for aging was 1 month, 5/25/79 to 6/25/79

3. Converging Nozzle with water particle injection - high velocity air with dense particle injection
4. High Pressure Jet Sweep - high velocity air
5. High Pressure Nozzle - high velocity air

Each of these head configurations, along with a presentation of tests performed, are further discussed in Sections 5.1.2 through 5.1.6.

The overall test setup used for all Concept 1 cleaning tests is schematically shown in Figure 5-1. Not shown in this figure is variable height indexing mount used for accurately positioning the cleaning head above the mirror. The major components of the test system are the air supply system, the cleaning head and shroud, and the vacuum system with electronic filtration.

In general, the air supply system can be designed as a high volume air supply with output at constant pressure or a fixed volume supply with pressure reduction as air flow is maintained.

Because of the short length of time expected to be required to clean a substantial test portion of the mirror, a blow-down from a static supply, controlled by solenoid valve, has been selected as the test operating mode. A ½ hp oil-less compressor is used to pressurize two portable air storage tanks having a combined volume of 2¼ $ft.^3$ and a maximum working pressure of 150 psig. A 3/8 inch solenoid valve with 300 psi maximum operating pressure and 226 SCFM maximum air flow is installed at the tank outlet. Eight feet of flexible hose with end fittings between the valve and Cleaning Head complete this portion of the Cleaning System.

The basic test head assembly is illustrated in Figure 5-2. The vortex nozzle is shown installed, however, any of the cleaning head configurations may be used.

Figure 5-1. Schematic of Test Setup for Cleaning Concept No. 1

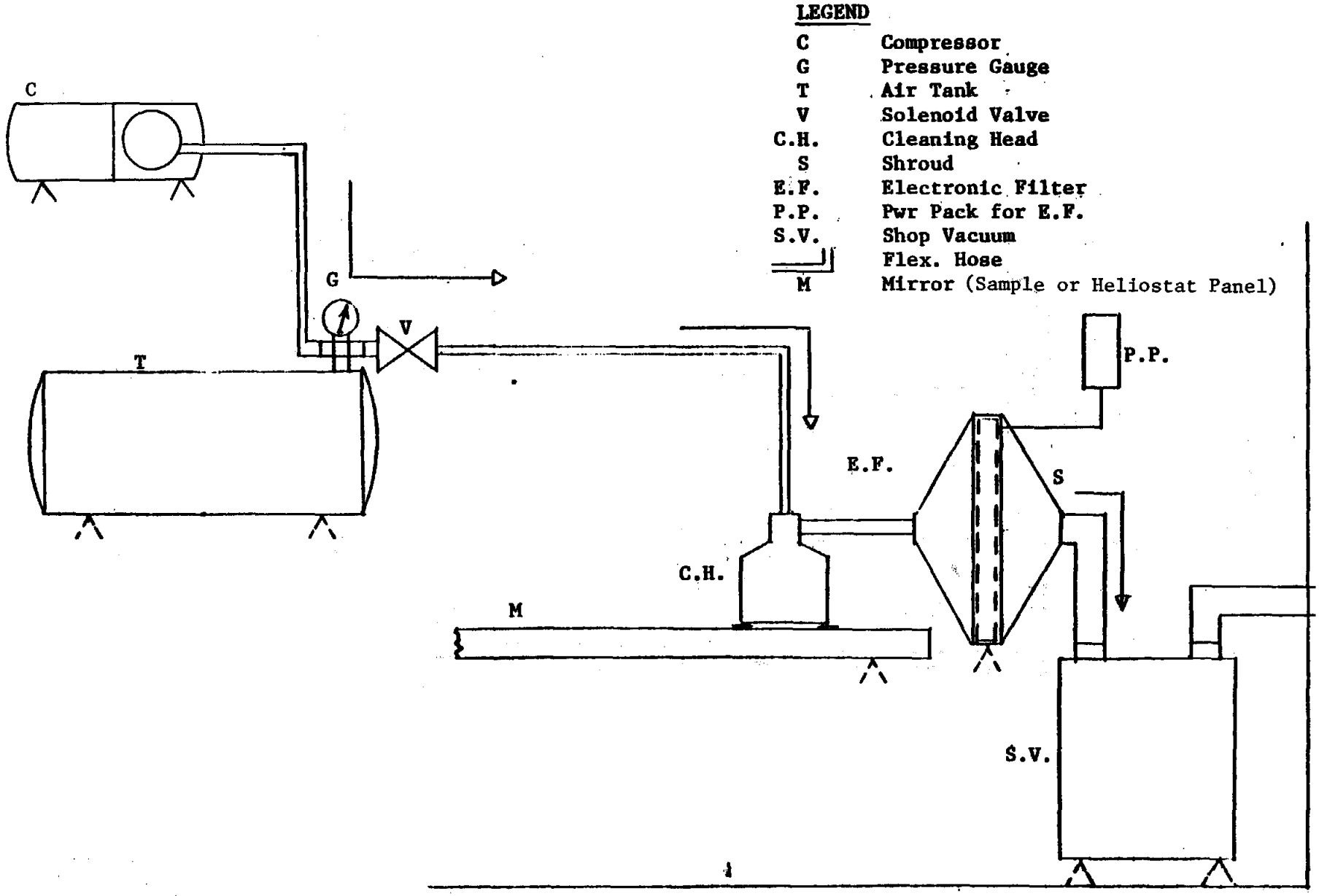

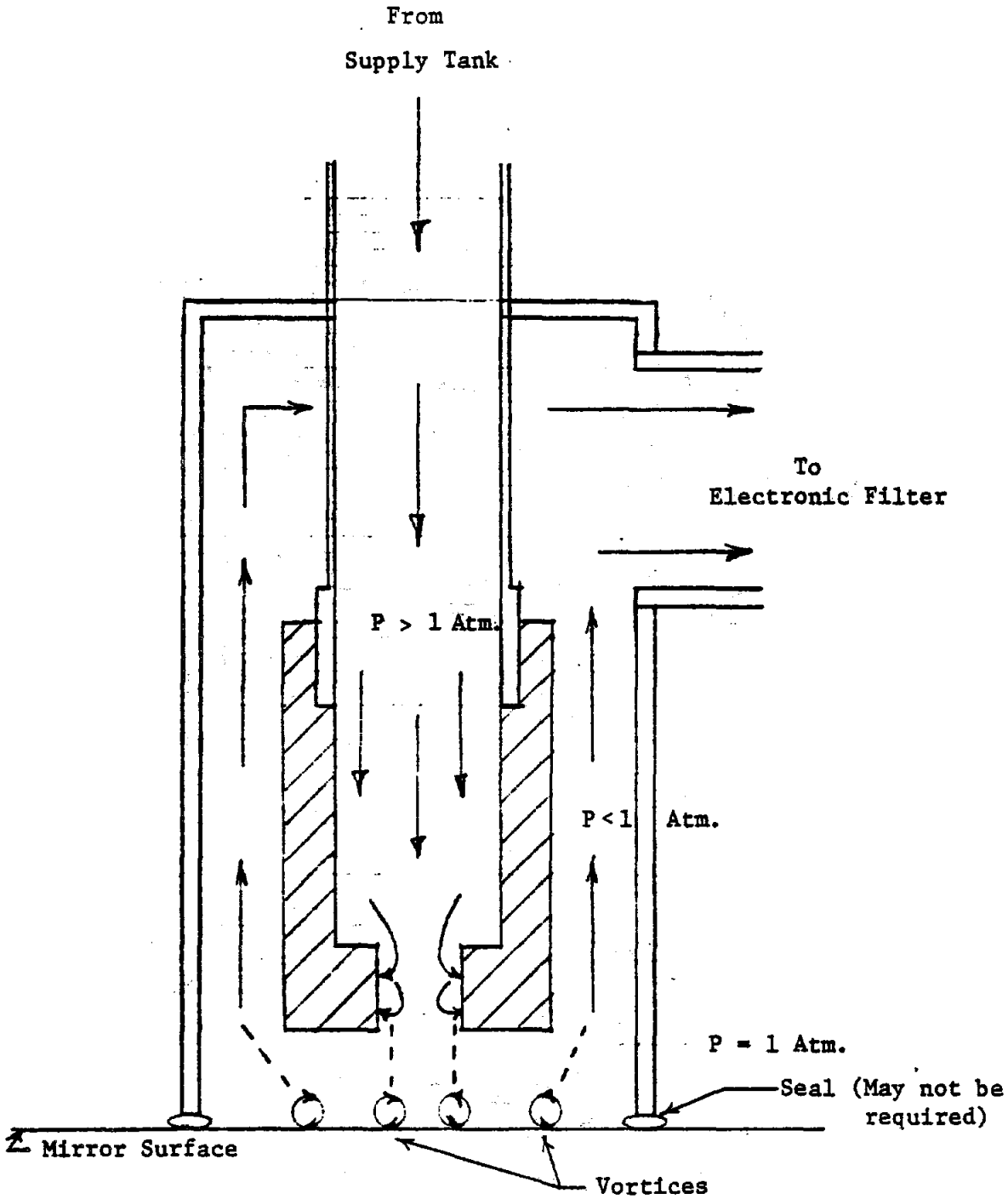

Figure 5-2. Schematic of Cleaning Head Test System

After the airflow passes through the cleaning head, the dust laden air is ready for cleaning and disposal. This is accomplished by providing a suction system containing an electronic filter. The vacuum unit itself is a shop type which delivers 104 CFM, 50" vacuum at 2½" tank orifice. The electronic air cleaner is an electrostatic filter designed to replace the conventional throw-away type used in heating and cooling systems. It is advertised to remove 75% of all airborne particles from 0.5 to 100 microns in size. A shroud including entry and exit transitions which connect to Cleaning Head and vacuum hoses, respectively, adapts the cleaner into the loop (open-ended since vacuum exhausts to atmosphere).

5.1.2 Vortex Generator Concept

The vortex generator head concept involves passing pressurized air through a circular, sharp edged, orifice thereby creating a high pressure air jet made up of rotating vortices. These vortices then pass along the mirror surface with a rotating scrubber effect which imparts a driving force to dislodge the dust particles adhering to the surface. The dislodged dust particles are then carried off by a vacuum hood over the head and removed from the cleaned area.

Figure 5-3 shows a typical orifice and illustrates vortex formation.

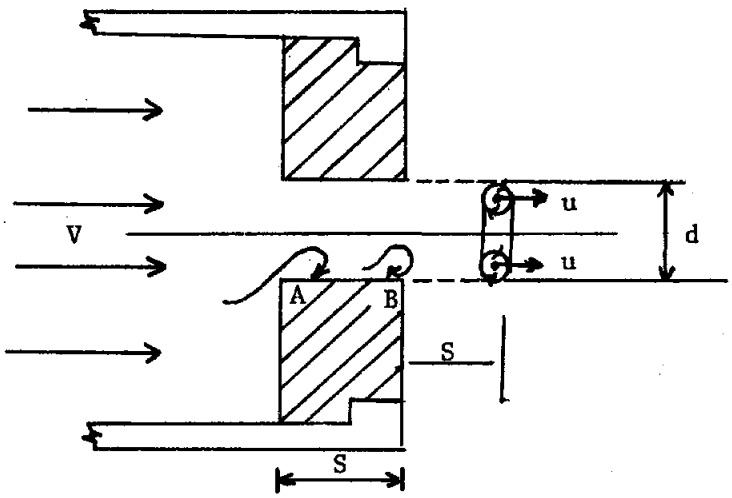

Figure 5-3. Vortex Formation at An Orifice

Vortex formation begins (Reference 23) when the air stream passes by the sharp edge at A. At this point, the air separates from the wall interface and rolls into a closed loop or vortex as point B is reached. The cross-section of the toroidal ring formed will have an outside diameter of approximately s/π with the distance between successive vortex rings approximately given by the orifice thickness, s. The shedding of each vortex at B causes a small pressure pulse which travels back at the speed of sound and provides feedback to aid in forming a new vortex between A and B.

With the translational velocity of the shedding vortices given as u, the generated sound frequency is simply,

$$f = u/s$$

The translational velocity, u, is proportional to the supply air velocity, V. Reference 23 states that the total fluid momentum entering the orifice converts to rotational and translational motion of approximately equal magnitudes such that $u \simeq 0.5\ V$. The combination of rotational and translational velocities provide a scrubbing action on the dust particles adhering to the mirror surface.

Figure 5-4 presents a cross-section of the test head orifice assembly. For the primary test head, d = .254 cm (.1 in), ℓ = .635 cm (.25 in.) and h varies.

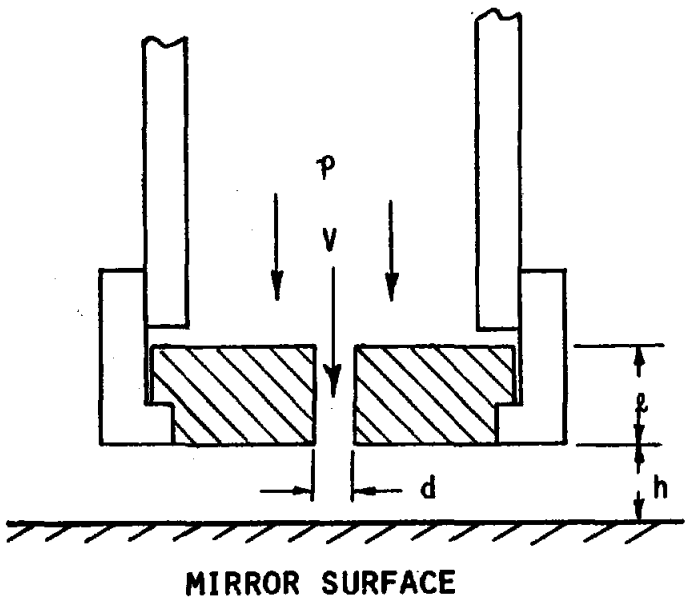

Figure 5-4. Vortex Nozzle Cross-Section

For the range of supply pressures used in testing (50 to 100 psi) the velocity at the nozzle exit is sonic at approximately 350 m/sec. This exit velocity is relatively non-varying with supply pressure, however, the flow rate through the vortex nozzle does increase with increasing supply pressure. The relationship between air flow rate and supply pressure for the vortex nozzle is presented in Figure 5-5. The supply pressure, for a supply tank volume of approximately 60 liters (0.0595 m^3 or 2.1 $ft.^3$), as a function of blowdown time using the vortex nozzle is shown in Figure 5-6. These plots are based upon empirical data taken with h = ∞

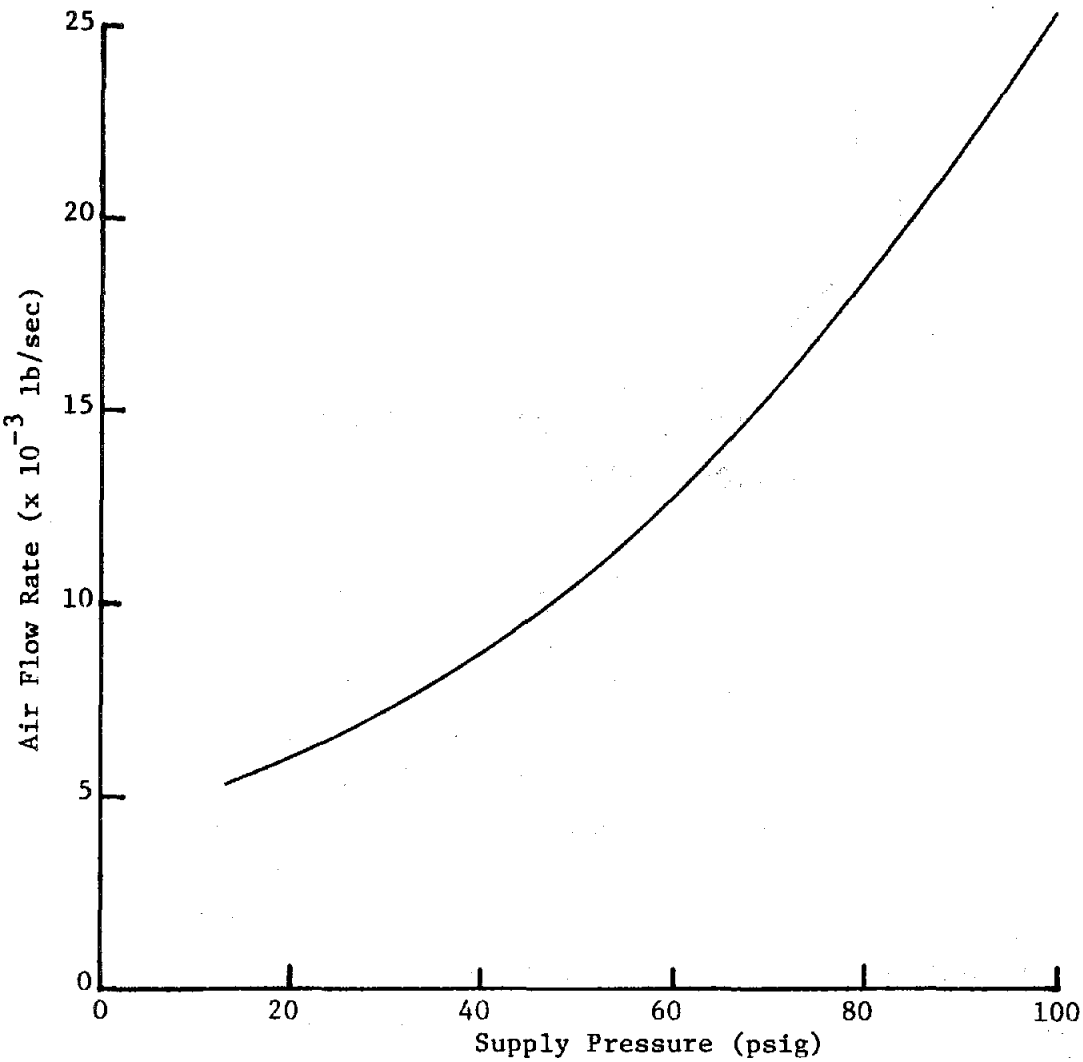

Figure 5-5. Air Flow Rate vs. Supply Pressure for the Vortex Nozzle Configuration (Based on Supply Pressure/Time Test Data)

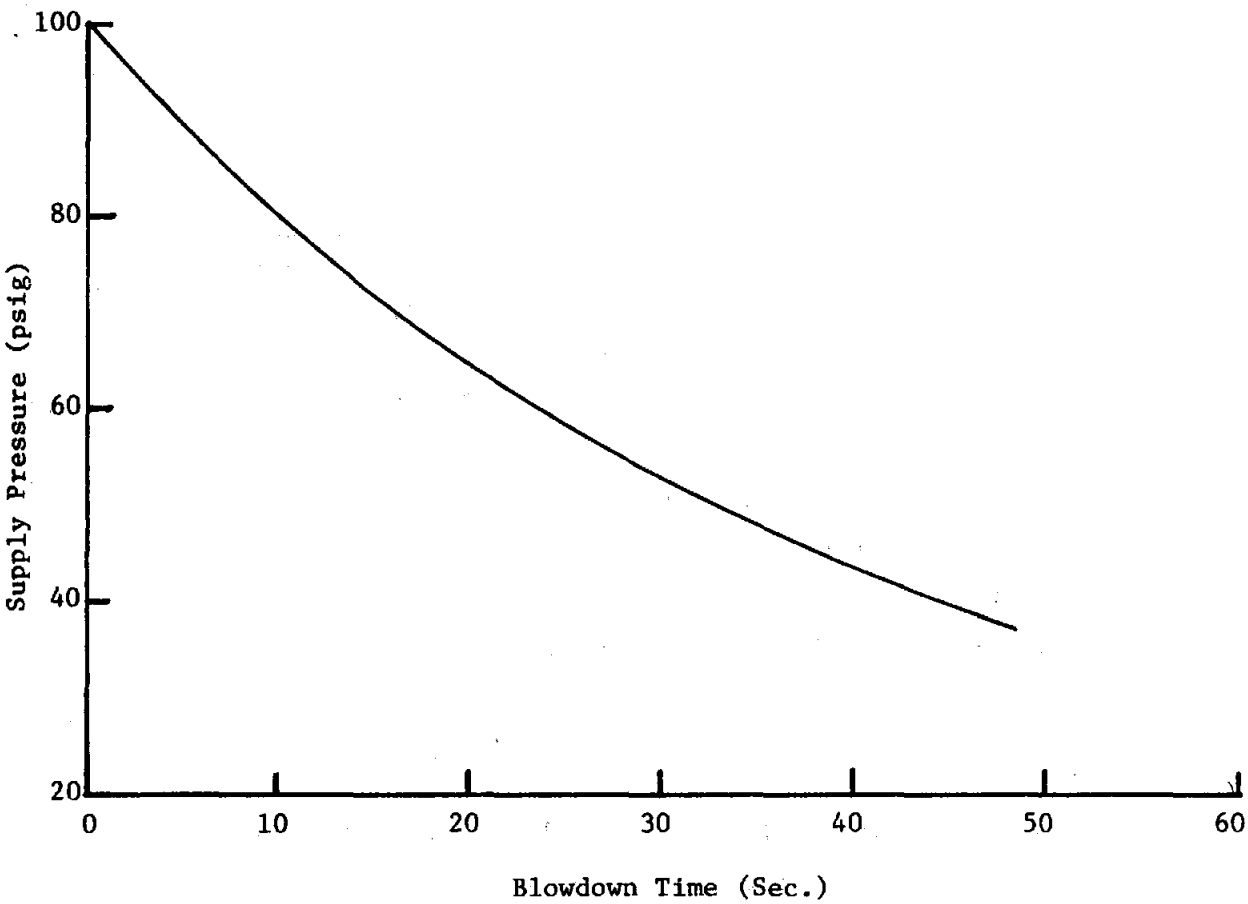

Figure 5-6. Supply Pressure vs. Tank Blowdown Time for the Vortex Nozzle Configuration, Tank Volume = 60 liters

For a velocity, V, of 350 m/sec, the expected sound frequency would be approximately given by:

$$f = \frac{350 \text{ m/sec}}{2(.00635)\text{m}} = 27{,}560 \text{ hz}$$

Sound measurement test data taken produced the following results.

Pressure (psig)	Sound Level (db)	Frequency (Hz)
100	104	27,800
90	104	27,340
80	103	27,700
70	103	28,860
	$\bar{f}$ =	27,925

These data were taken using a Brüel and Kjaer Type 2209 Impulse Precision Sound Level Meter with a B & K Type 4133 ½ inch microphone. Using this meter/mike combination, the measurement ranges on sound pressure level and frequency are 36 to 150 dB and <10 to 40,000 Hz., respectively. The mike was positioned perpendicular to the air jet at nozzle exit level and 33 cm away from the nozzle centerline. The AC output from the sound level meter was used to drive a Heathkit IM-4110 frequency counter.

Cleaning tests performed using the vortex nozzle include variations of height off mirror, surface velocity (movement of the cleaning head across the mirror surface) and the mirror parameters of aging and coating treatments. All tests were performed with an initial supply pressure of 100 psig. The vacuum shroud was not used for these initial tests.

Figure 5-7 illustrates the effect of varying the nozzle height off the mirror surface. From these few tests performed it can be seen that the reflectance loss recovery and cleaned width do not vary significantly with nozzle height for the heights tested. It was

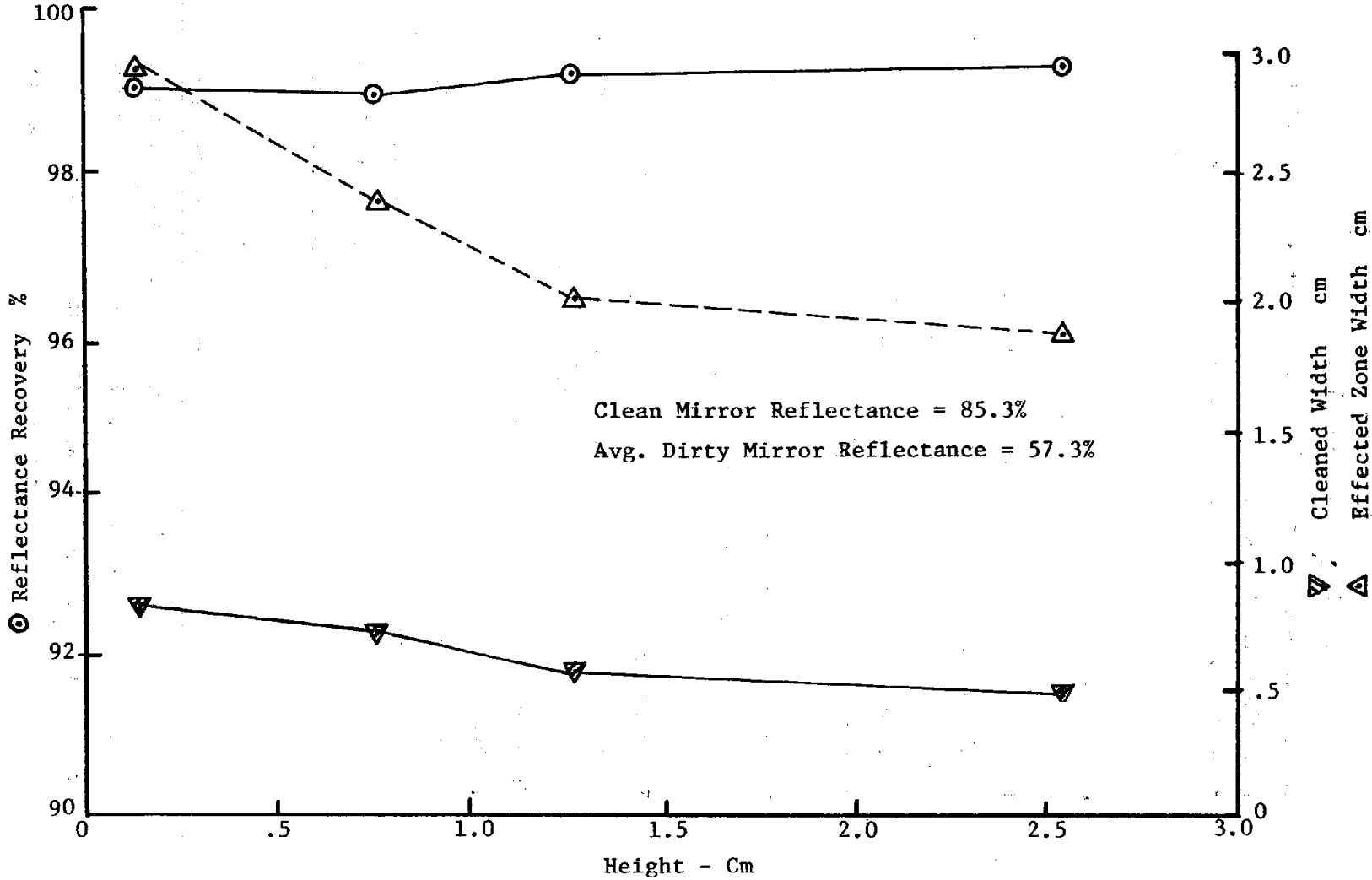

Figure 5-7. Vortex Nozzle Reflectance Recovery and Cleaned Width vs. Nozzle Height Off Mirror V = 2.85 cm/sec, Unaged Mirror

found that for nozzle heights greater than 5 to 6 cm the vortex nozzle lost much of its effectiveness. The clean path width is quite small and may preclude efficient use of this nozzle in a full scale system. The effected zone width is that width of mirror area showing some change in the dusty surface due to the passage of the air nozzle. Although quite a bit wider than the "clean path width" it is expected that this area would not be adequately cleaned on aged samples.

The effect of cleaning head velocity relative and parallel to the mirror surface is shown in Figure 5-8. Again, for the unaged mirror specimen, reflectance recovery and clean width are not largely affected over the range of velocities tested.

Typical cleaning profiles of the clean path and surrounding mirror area are presented in Figure 5-9.

Tests on aged mirror specimens were also performed. The 4 and 8 day samples were aged on a rooftop in Sacramento. The mirrors were deposited in the lab wind tunnel at Schumacher and Associates and placed on the facility rooftop under a protective box with a clear Saran wrap top to allow solar radiation to reach the mirror surface. Sufficient air holes were present to allow environmental air exchange. The 30 day specimens were aged in similar fashion at Bass Lake, California (1200 ft. elevation). See Table 5-1.

The vortex nozzle tests on the aged specimens revealed a much poorer cleaning ability. In fact, in most cases a dirty streak was left down the middle of the cleaning path of a width equal to what the expected cleaned path would be. Reflectance profiles of these tests are shown

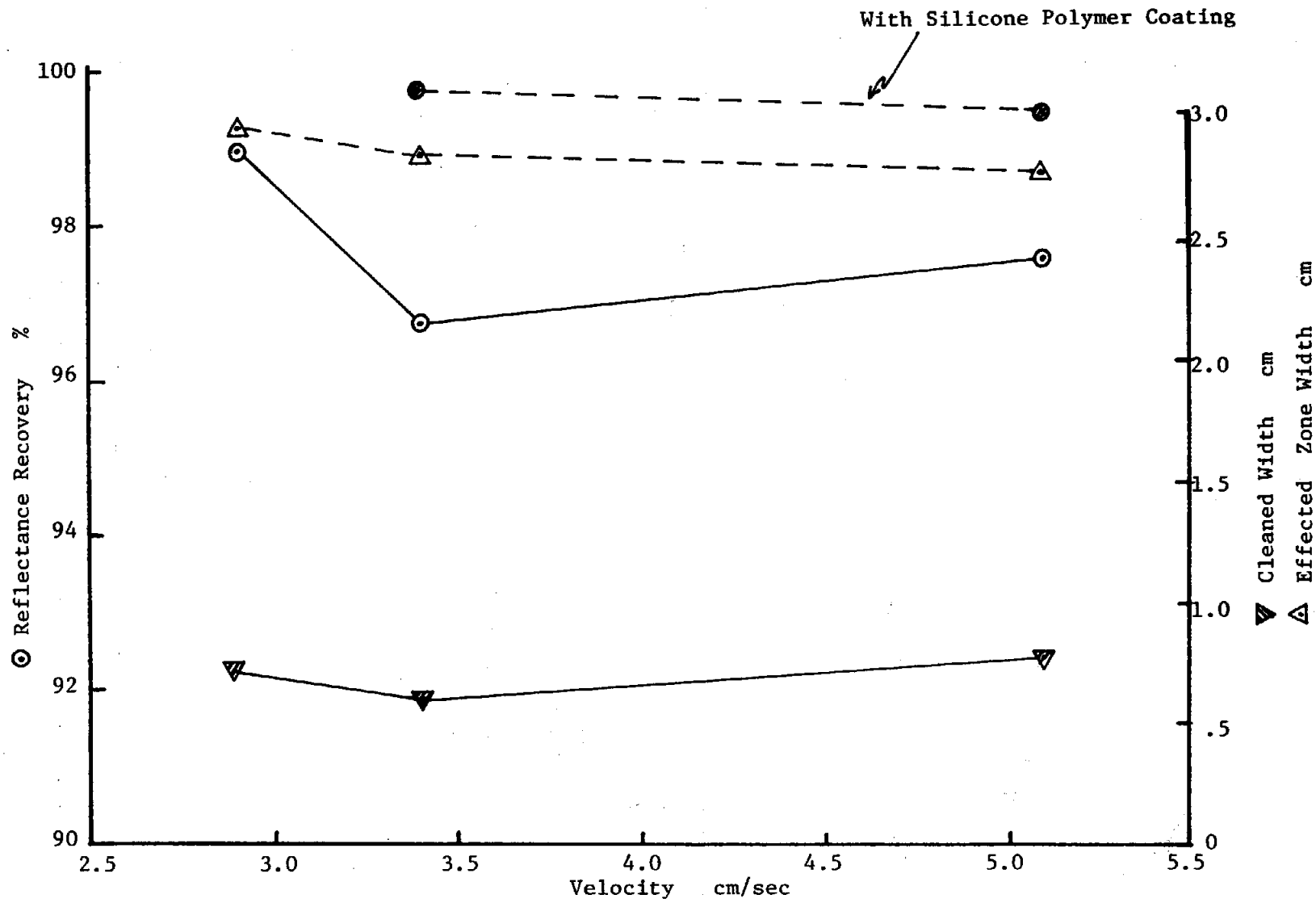

Figure 5-8. Vortex Nozzle, Reflectance Recovery and Cleaned Width vs. Cleaning Speed, h = .76 cm, Unaged Mirror

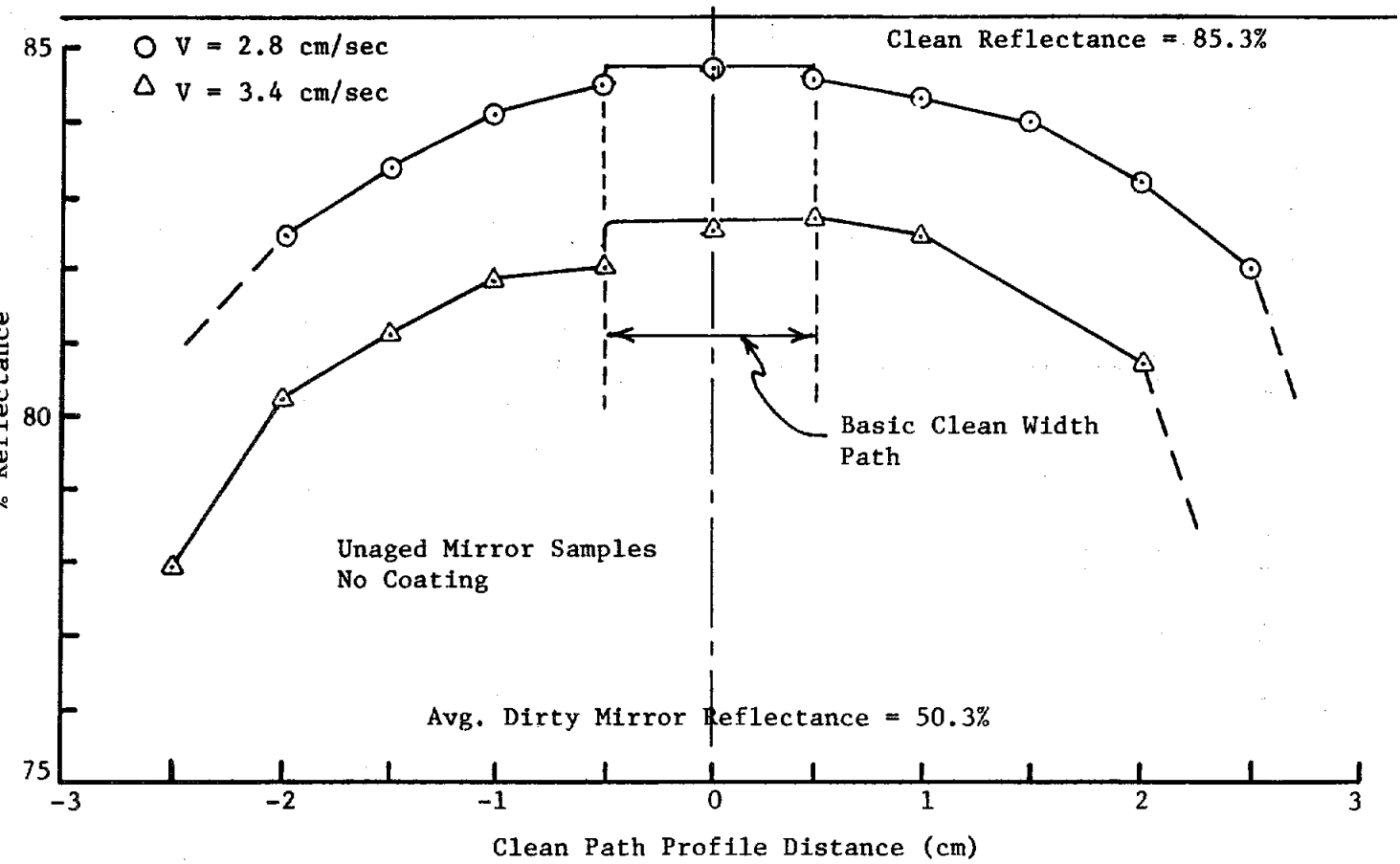

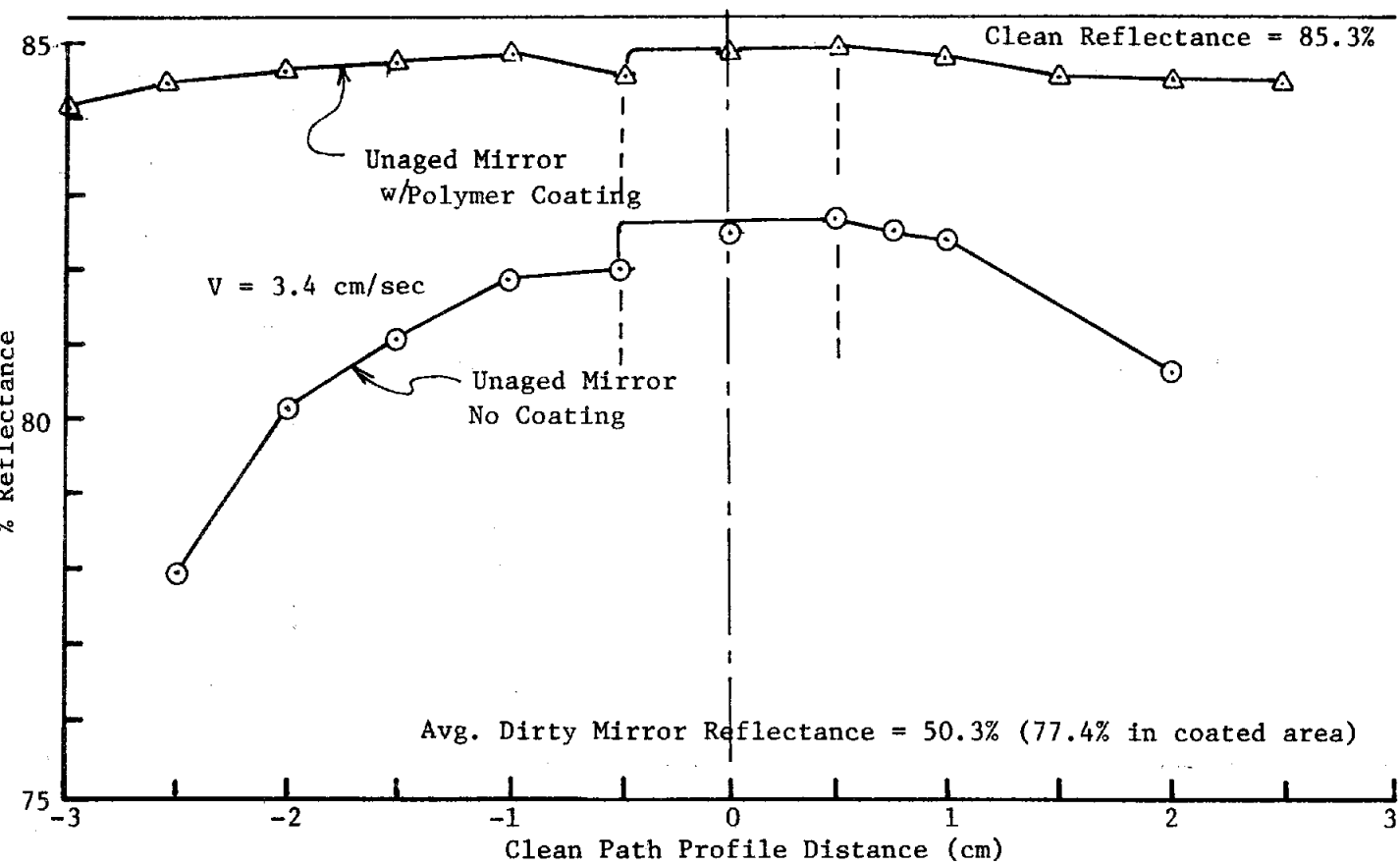

Figure 5-9. Vortex Nozzle Clean Path Reflectance Profiles, for Uncoated and Coated Mirror Samples, h = .76 cm, unaged Mirror Samples

in Figure 5-10. While Figure 5-11 illustrates the effect of mirror aging on cleanability and clean path width. To be noted again is the fact that the clean path width in this case is really the effected streaked path.

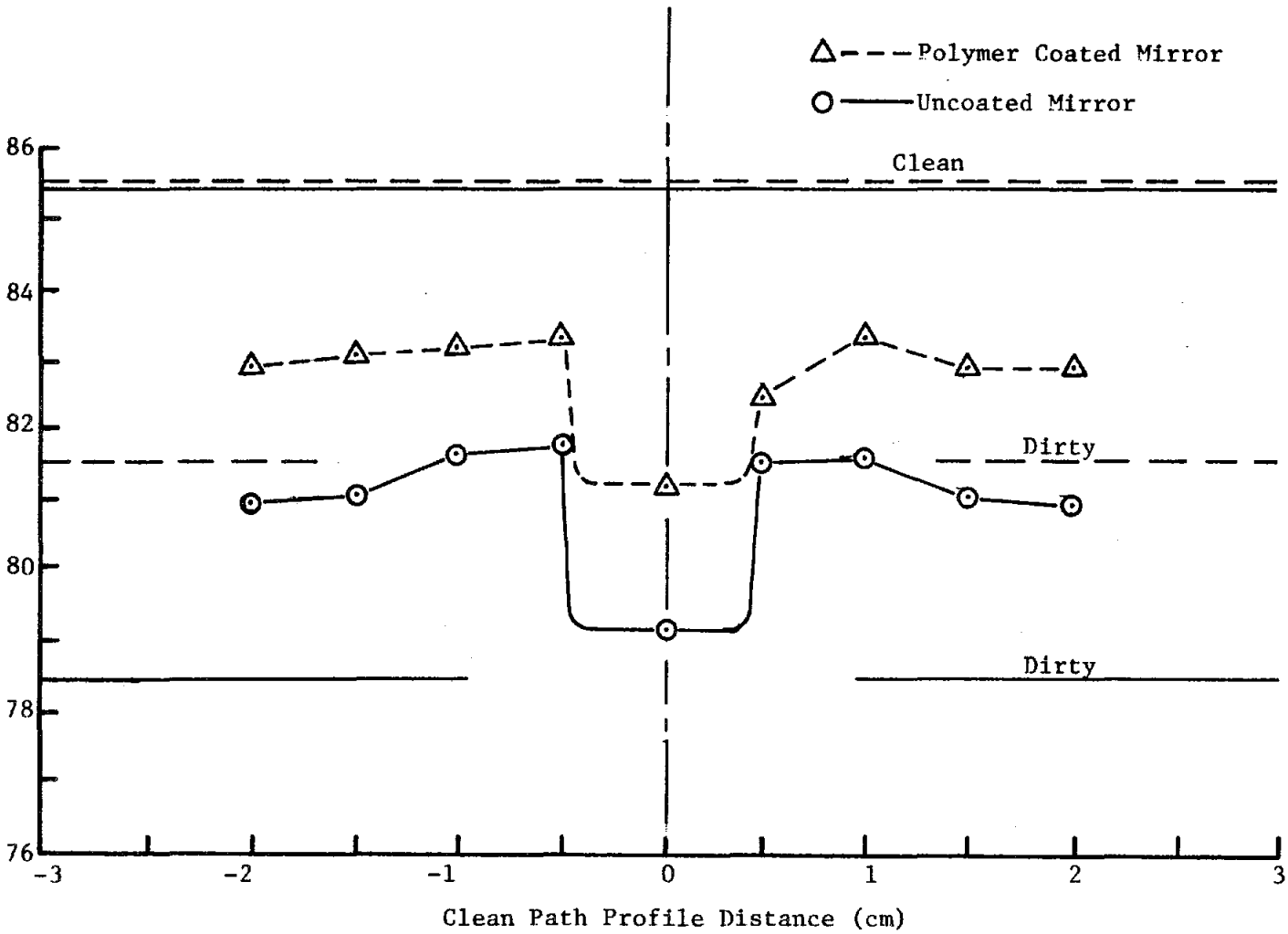

Figure 5-10. Vortex Air Nozzle, Cleaned Path Reflectance Profiles for Uncoated and Coated 8 Day Aged Mirror Samples, h = .76 cm, V = 3.56 cm/sec

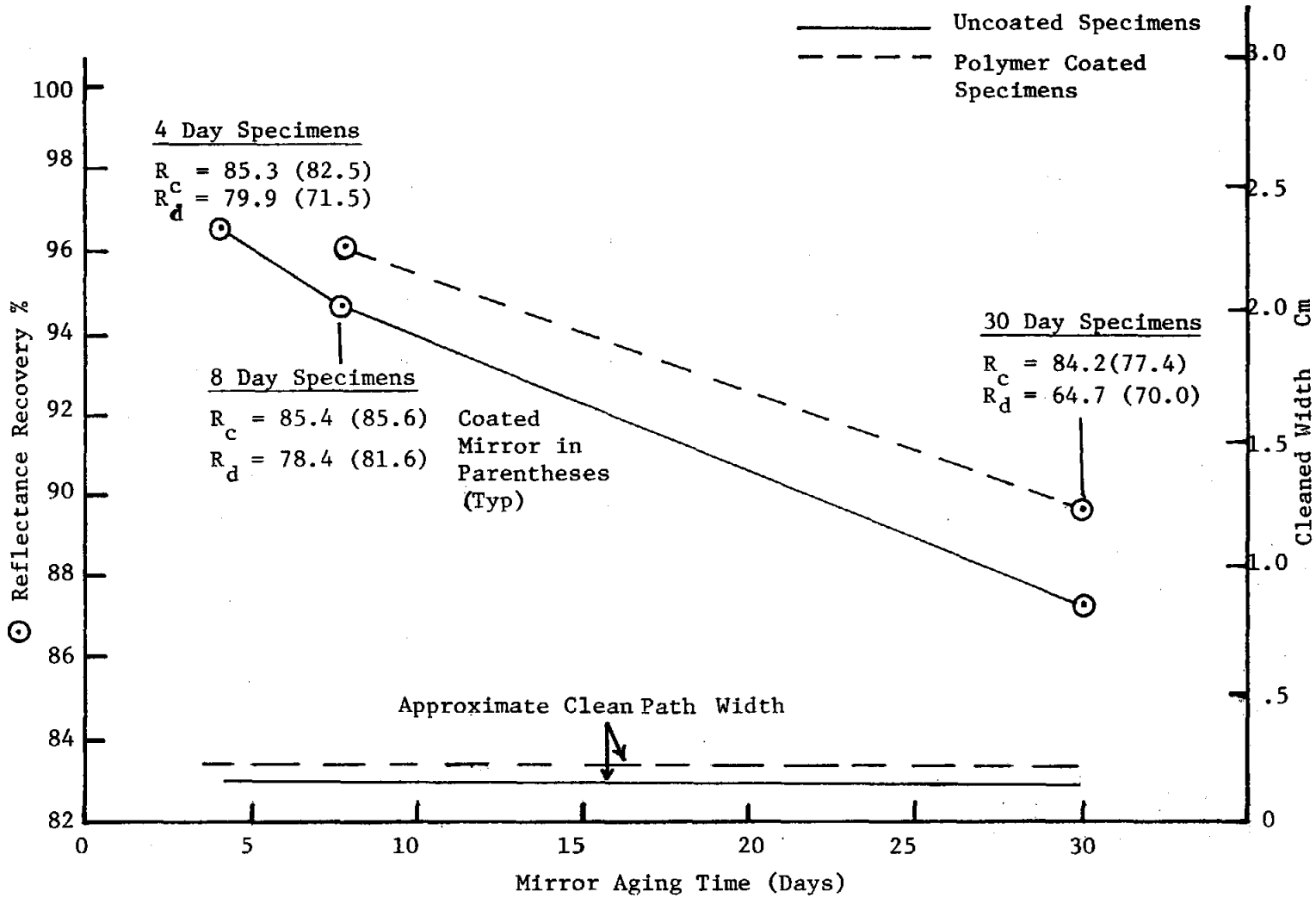

Figure 5-11. Vortex Air Nozzle, Reflectance and Cleaned Width vs. Mirror Aging Time, h = 0.76 cm, V = 3.6 cm/sec

To improve stabilization of the vortex formation a jet edge feedback system, such as described in Reference 23 and elsewhere, was tried. This consisted of a jet edge bar placed downstream from the orifice exit plane as shown in Figure 5-12 below. From sound level measurements taken on the unit fabricated, this does substantially increase the acoustic pressures generated. However, the required separation, s, caused the distance, h, to be so large that after the airflow was split by the jet edge the air jet energy was so dispersed as to preclude any effective amount of cleaning.

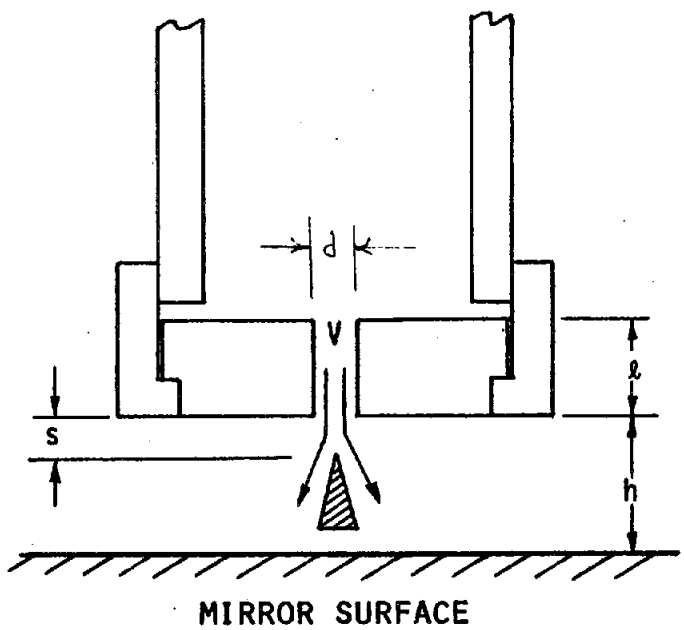

Figure 5-12. Vortex Nozzle with Jet edge Feedback

frequency, $f = \frac{naV}{s}$

where n = stage of operation
a = f(d,n)

5.1.3 Converging Nozzle with Acoustic Cavities

The reason for investigation of this concept was to try to aid the air washing technique with an additional energy in the form of local acoustic power. There are numerous well known devices for generating high acoustic pressures in air or liquid. In addition to sirens and whistles, a great many applications are found in industry such as liquid emulsification and homogenization.

The fluid dynamic device chosen is the Hartmann generator (References 23 and 24). Figure 5-13 illustrates the head configuration. Shown is an optional shroud to aid in focusing the acoustic energy towards the mirror surface. The optimum cavity diameter for maximum acoustic energy development is $d_2 = 1.3\ d$ (Reference 24). This nozzle size as well as two others ($d_2 = .5d$ and $1.0d$) were investigated at various separation distances, s. The optimum parameters were found by measurement of acoustic sound pressure for each variation of the parameters s, d_2, and 1. ($s = 1.5d$, $d_2 = 1.3d$), see Figure 5-14. Although substantial acoustic energy was developed in its optimum configuration (150 db 9 cm from the nozzle source) the energy was difficult to focus and concentrate on the mirror surface. Significant cleaning was not able to be demonstrated.

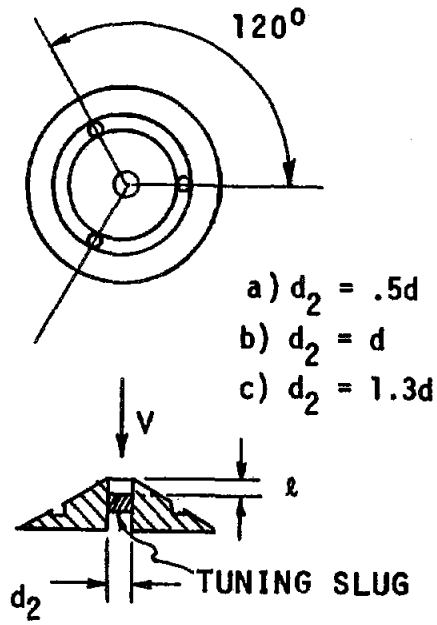

ACOUSTIC CAVITY

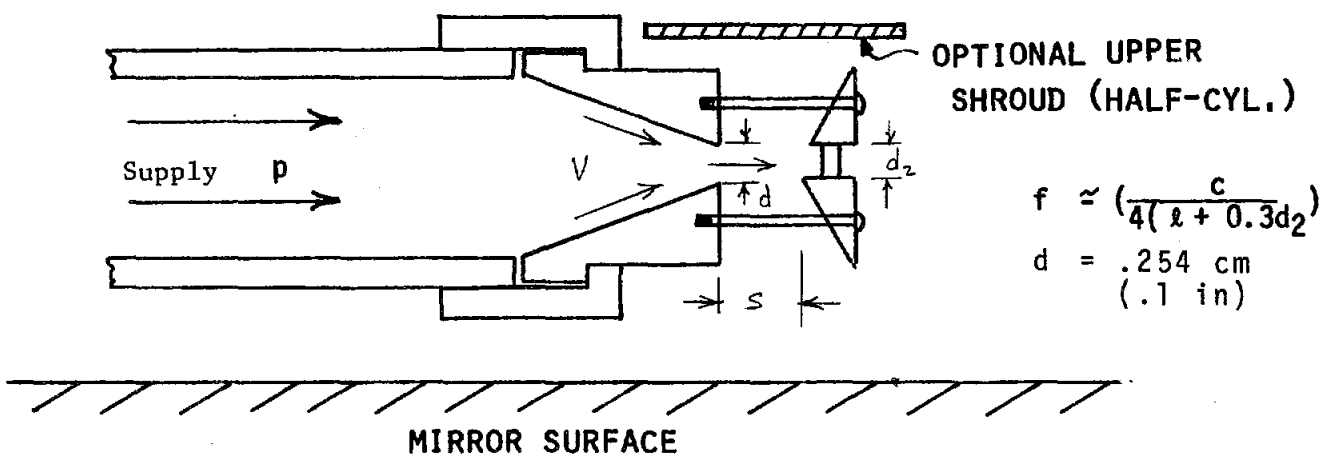

ASSEMBLY (SHOWN IN HORIZONTAL CONFIGURATION)

Figure 5-13. Converging Nozzle with Acoustic Cavity

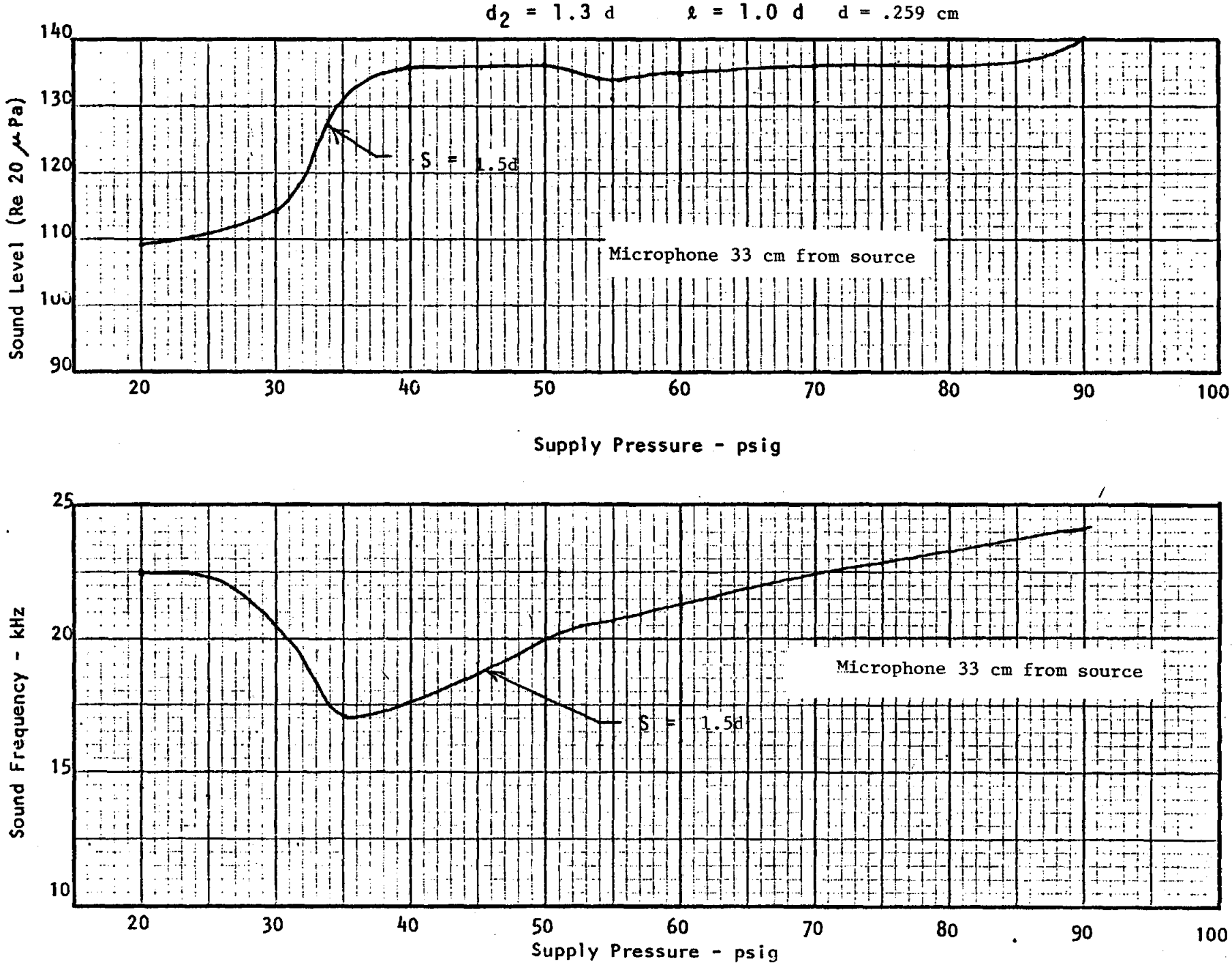

Figure 5-14. Converging Nozzle with Acoustic Cavity, Frequency - Sound Pressure Level vs. Supply Pressure

5.1.4 Converging Nozzle with Water Particle Mist Injection

This design variation proved to be the most effective of Concept 1 configurations for cleaning mirror surfaces. The high velocity air stream with injected water particles provided reasonably effective cleaning of unaged and aged mirror specimens.

Figure 5-15 illustrates the test head nozzle configuration.

Numerous tests were performed using this nozzle configuration. The basic parameters varied were the nozzle to mirror height, h, the water flow rate, Q, and the head traverse velocity, V, relative to and parallel to the mirror surface. As in all Concept 1 nozzle testing the supply air pressure was initially 100 psig and allowed to depress to a final value (usually greater than 70 psig) during the test.

As with the vortex nozzle the velocity at the exit of the converging nozzle is sonic (approximately 350 m/sec.) The relationship between air flow rate and supply pressure for the converging nozzle is presented in Figure 5-16. The supply tank pressure as a function of blowdown time using the convering nozzle is shown in Figure 5-17. These plots are based upon empirical data taken with $h = \infty$.

Figures 5-18, 5-19 and 5-20 show the effects of varying h, Q and V on the reflectance recovery and clean path width. These curves are all based upon unaged mirror samples. From these plots an optimum set of parameters were chosen for use in the aged mirror cleaning tests. These were: h = 10.2 cm (4 in.), Q = 2.14 ml/min., V = 7.11 cm/sec.

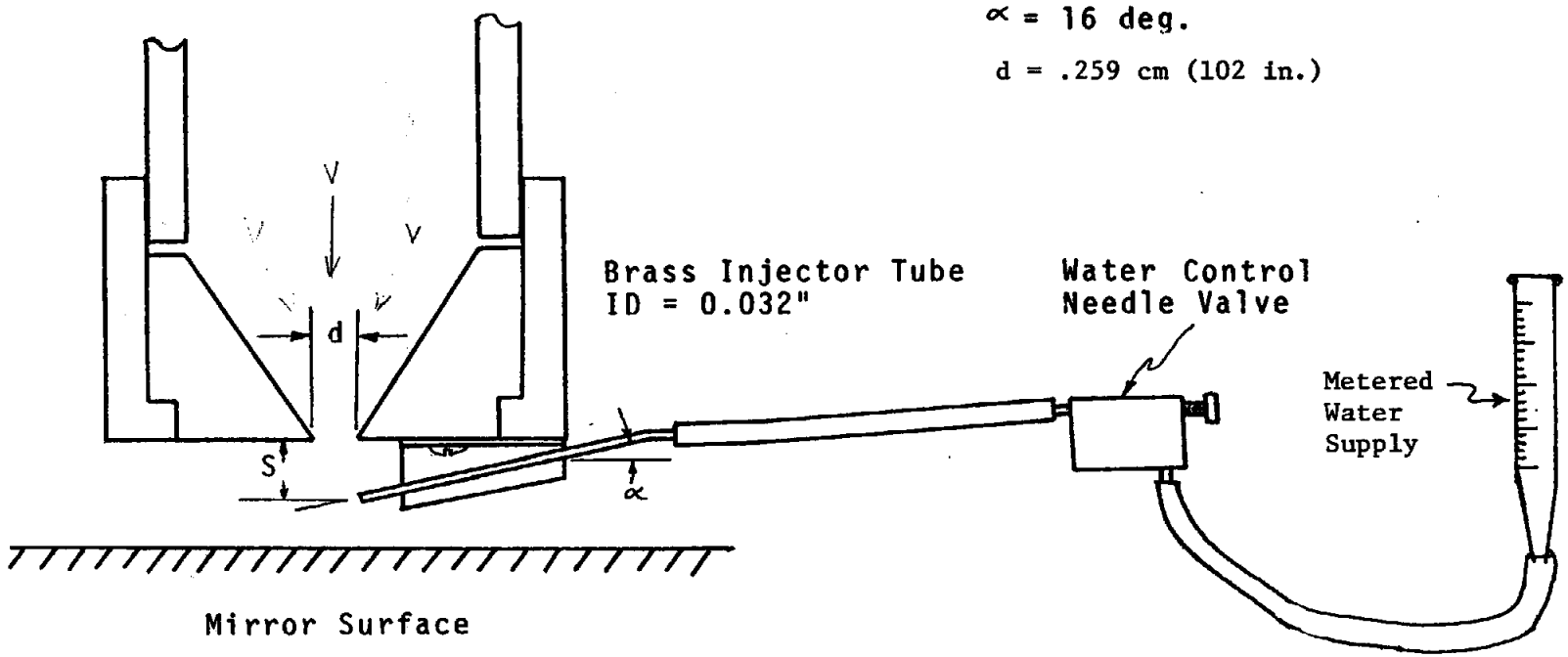

Figure 5-15. Converging Nozzle with Water Particle Injection

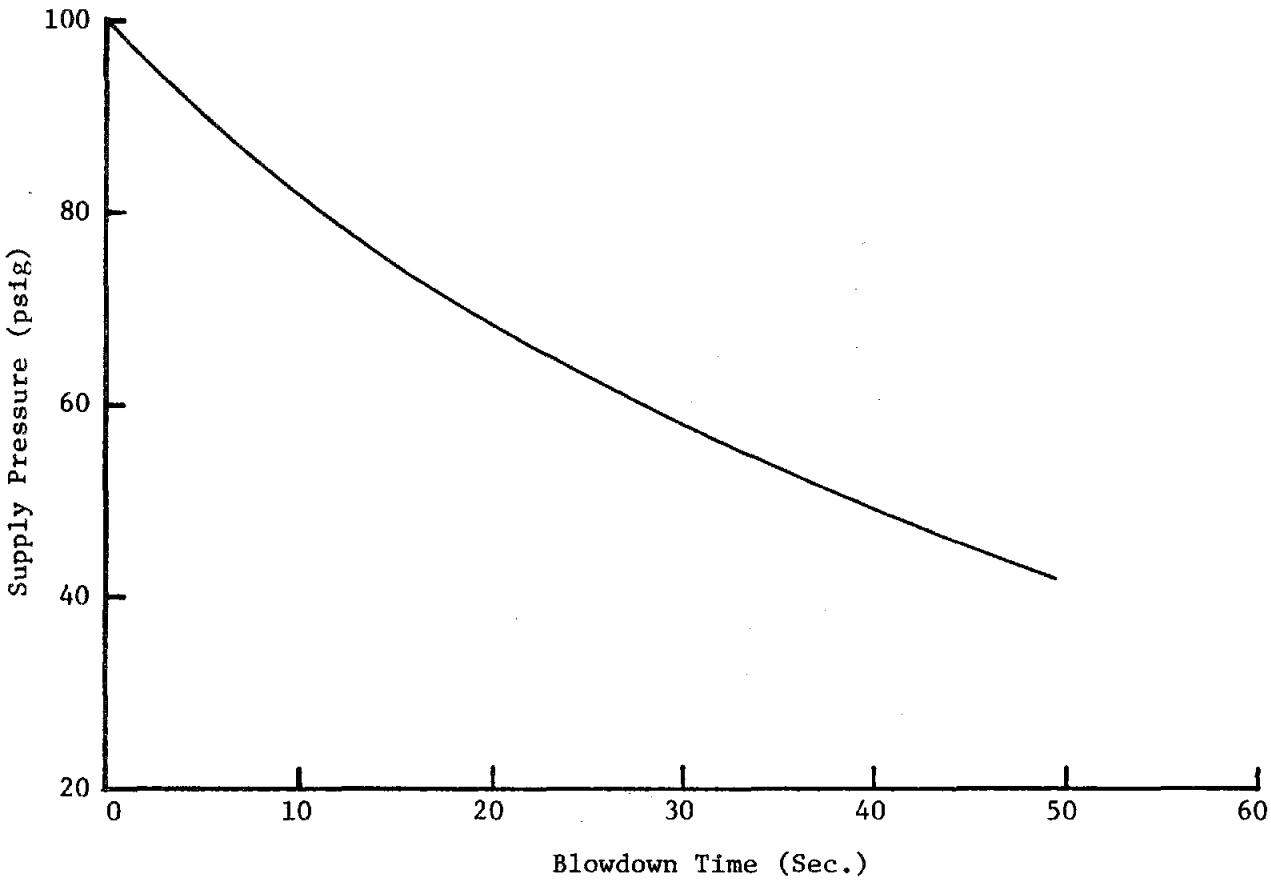

Figure 5-16. Supply Pressure vs. Tank Blowdown Time for the Converging Nozzle Configuration, Tank Volume = 60 liters

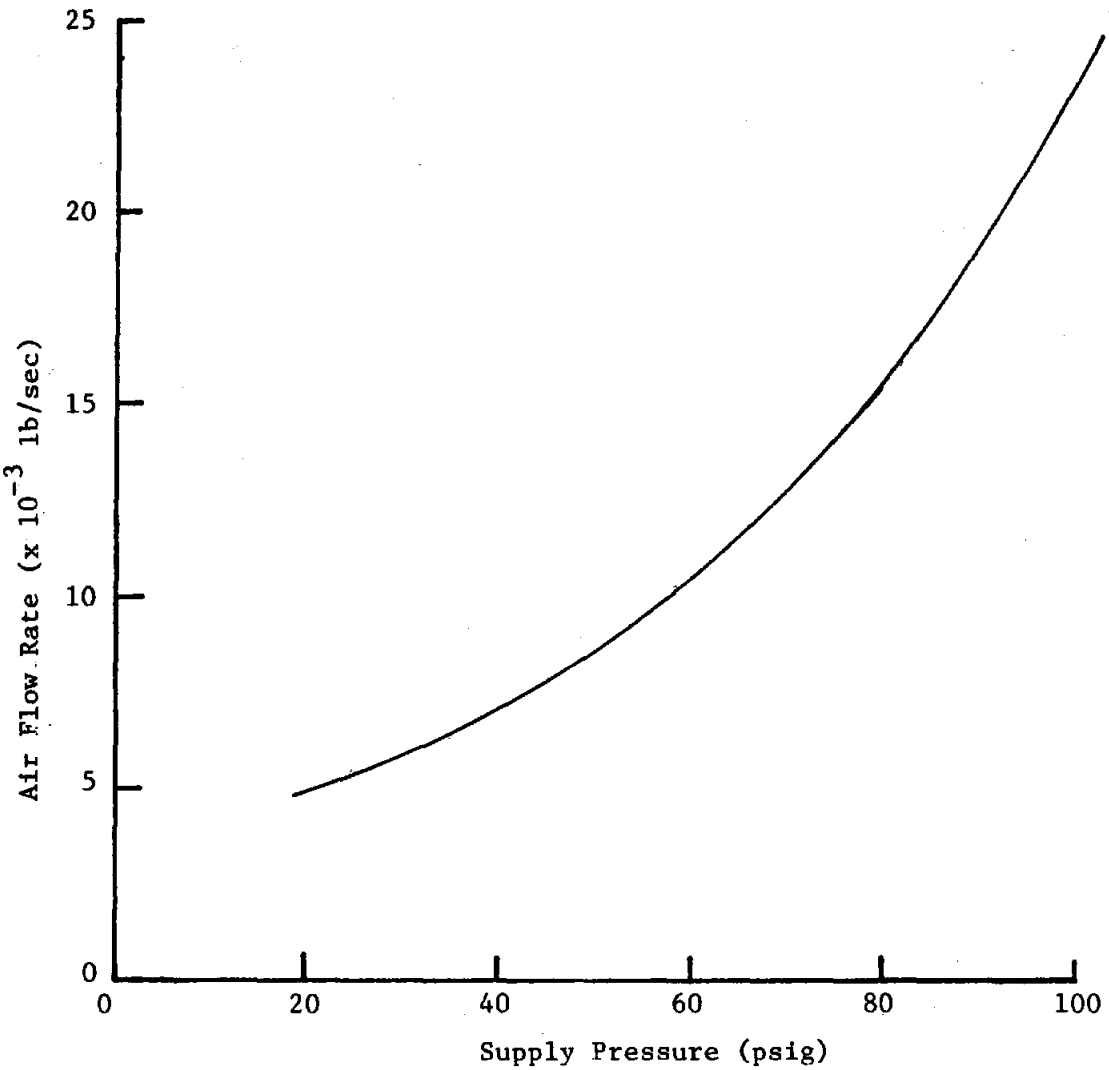

Figure 5-17. Air Flow Rate vs. Supply Pressure for the Converging Nozzle Configuration (Based on Supply Pressure/Time Test Data)

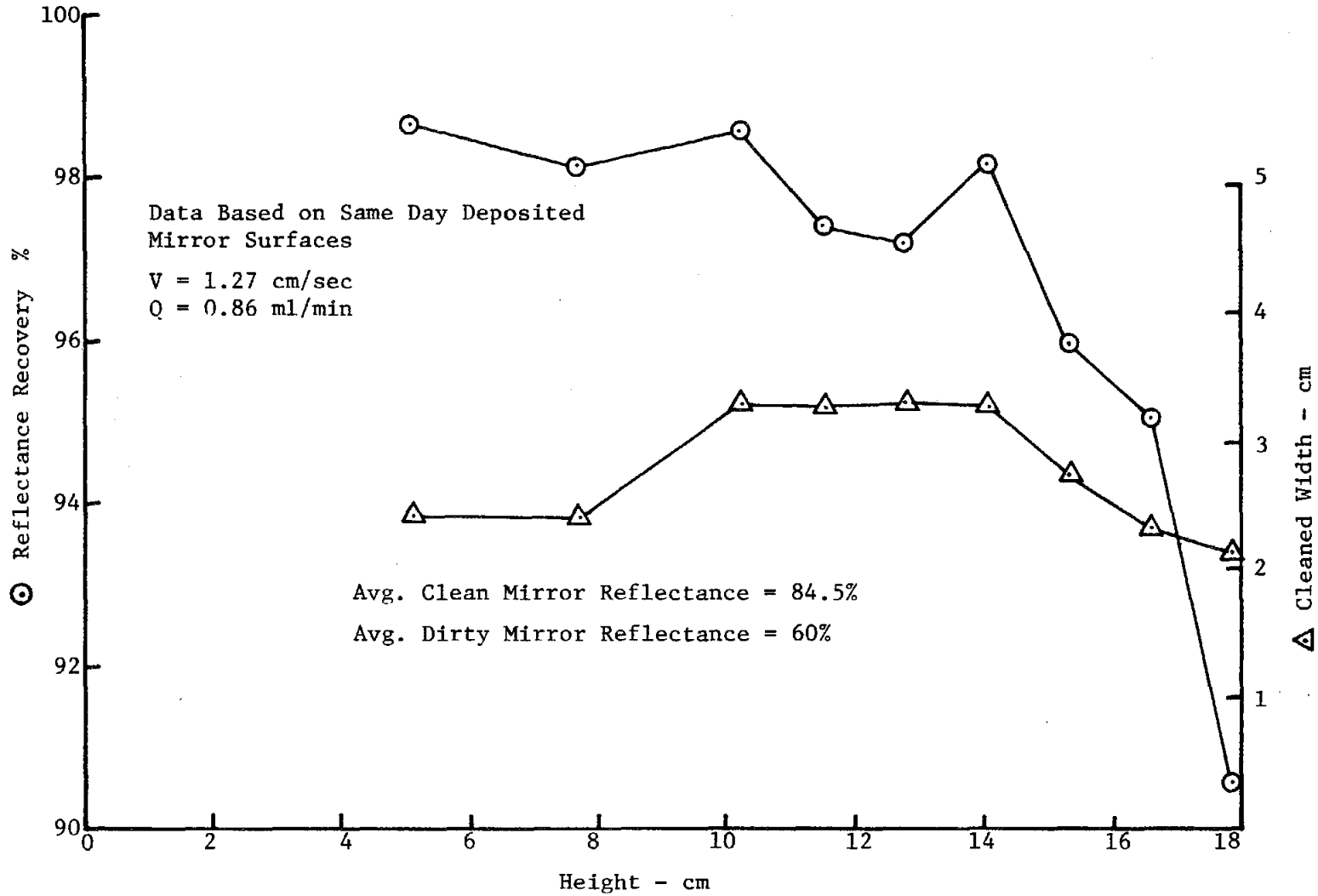

Figure 5-18. Converging Air Nozzle with Mist Injector Reflectance Recovery and Cleaned Width vs. Nozzle Height Off Mirror

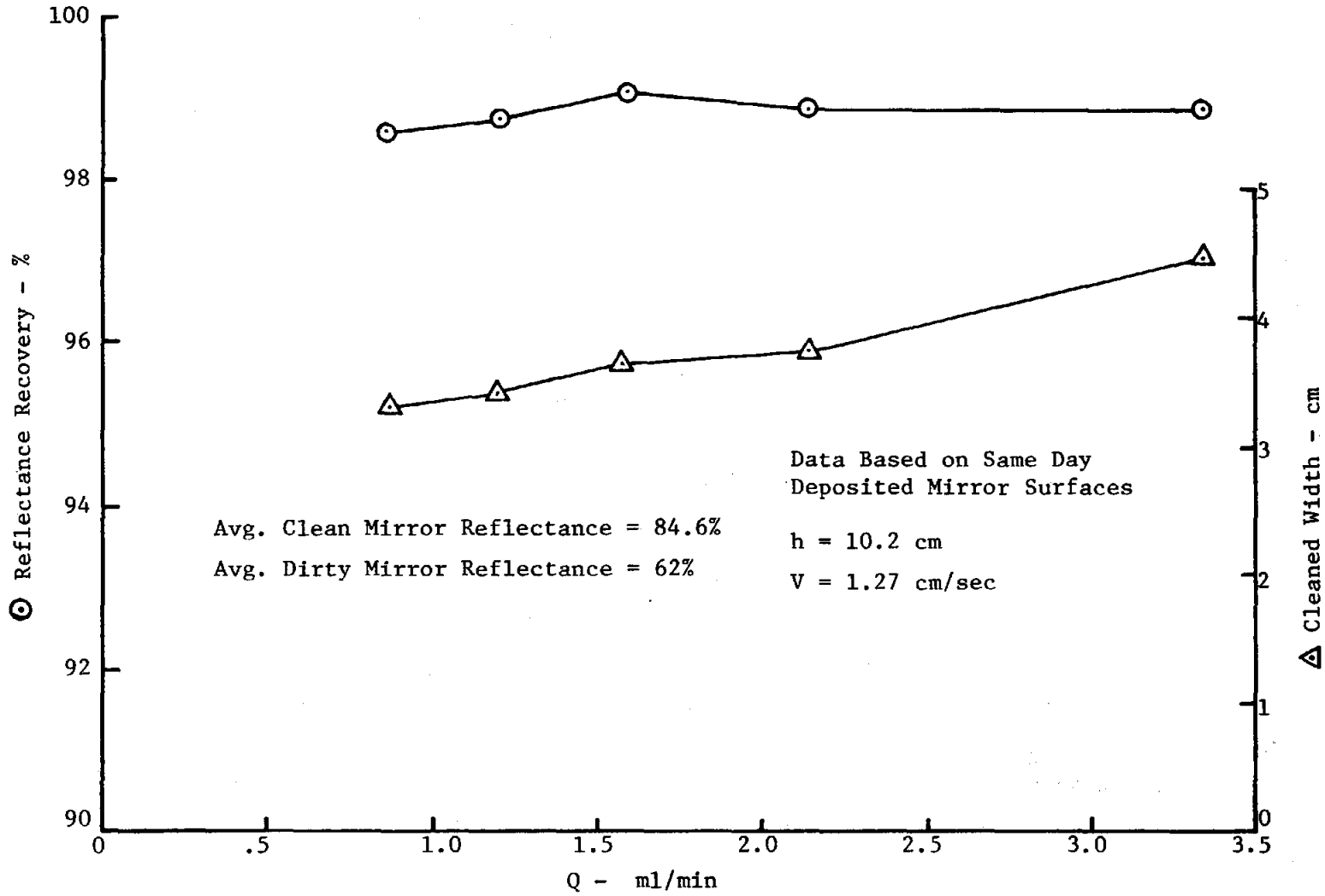

Figure 5-19. Converging Air Nozzle with Mist Injector, Reflectance Recovery and Cleaned Width vs. Water Flow Rate

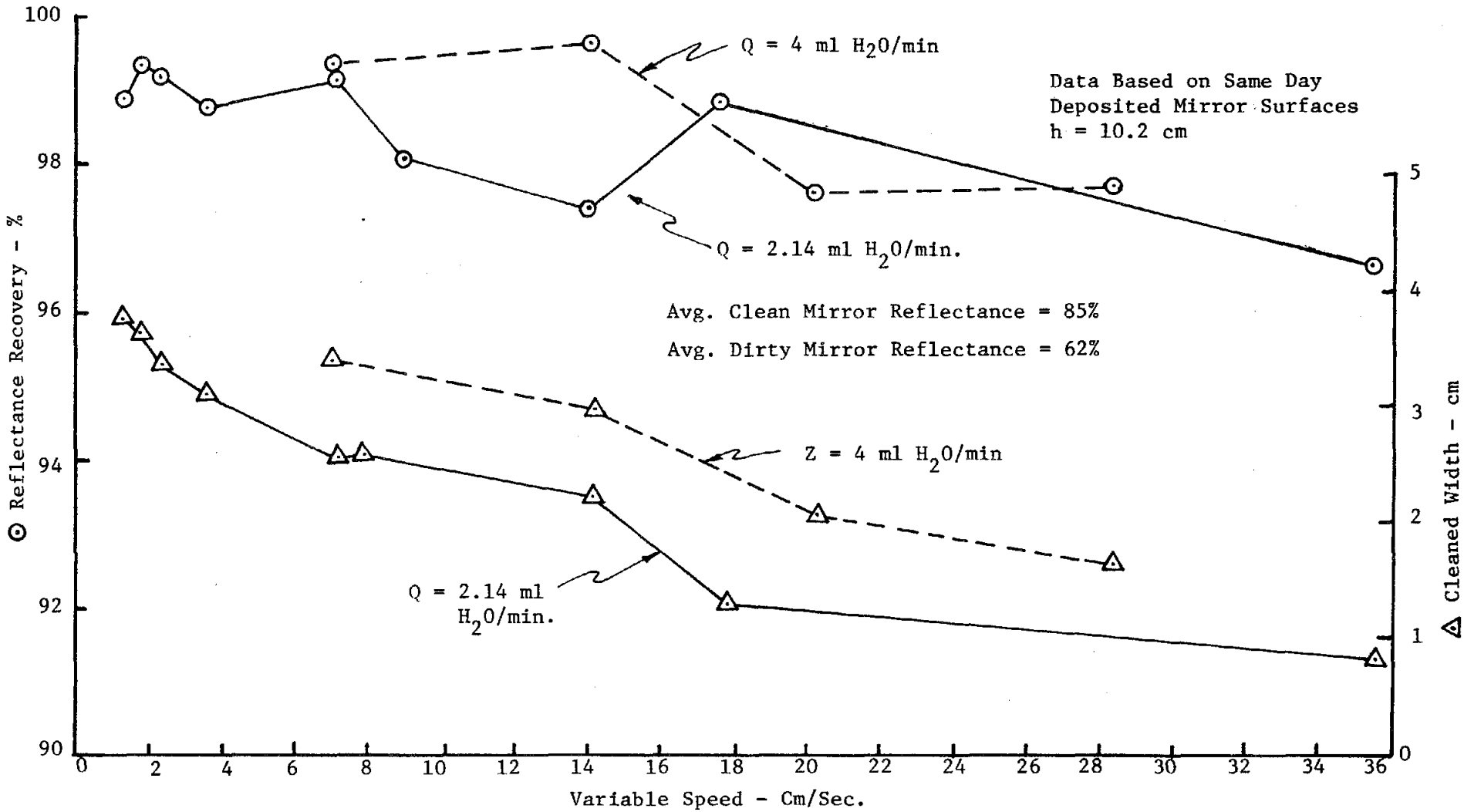

Figure 5-20. Converging Air Nozzle with Mist Injector, Reflectance Recovery and Cleaned Width vs. Cleaning Speed, h = 10.2 cm

Plots of reflectance profile over the width of the clean path are presented in Figure 5-21. The presence of the polymer coating provided for substantial improvement in clean path width with little improvement in reflectance recovery. This is further illustrated in the photograph of Figure 5-22.

The effects of mirror aging on cleanability were also investigated. The aged mirror samples were the same specimens as used in the vortex nozzle tests. The three aging times used were 4, 8 and 30 days. Figure 5-23 illustrates the expected loss in cleanability over the 30 day period as well as the loss in cleaned path width. The latter is important when considering nozzle spacing of a full scale prototype. Typical cleaned path reflectance profiles for the aged mirrors are shown in Figure 5-24.

Although the testing is limited to date, the results thus far do indicate that aged mirror samples may be effectively cleaned.

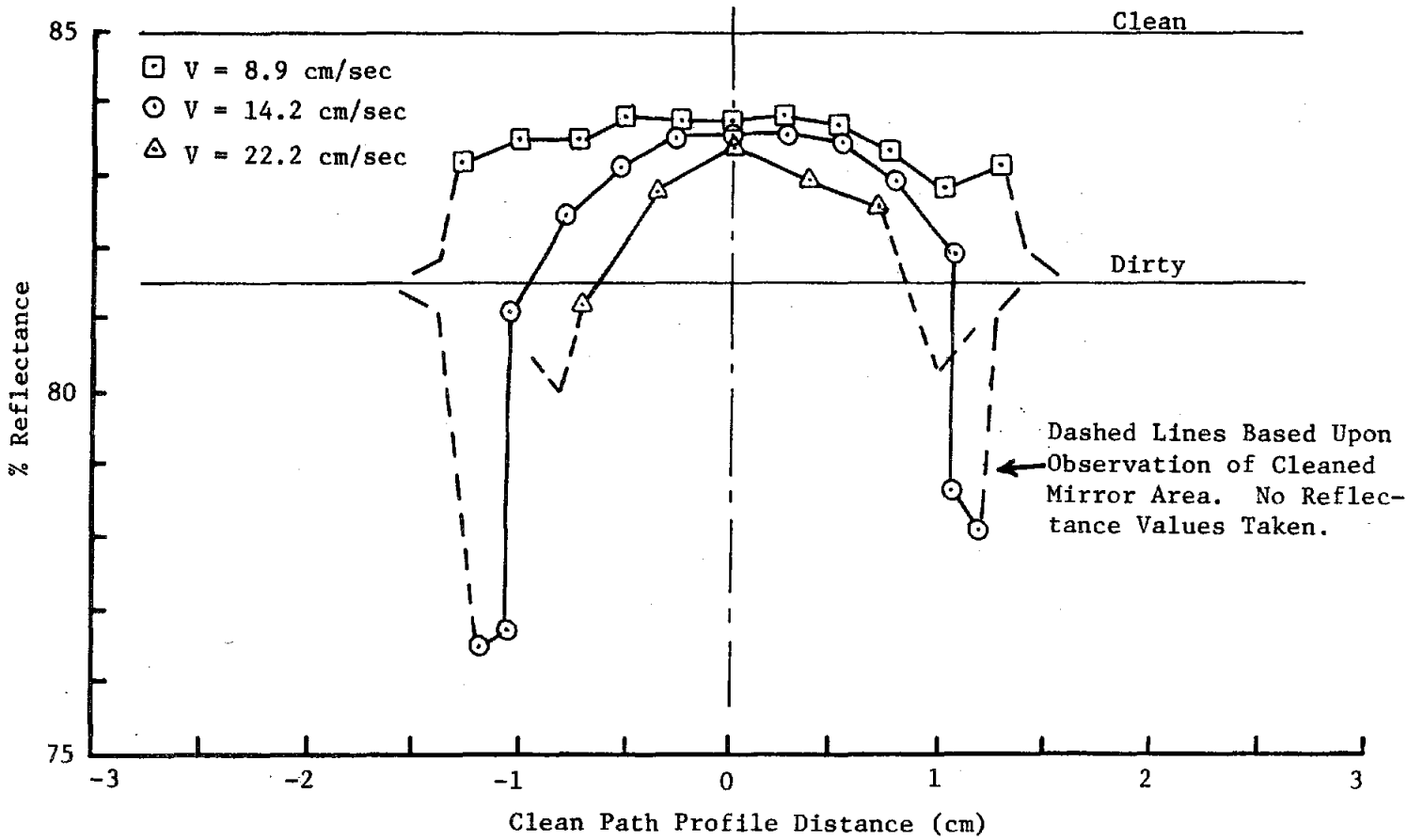

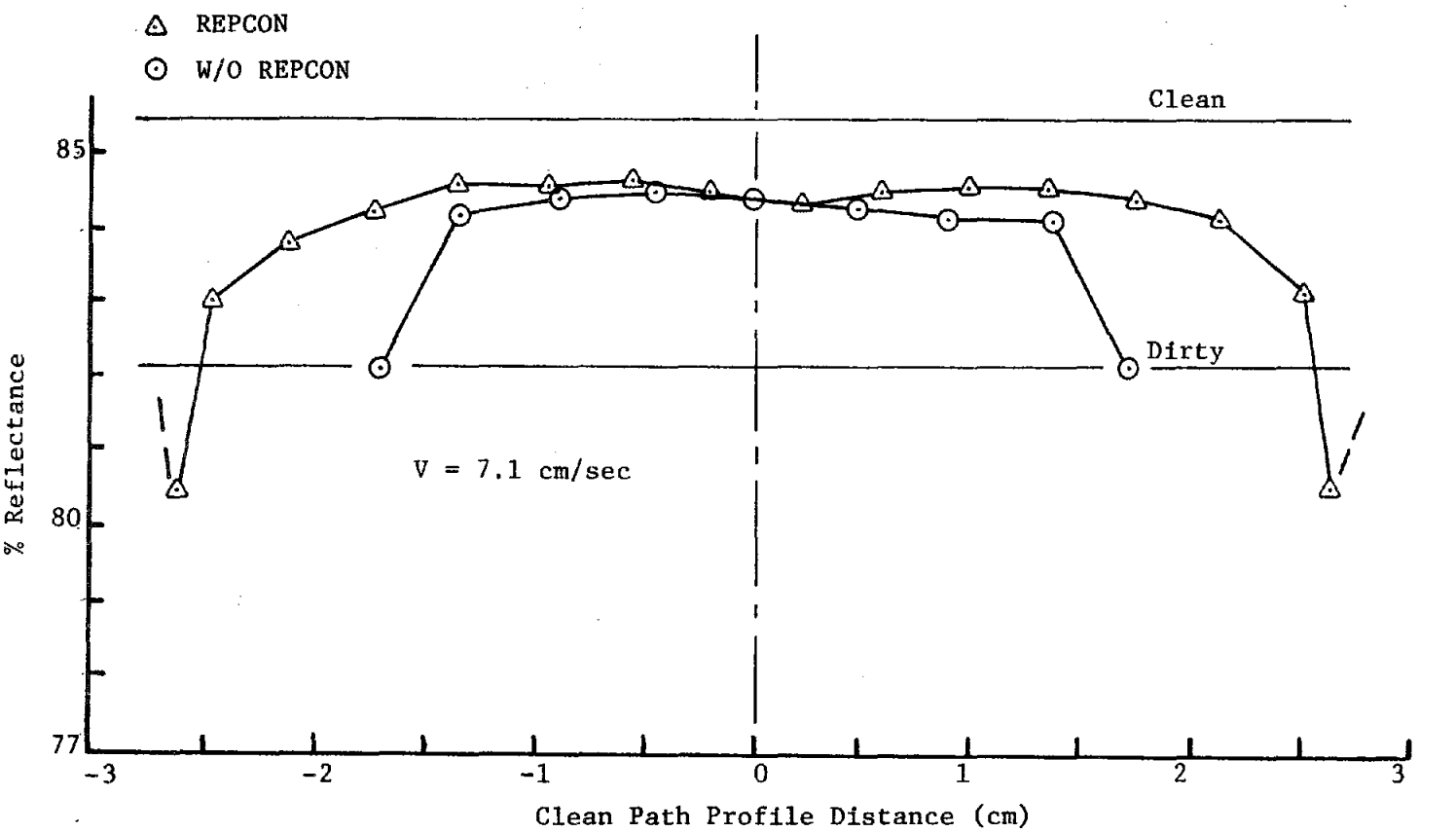

Figure 5-21. Converging Air Nozzle with Mist Injector, Cleaned Path Reflectance Profiles for Uncoated and Coated Unaged Mirror Samples, h = 10.2 cm Q = 2.14 ml/min

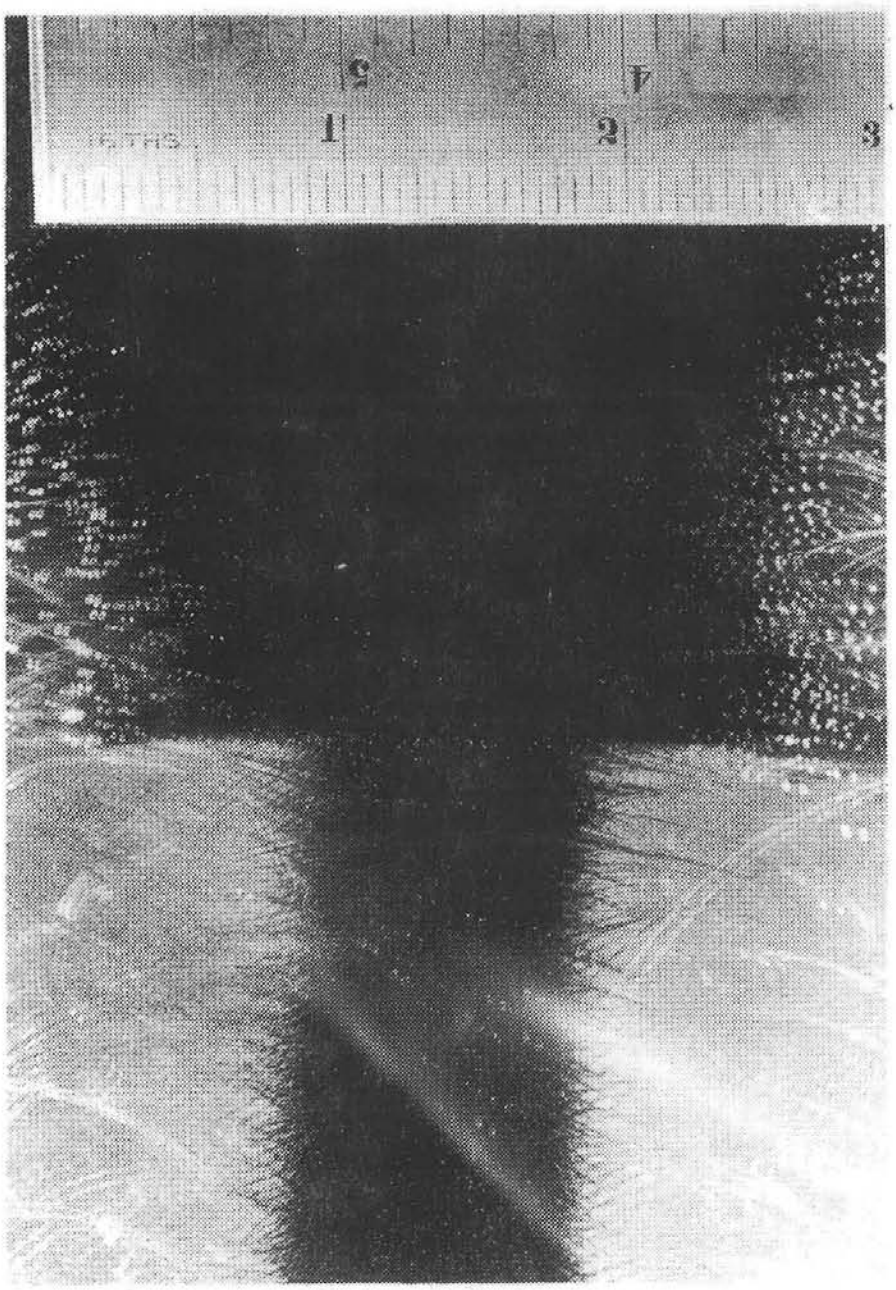

Figure 5-22. Converging Nozzle with Mist Injector, Comparison of Cleaning Path Width on Uncoated and REPCON Coated Unaged Mirrors

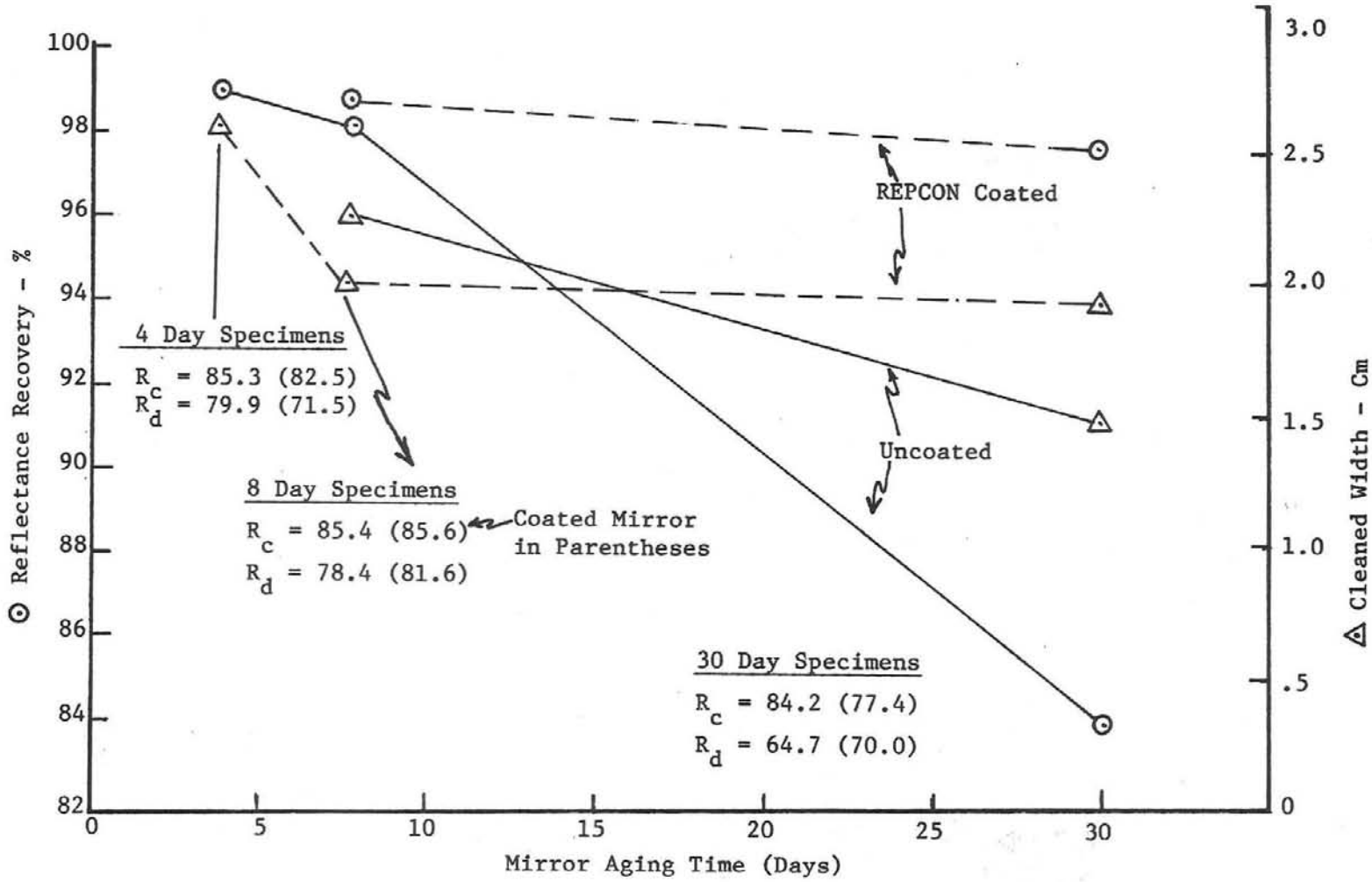

Figure 5-23. Converging Air Nozzle w/ Mist Injector, Reflectance and Cleaned Width vs. Mirror Aging Time, h = 10.2 cm V = 7.1 cm/sec, Q = 2.14 ml/min.

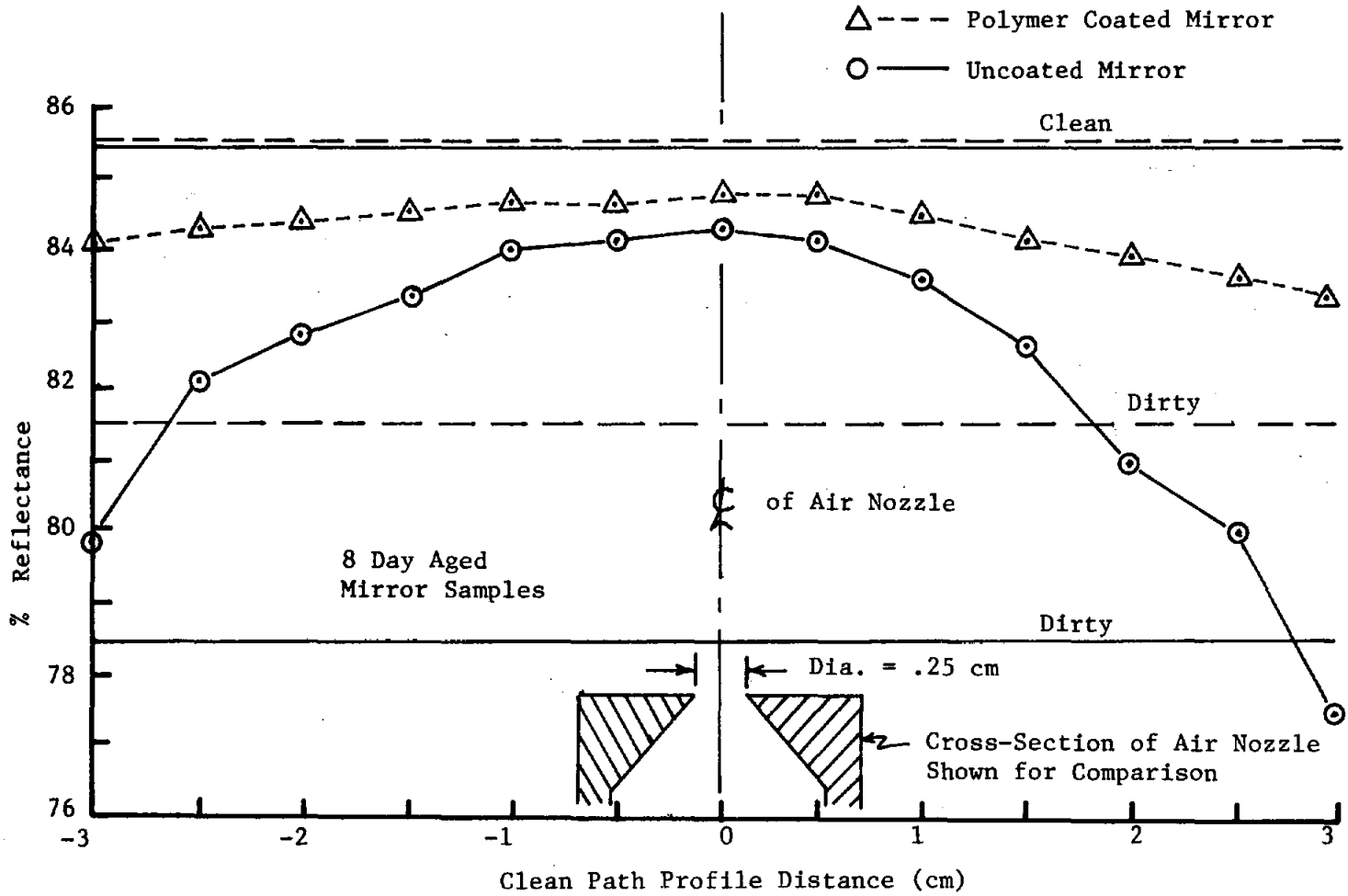

Figure 5-24. Converging Air Nozzle With Water Mist Injector, Cleaned Path Reflectance Profiles for Uncoated and Coated 8 Day Aged Mirror Samples, h = 10.2 cm, V = 7.1 cm/sec., Q = 2.14 ml/min.

5.1.5 High Pressure Jet Sweep

This concept is shown in Figure 5-25. The primary reason for its' design was to be a compliment to the ultrasonic radiating plate concept described in Section 5.2.

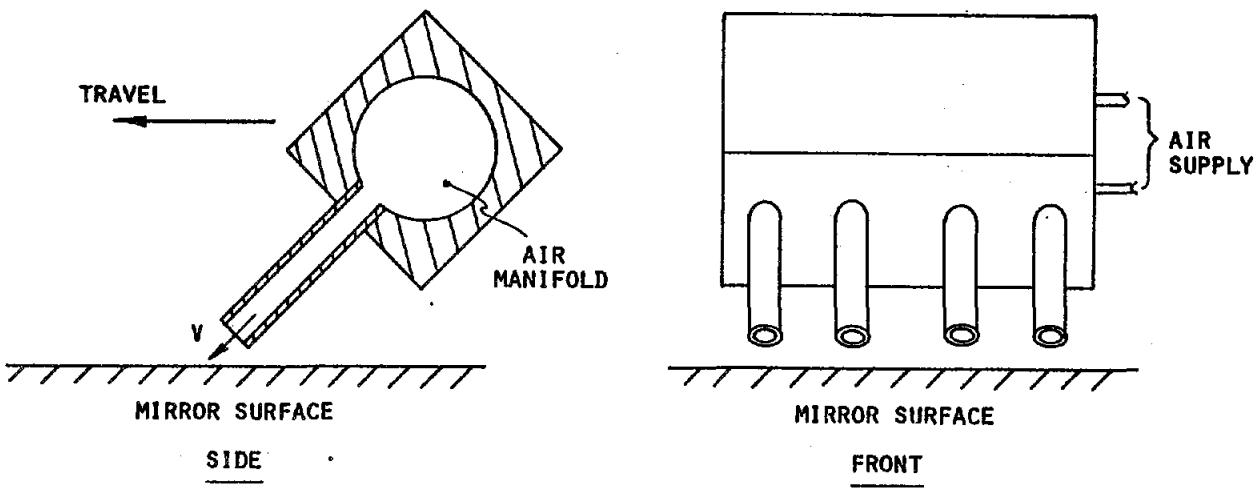

Figure 5-25. High Pressure Jet Sweep

The head was also tried as a cleaning article on its own. The results were not significant primarily due to the low air velocities generated. This was due to the inadequate air supply in the case of the air compressor/tank system and supply line and regulator restrictions in the case of the high pressure nitrogen supply tested.

5.1.6 High Pressure Nozzle

The high pressure nozzle was considered in order to obtain some evaluation of elevated pressure (well over 100 psig) on cleaning. Figure 5-26 illustrates the basic nozzle configuration.

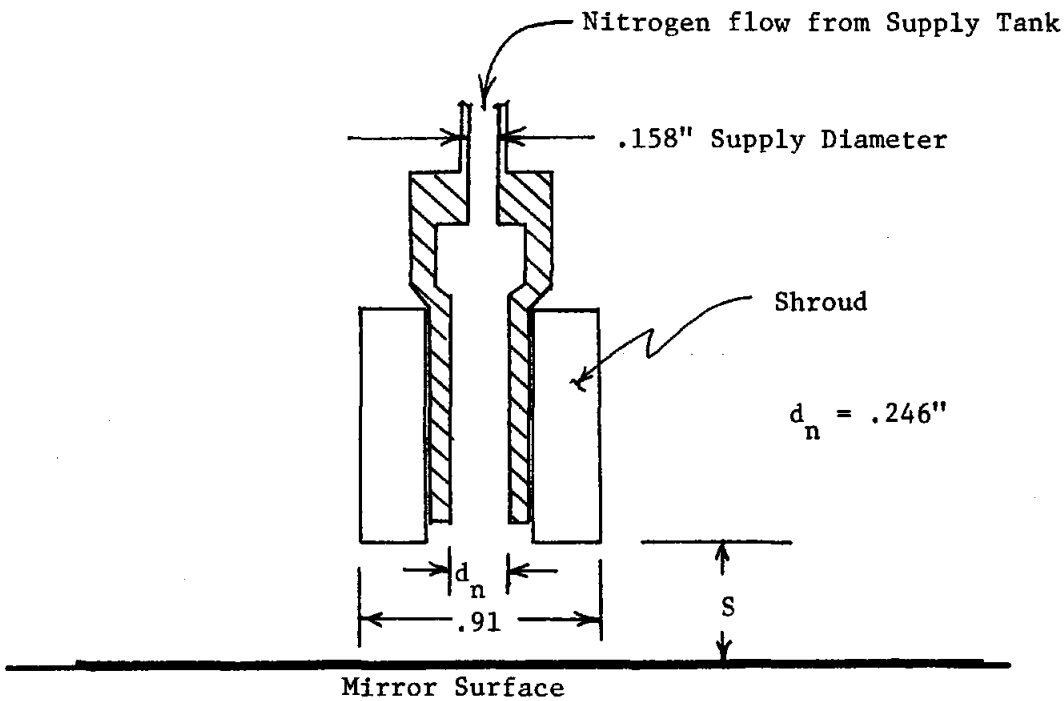

Figure 5-26. High Pressure N_2 Nozzle

The nozzle was tried with and without the shroud and a supply pressure of 320 psig nitrogen maximum. The actual nitrogen tank supply was at a pressure of 2000 psig but the high flow rate required and the low restriction of the nozzle permitted the maximum pressure under flow of 320 psig.

Tests were performed before the reflectometer was fabricated and checked out so that no reflectance readings are available.

However, subjective evaluation of the performance indicated that the shroud was an aid in keeping the air stream down on the mirror surface after exit from the nozzle which, in turn, increased the cleaned spot diameter. Cleaning action on the mirror surface was not as good as that produced by the vortex nozzle, however, further nozzle design would produce a more optimum configuration.

5.1.7 Conclusions and Recommendations for Concept 1

Based upon the Concept 1 configurations developed and the tests performed, the following conclusions can be drawn:

1. The nozzle designs with acoustic cavities and jet edge feedback mechanisms, while producing elevated acoustic power levels, are not capable on their own of significant cleaning action. It is possible that they could be used to impart oscillating energy to another jet stream thereby enhancing its cleaning ability.

2. The vortex generator is capable of producing reasonable cleaning results when in close proximity to the mirror surface (.75 cm). However, these cleaning levels can be reached or exceeded by the converging nozzle.

3. The converging nozzle with water particle injection is the most favorable of the concepts tried. It is reasonably effective at moderate distances from the mirror surface (10 cm) and appears to be capable of cleaning aged surfaces to an acceptable degree.

It is recommended that the converging nozzle alone and with the mist injector be investigated further with regards to scaling up and possible use alone or in conjunction with the acoustic radiating plate of Concept 2 described in the following section. Additionally, further testing of aged mirror samples is necessary to more properly characterize this concepts cleanability.

5.2 Concept No. 2 - Airborne Ultrasonic Transducer Cleaning Head

5.2.1 Basic Principles of Operation and Test Setup

The previous subsections in Section 5.1 investigated dust particle removal from a mirror surface with the use of high velocity air with and without water particle injection in the air stream. Concept No. 2 also relies on air flow to remove the dust particles but, in addition, attempts to greatly reduce the dust to mirror bond forces through the use of ultrasonic energy directed at the mirror surface.

Section 1.0 briefly discusses dust to mirror adhesive forces as well as basic cleaning mechanisms pertinent to this report. As presented in Section 1.0 conventional liquid media ultrasonics relies on cavitation and acoustic streaming for the removal of particles from a surface. The cavitation effect predominates and breaks particle bonds by direct erosion using imploding air bubbles and by fatigue using pulsating bubbles entrapped under and next to particles adhering to a surface.

Removal of dust particles by air flow involves erosion and denudation by air velocity forces and by collision forces between airborne and attached particles. The cleaning effect can be enhanced by increasing the air stream velocity, by injection of high mass particles into the air stream (dust, water, glass or plastic beads, etc.) or by the superposition of a vibrational field. (Ref. 5)

Cleaning Concept No. 2 is a combination of the mechanisms of air flow and particle vibration. In this case the dust particles are subjected to oscillating forces propagated in air by an ultrasonic (21 kHz) radiating plate. The action of these forces on the particles is somewhat analogous to the fatigue mechanism present in liquid media ultrasonics. Upon

application of the high intensity acoustic pressure forces to the dust particles, the bonding forces will be reduced thereby allowing the particles to be more easily removed with the high velocity air flow.

The actual acoustic pressure level output in decibels (referenced to 20μ Pa) required of the transducer head to reduce or eliminate the dust to mirror bonds is not known. From Zimon (Reference 5) bond force-acoustic pressure level equivalents of approximately 118 dB may be calculated. This, however, is based on bond forces for 60μ diameter magnesite particles on a glass surface and assumes total energy transfer from the incident acoustic sound field to the dust particle and, further, that all the energy absorbed by the particle goes into bond breakage. Additionally, Zimons monograph suggests that there is a rise in adhesive force (at least molecular attraction) with decreasing particle size for microscopic particles. In reality, the incident acoustic energy required to break bonds of small (<10μ) dust particles is expected to be substantially higher than this, perhaps at least as much as 100 times (>40 dB increase) for a total of greater than 160 dB required incident acoustic pressure level available at the mirror surface after propagation through air from the source.

The efficient transmission of high power ultrasound through air is very difficult to achieve due to the low specific acoustic impedance and high absorption characteristics of the air. However, experimentation by Gallego-Juarez et al (References 9, 10, 25, 26, 27) has led to the development of a transducer/radiating plate concept which allows the efficient propagation of high intensity ultrasound in gases. With their design they have aimed for a good impedance match between the generator and the air, high amplitudes of vibration and high directivity of the radiator. It is this type

of transducer which is used in Concept No. 2 for generation of the sound pressure field.

The basic structure of the transducer is shown in Figure 5-27. It is made up of three basic conceptual parts: (1) a piezoelectric transducer in a sandwich configuration, (2) an amplification horn and (3) a radiating plate. An electronic amplifier (not shown) provides a high frequency voltage source to the piezoelectric discs which transform the voltage waveform into a longitudinal mechanical vibration. This vibration is amplified by the mechanical amplifier before it drives the radiating plate at the plates center. The radiating plate then drives the air in front of it at the plates radiating frequency. The large area of the plate and its stepped design provide for a good impedance match with the air. It is important to mechanically shape all of the components such that all the desired natural vibration frequencies of the three elements coincide. This turned out to be difficult to achieve as is brought out in the following subsections.

Evaluation of Concept No. 2 involves two basic types of testing; (1) characterization of the cleaning head and (2) mirror cleaning tests. Characterization tests are first performed with the intent of determining the head assembly resonant frequencies and the output sound pressure levels generated. During this phase of tests the mechanical/electrical parameters of the system are optimized so that maximum acoustic output may be obtained from the radiating plate prior to beginning the cleaning tests. Figure 5-28 presents a schematic of the characterization test system. Components of this system allow variable input frequency and power level, measurement of input frequency and power level as supplied by the ultrasonic generator, measurement of output sound pressure level and frequency as well as observation of the wave form of the sound signal being generated at the radiating plate. Also provided is a thermistor for temperature measurement at various high stress

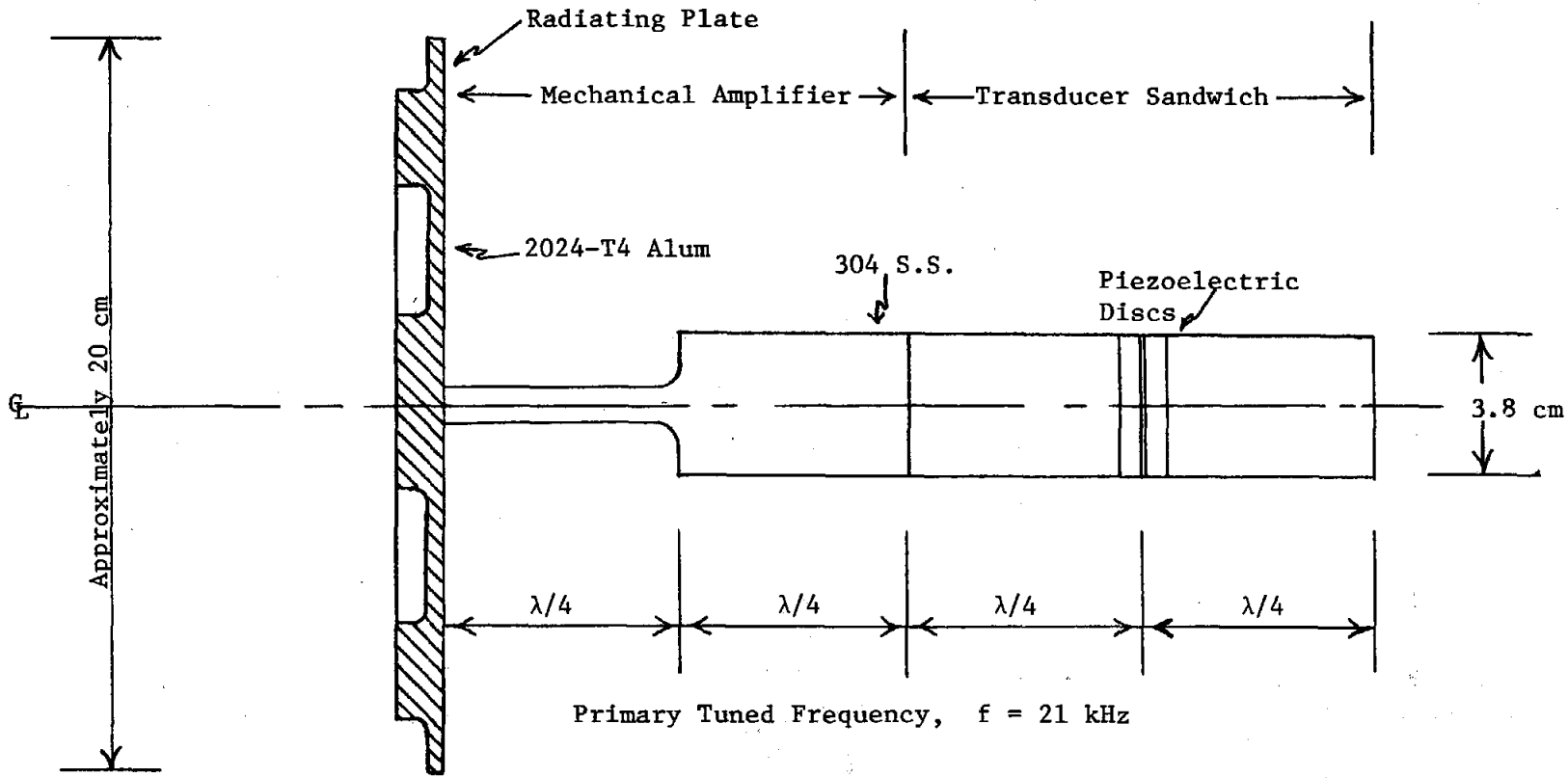

Figure 5-27. Concept No. 2, Transducer for Radiating Air Propagated High Intensity Ultrasound, General Representation

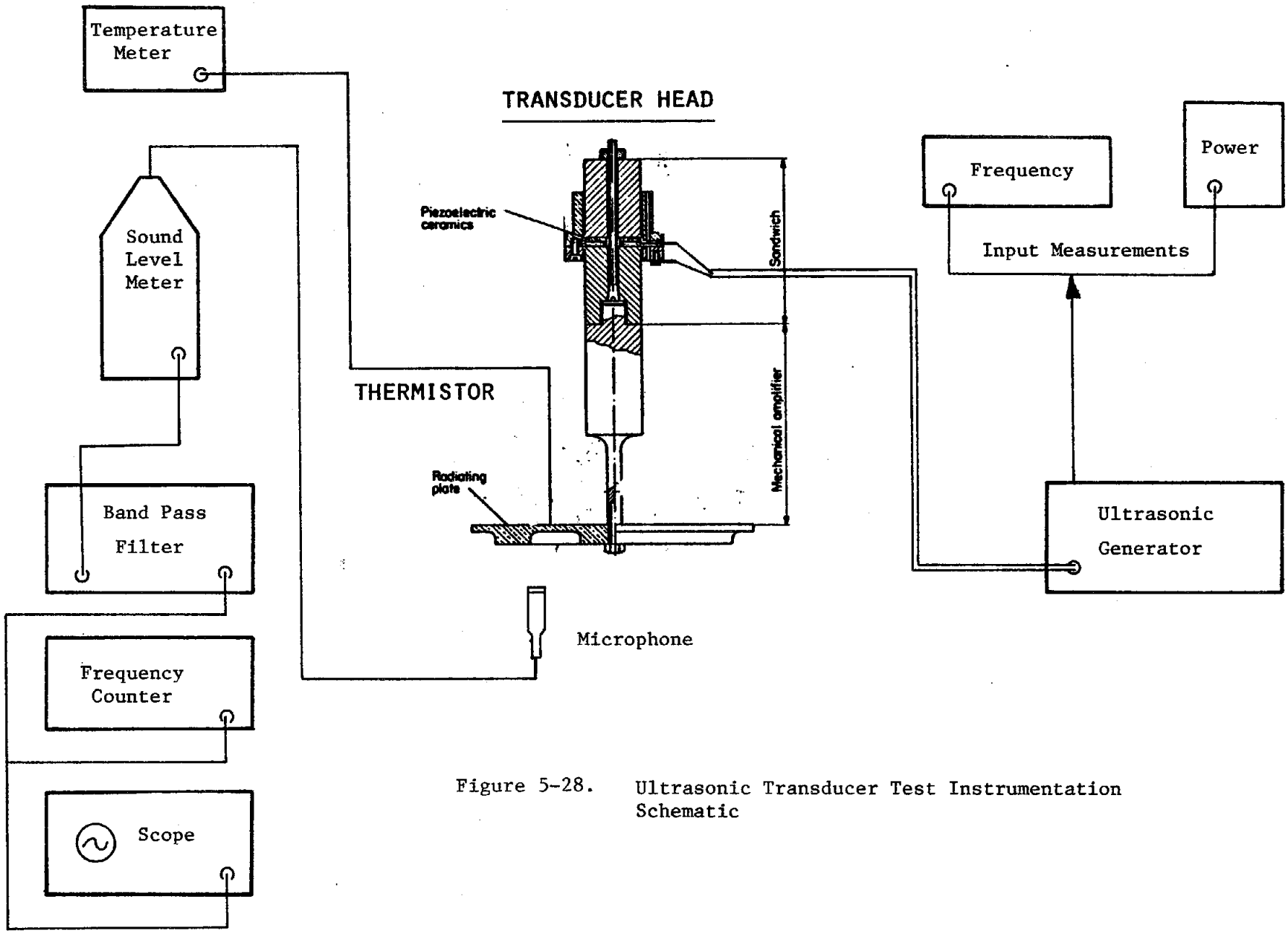

Figure 5-28. Ultrasonic Transducer Test Instrumentation Schematic

points of the transducer. This is included since, at higher power levels, the Juarez transducers structurally failed in high temperature fatigue of the radiating plate and, in fact, were water cooled to aid in reducing the temperature and increase the fatigue strength of the plate. The principal instruments used are as follows:

1. Ultrasonic Generator - Fibrasonics Model G-100 Mark III
2. Sound Level Meter - Brüel and Kjaer, Model 2209
3. Microphone - B & K Type 4133 - ½ inch (Measurement capability: 36 to 150 dB <10 to 40,000 hz
4. Band Pass Filter - Krohn-Hite, Model 3202
5. Frequency Counter - Heathkit IM-4110
6. Oscilloscope - Heathkit IO-4530

Figure 5-29 shows the orientation of the ultrasonic radiating head, air jet and mirror as used for the cleaning tests.

The following section presents the design of the ultrasonic transducer head while sections 5.2.3 and 5.2.4 cover the transducer characterization tests and Concept No. 2 cleaning test results, respectively.

5.2.2 Design Description of Cleaning Head

The design of the ultrasonic transducer head of Figure 5-27 follows closely the latest design arrived at by Gallego-Juarez et. al. (Reference 10). The design frequency chosen is 21,000 Hz. The design process may be considered as two somewhat separate steps; the design of the flexurally vibrating plate and design of the longitudinally vibrating transducer sandwich and amplifier sections.

The design of flexural vibrating free-edge plates for propagation of ultrasound has been investigated in depth by Barone and

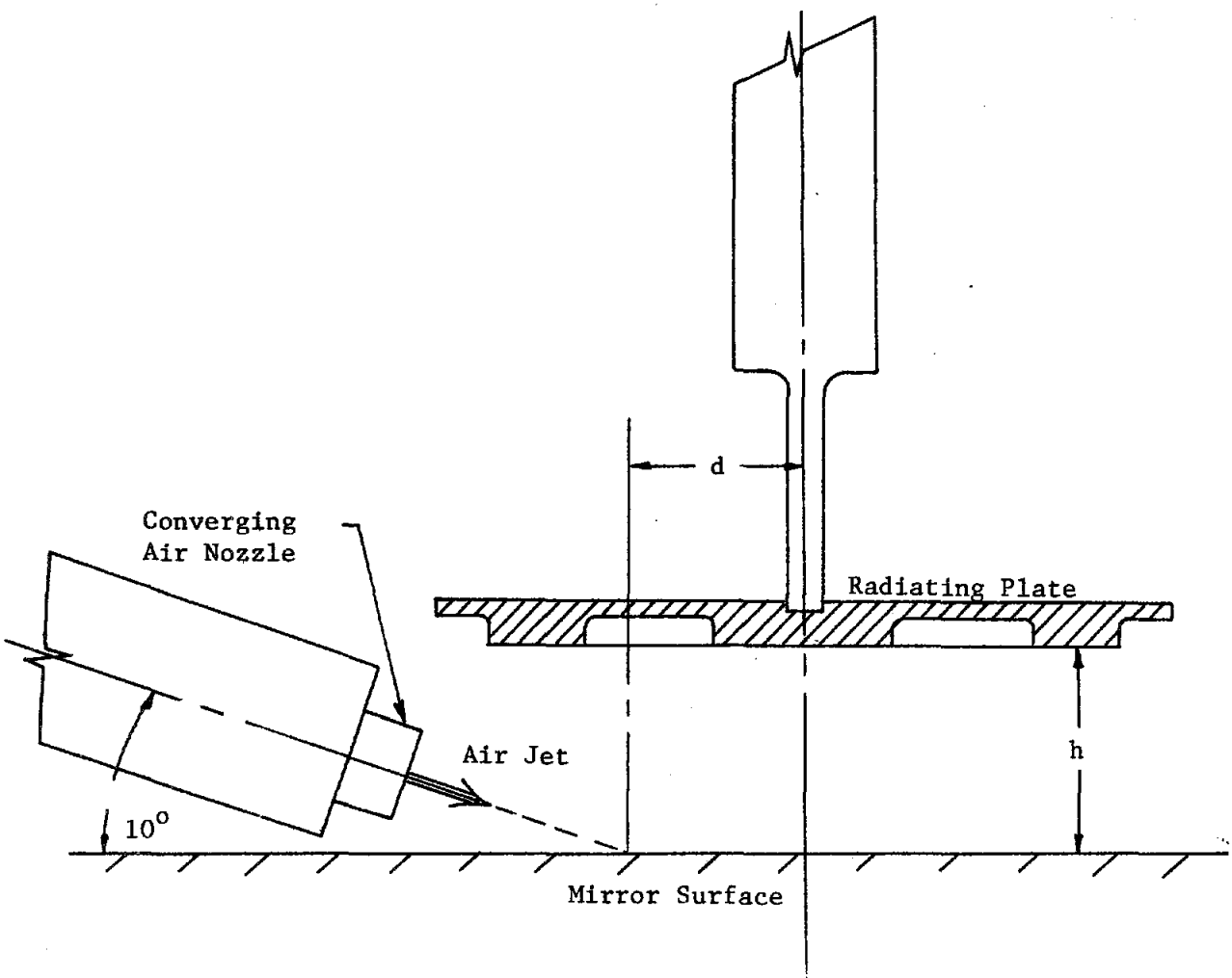

Figure 5-29. Concept No. 2, Cleaning Head Test Setup

Gallego-Juarez in References 25, 26 and 27. The design chosen for use in this investigation is the same as presented in Reference 10 which is a plate based on the preceding three references but which is improved for more efficient, directional high power applications. Not all required plate dimensions are given in Reference 10, therefore, a computer design was performed for the plate using the basic dimensions available in Reference 10 as a starting point for design.

The computer model used is an axisymmetric finite element method (FEM) elastic model of the plate cross-section. Since the plate is axisymmetric only the cross-section need be specified with the constraint and behavior of the full plate accounted for within the computer code. Figure 5-30 presents the cross-section of the radiating plate with pertinent dimensions as input to the computer. All dimensions were held fixed with the exception of the basic plate thickness, t. A separate normal modes analysis was performed for each of these different values of t. The mode shapes and natural frequencies thus obtained allowed interpolation to the required value t for the desired frequency of 21 kHz. The computer code used is EAC/EASE2 as documented in Reference 28.

Figure 5-31 presents the lowest six mode shapes for axisymmetric flexural vibration of the radiating plate. From Reference 9 and 10 the desired mode is the fourth fundamental mode. Table 5-2 summarizes the first six natural frequencies of the plate for each of the three plate thicknesses investigated. The variation of fourth mode natural frequency with t is plotted in Figure 5-32. From this plot a thickness of 5.46 mm (.215 inches) was chosen for a natural frequency of 21 kHz.

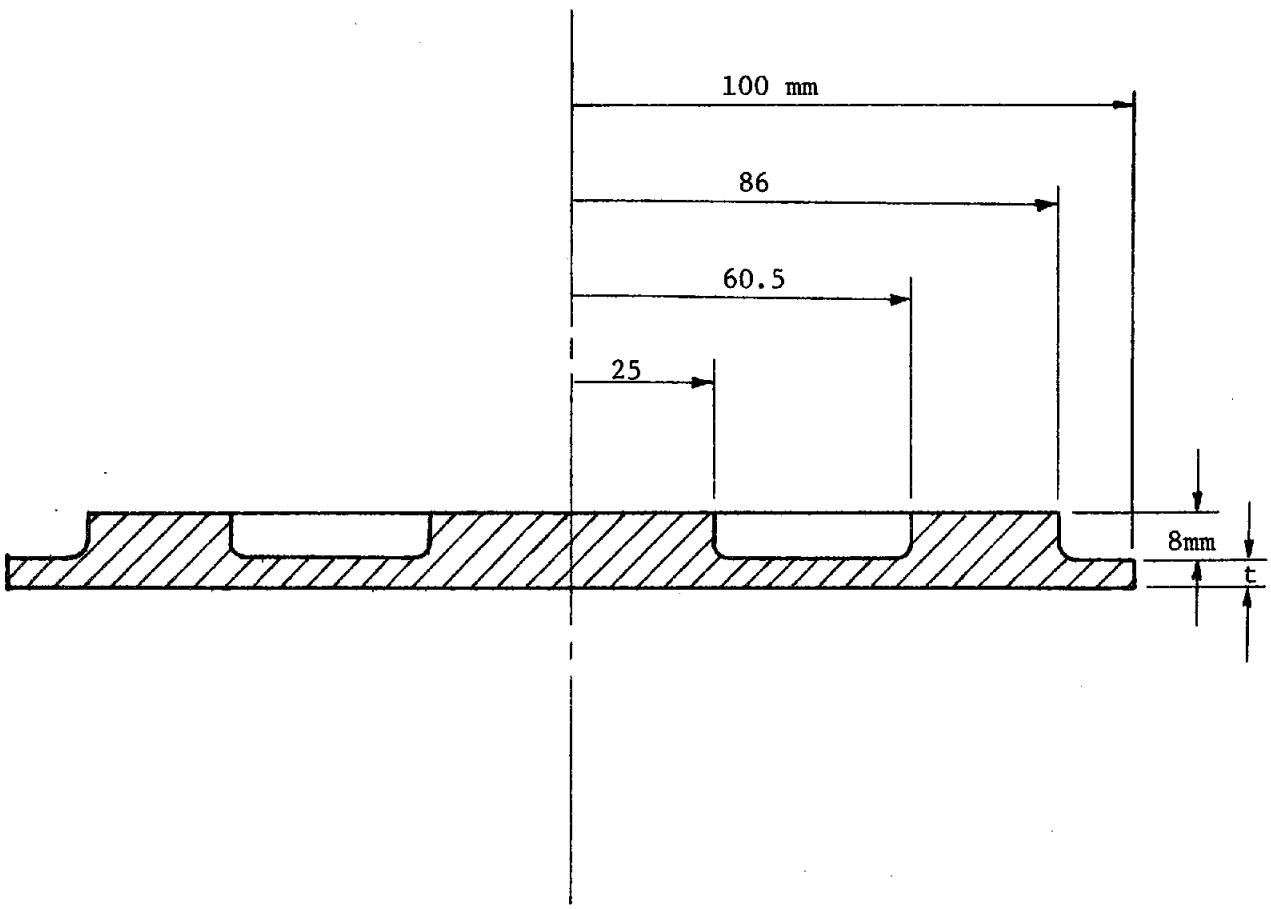

Figure 5-30. Ultrasonic Radiating Plate Dimensions used for Axisymmetric Finite Element Analysis of Plate Natural Frequencies

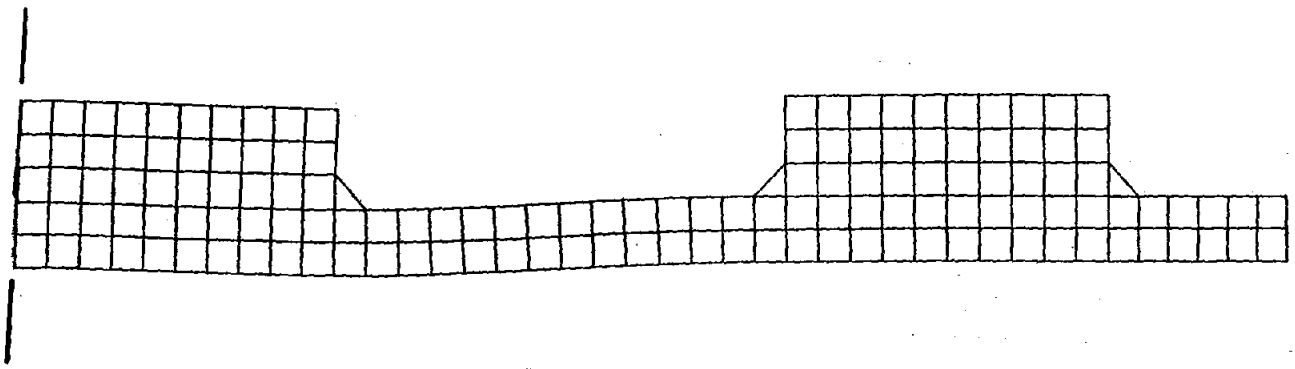

FIRST MODE

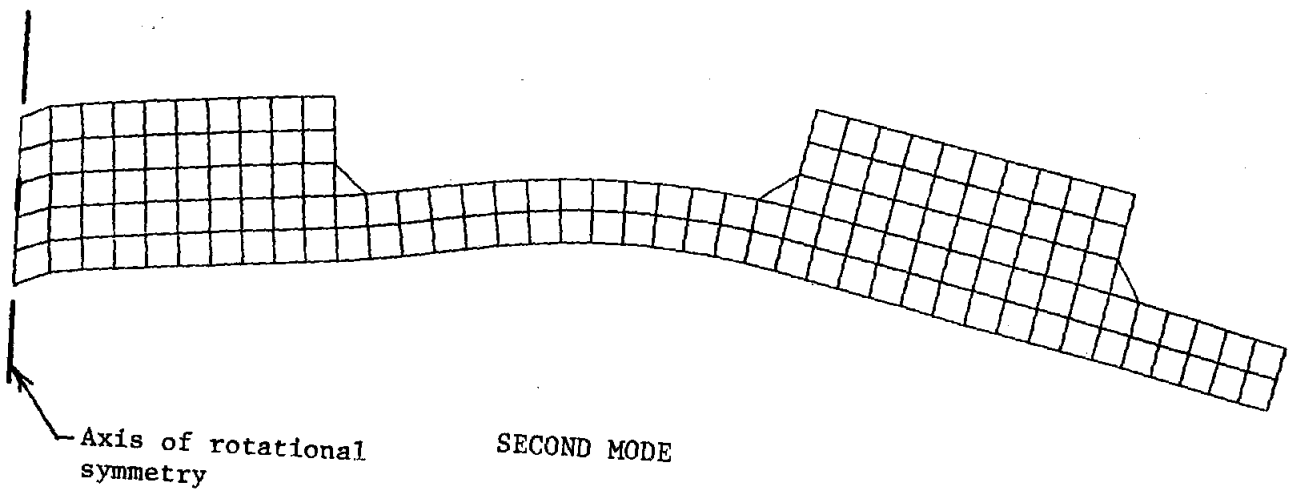

SECOND MODE

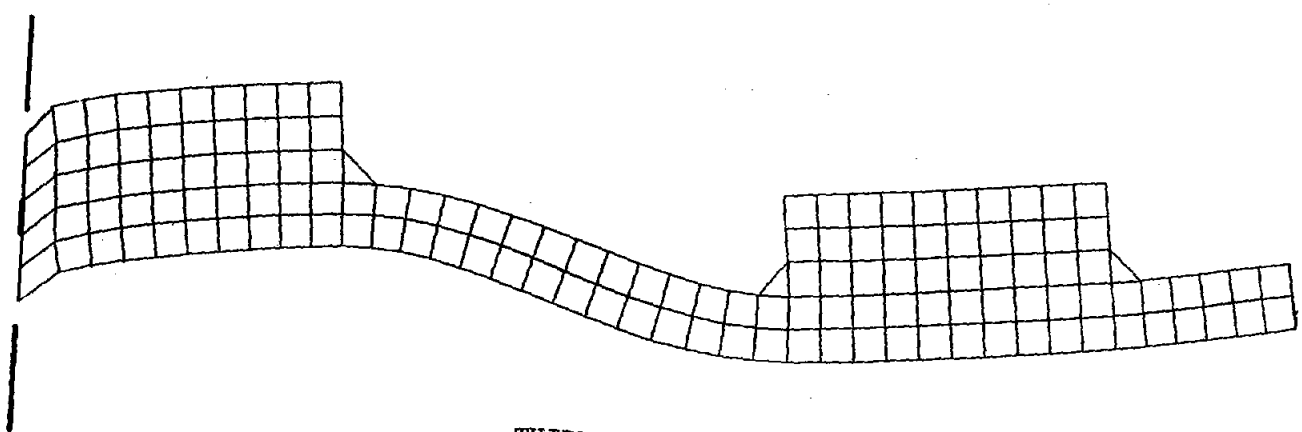

THIRD MODE

Figure 5-31. Ultrasonic Radiating Plate Finite Element Analysis Model, Normal Modes

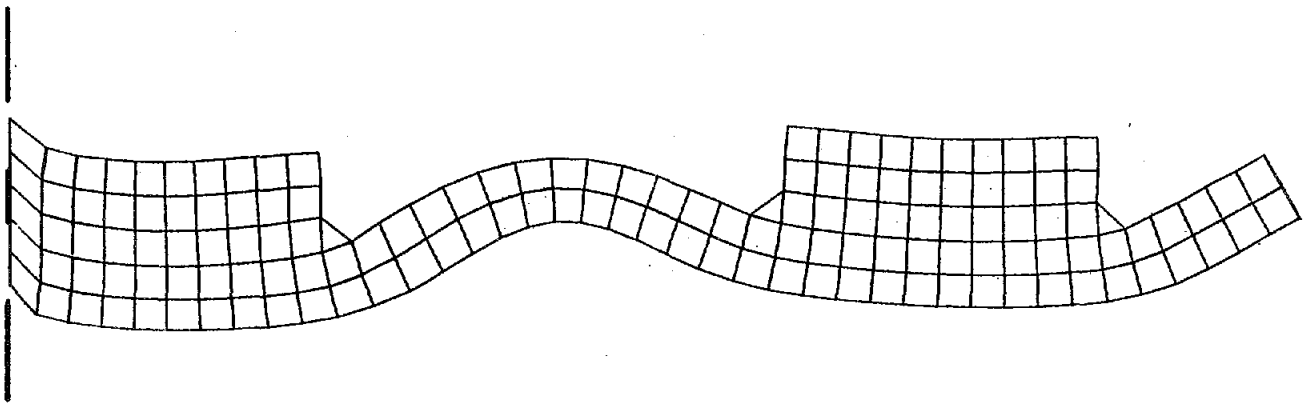

FOURTH MODE

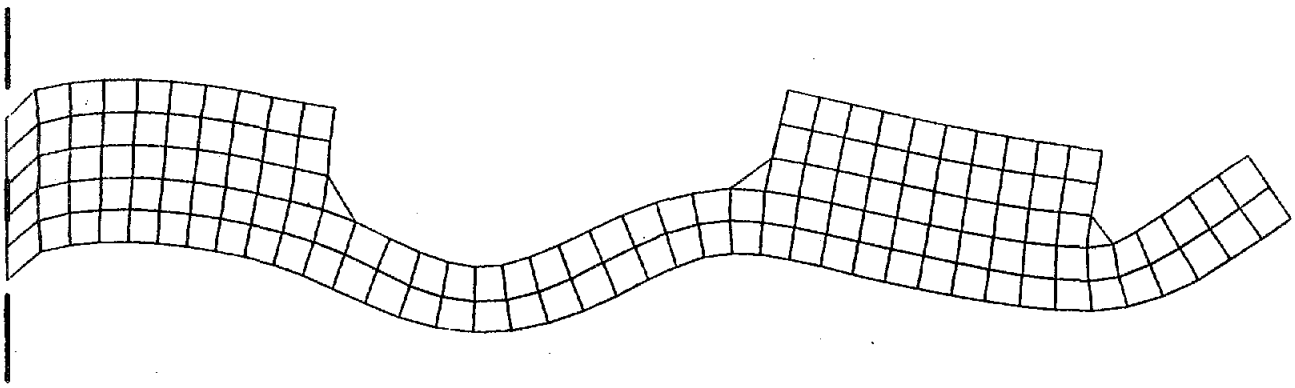

FIFTH MODE

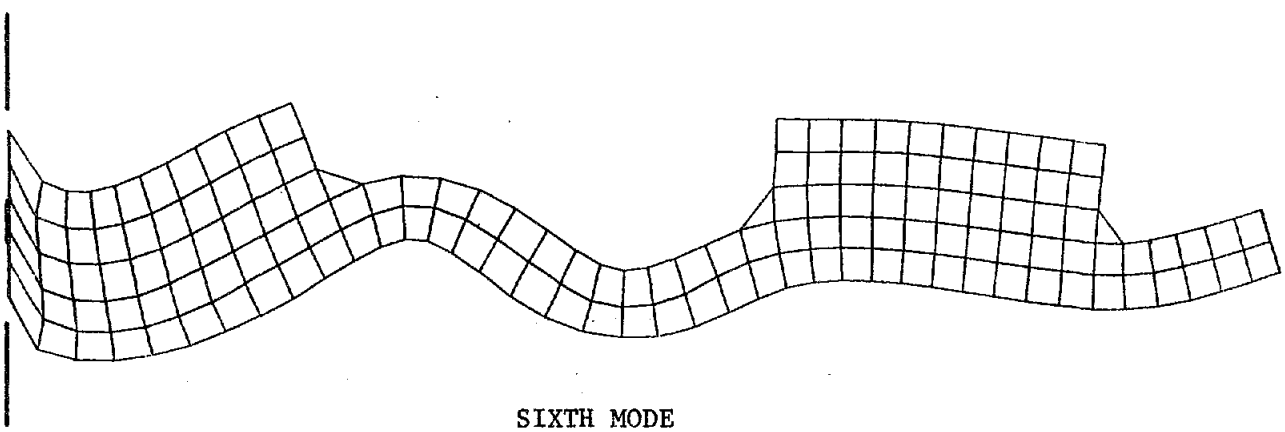

SIXTH MODE

Figure 5-31. (Cont'd) Ultrasonic Radiating Plate Finite Element Analysis Model, Normal Modes

Table 5-2. Ultrasonic Radiating Plate Finite Element Model, Natural Frequencies

n	f_n (Hz)		
	t = .20 in (5.08 mm)	t = .22 in. (5.59 mm)	t = .24 in. (6.10 mm)
1	902	947	988
2	5,118	5,251	5,377
3	10,102	10,525	10,945
4	20,211	21,241	22,199
5	27,178	28,862	30,433
6	41,028	42,689	44,271

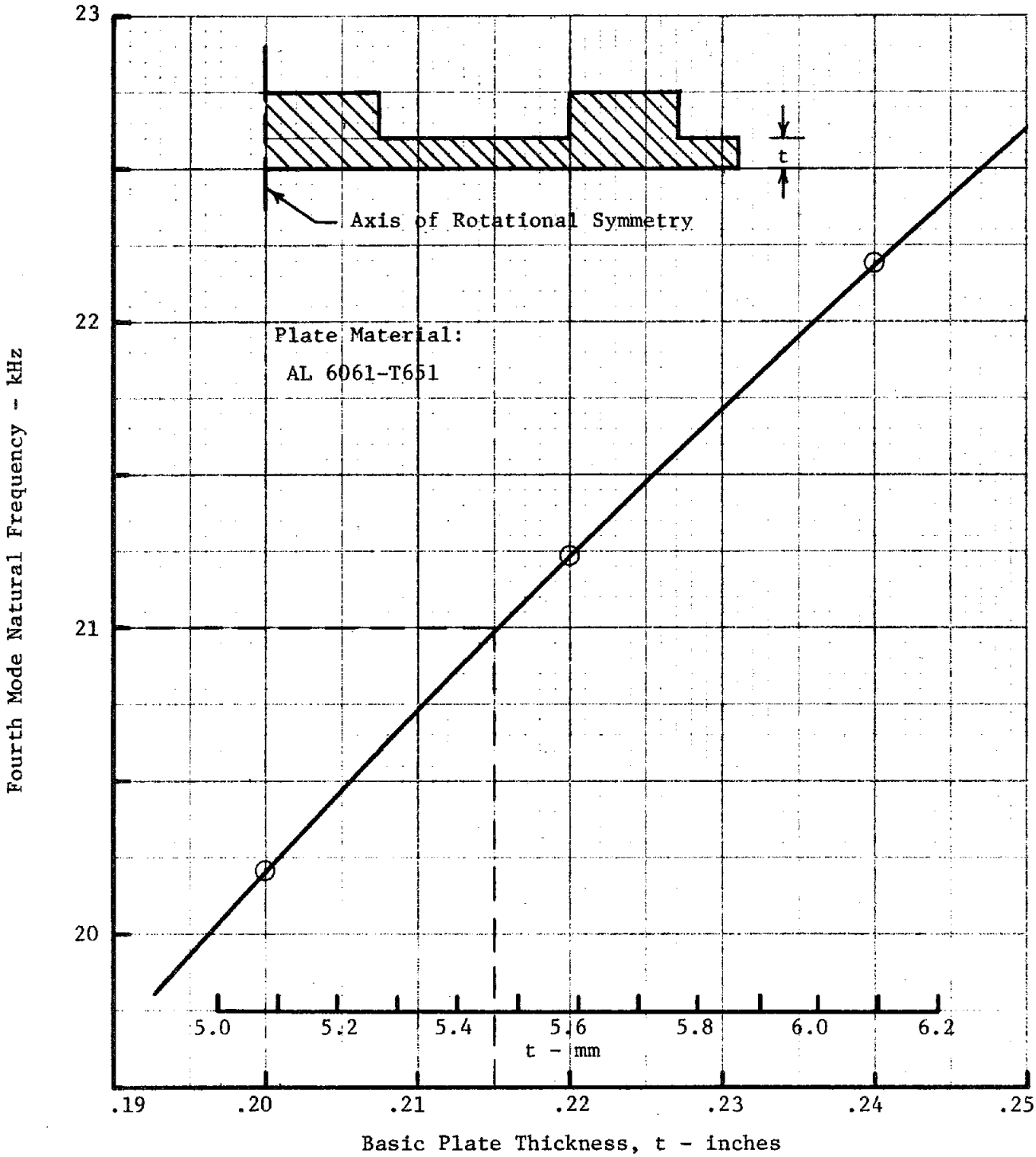

Figure 5-32. Ultrasonic Radiating Plate Finite Element Model, Variation of Fourth Mode Natural Frequency with Plate Thickness

Two transducer sandwich/amplifier heads were designed and fabricated for testing. The first one is based entirely on the design of Reference 10 and attempts to duplicate that transducer as closely as possible with slight length changes required for operation at 21 kHz instead of 20.4 kHz as used in Reference 10. This design, with its dimensions, is presented in Figure 5-33.

The second transducer was fabricated after preliminary testing of Design #1 produced sound pressure intensities less than predicted and desired (See Section 5.2.2). Since every material interface, discontinuity or joint is a source of reflective loss and reduction in overall efficiency, Design No. 2 attempted to remove as many of these as possible. In addition, the component lengths were recalculated based upon the Langevin expression for sandwich transducers, (References 9 and 23), and the experimentally measured fabricated plate natural frequency of 20.16 kHz. This design is presented in Figure 5-34.

5.2.3 Transducer Head Characterization and Acoustic Testing

Prior to the cleaning tests, characterization studies were performed on the transducer assembly. The primary goals being to: (1) determine the frequency and output power characteristics of the radiating head and (2) to maximize the output sound pressure level.

The first tests included checking the radiating plate natural frequencies. To determine the plate frequencies the head assembly was placed in a vertical position and talcum powder evenly distributed over the back surface of the plate. The ultrasonic generator allows tuning through a range of frequencies from about 12.5 kHz to 100 kHz. Upon reaching a natural frequency of the plate, the plate vibrates in the associated mode shape and the talcum particles are driven

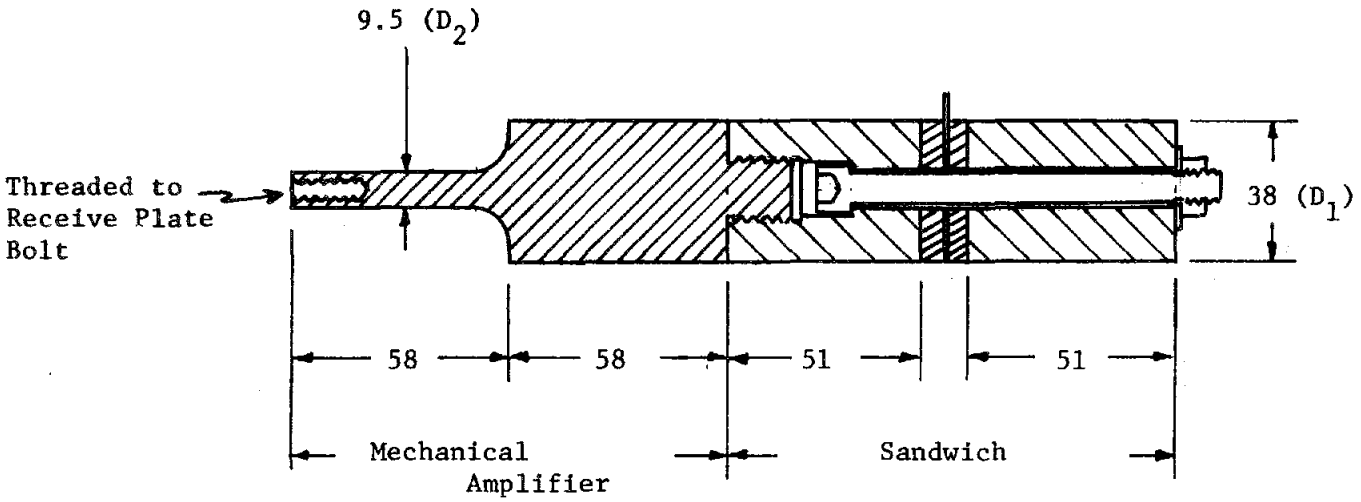

All Dimensions in mm
C varies from 12.8 mm to 17.5 mm
$D_1/D_2 = 4$

Figure 5-33. Ultrasonic Transducer Sandwich and Mechanical Amplifier, Design #1

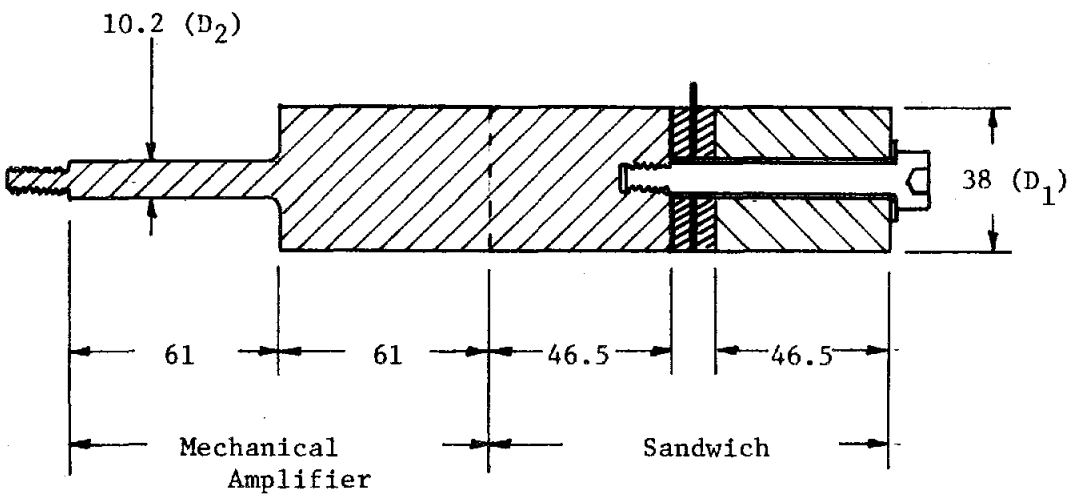

All Dimensions in mm
$D_1/D_2 = 3.7$

Figure 5-34. Ultrasonic Transducer Sandwich and Mechanical Amplifier, Design #2

to the nodal circles. The two strongest modes of the plate above 12.5 kHz occurred at 15.46 kHz and 20.16 kHz. Photographs of the vibrating plate at each of these two frequencies are presented in Figure 5-35.

Figure 5-36 portrays the overall test setup for output sound level and frequency measurements. Closeups of the radiating plate with microphone probe and the ultrasonic generator are shown in Figure 5-37.

Sound level/frequency studies performed resulted in maximum outputs of 134 dB at both 15.4 kHz and 20.16 kHz for transducer Design No. 1. These measurements were taken 76 mm from the plate surface. The ultrasonic generator was at maximum output in all cases, however, the power to the load is substantially less than 100 W. The vibrational mode at 15.4 kHz was fairly easy to stabilize, however, the mode at 20.16 kHz was difficult to place in resonance and even more difficult to maintain for any length of time.

Much effort was expended in trying to improve on the output of the transducer head including experimentation with joint couplants and nodal mounting techniques of the assembly. At one time an output of 150 dB was obtained at 20.16 kHz, however, this was difficult to tune and unstable when tuned in. Further experimentation did not produce as high an output and, in fact, it was not possible to return to the original configuration which produced 150 dB. At no time did the transducer/plate assembly generate significant heat either from the stepped down amplifier section or from the higher stressed areas of the radiating plate. This is contrary to heating phenomena associated with the Reference 10 transducer head, which showed high temperature levels due to flexure. So important is temperature to the Reference 10 design that it

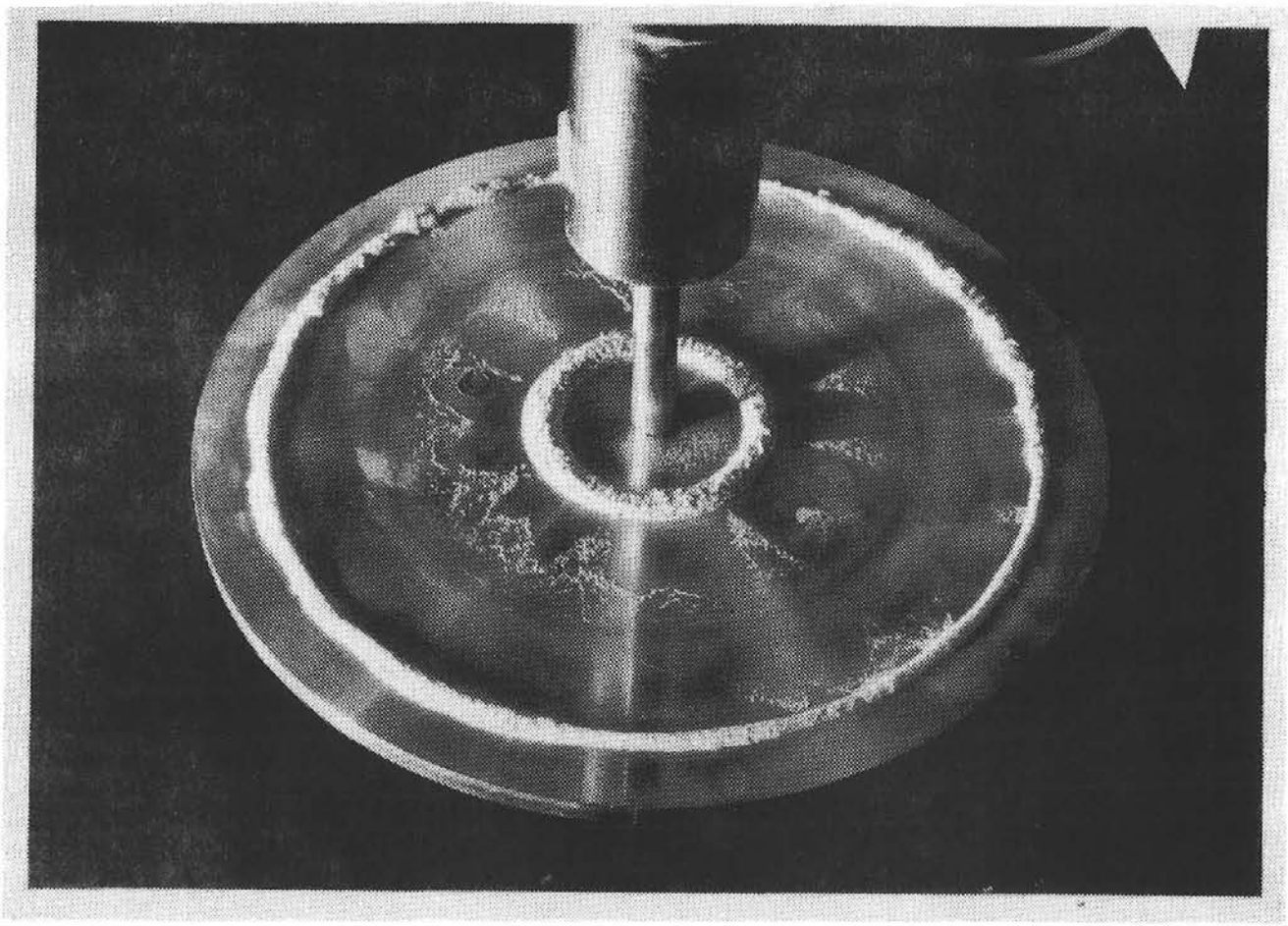

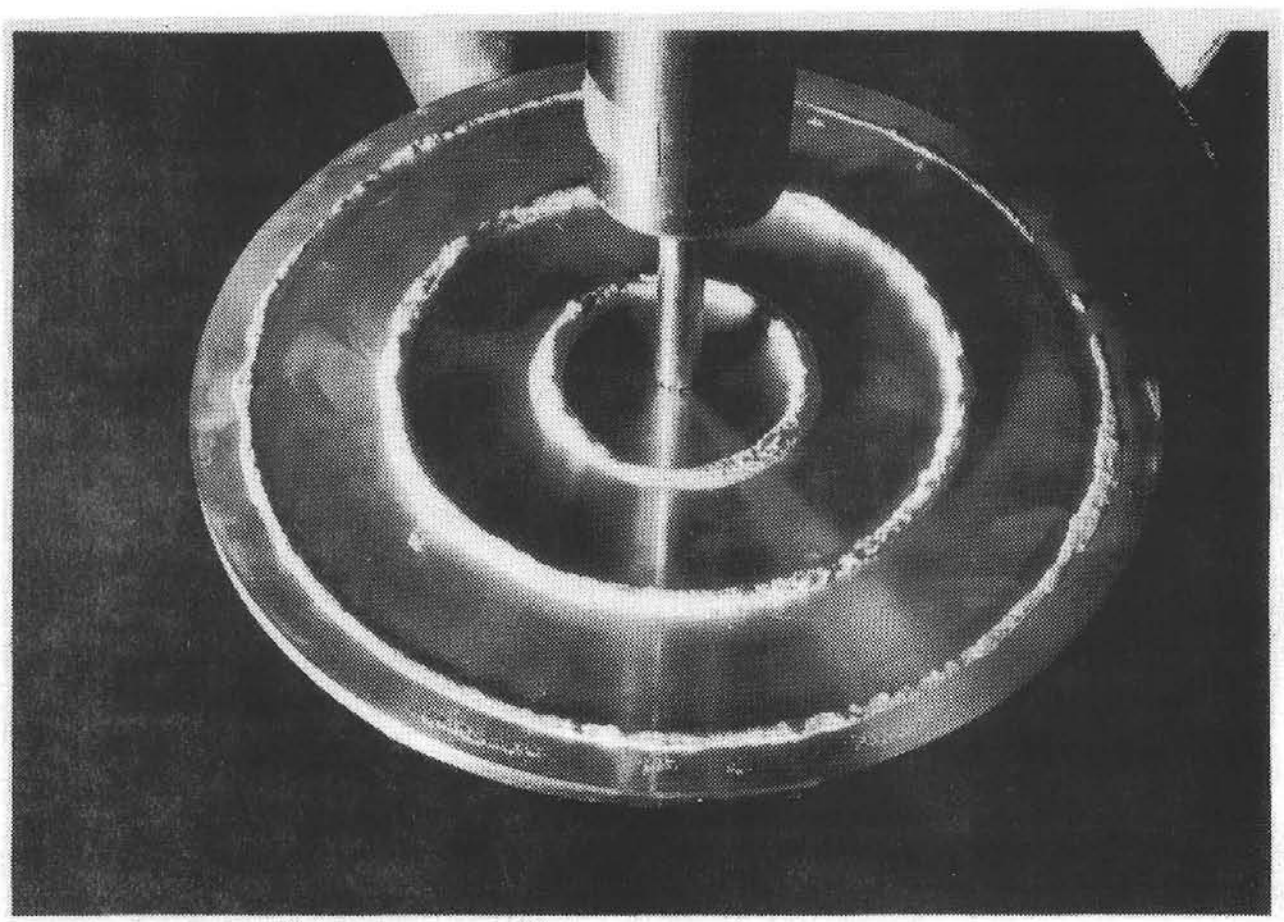

Figure 5-35. Ultrasonic Radiating Plate Vibrational Modes, 15.46 kHz (Top), 20.16 kHz (Bottom)

Figure 5-36. Test Setup for Ultrasonic Transducer Sound Level and Frequency Measurements

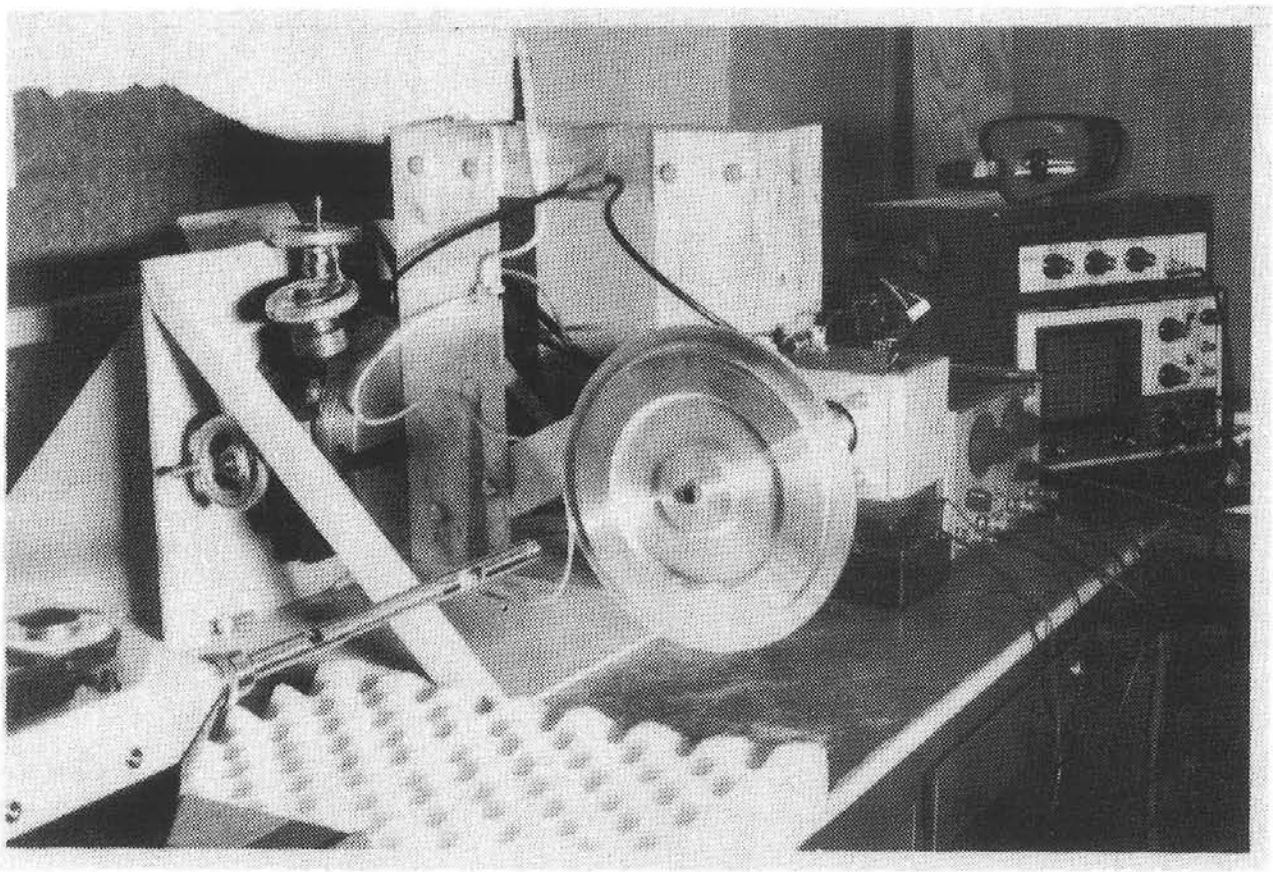

Figure 5-37. Ultrasonic Transducer Radiating Plate and Sound Level Meter Microphone Probe

was necessary to cool the back of that radiating plate with water to improve the fatigue strength of the material. Even so, the aluminum plate used would totally fail in fatigue at input power levels greater than 130 watts.

The conclusion is then that the assembly tested herein draws very little of the available 100 watts output of the ultrasonic generator. This is possibly due to either electrical mismatch of the transducer to the generator or mechanical mismatch of the fabricated components with regard to their dimensions.

Transducer Design No. 2 produced characteristics which were not significantly better than Design No. 1. The overall acoustical behavior was somewhat cleaner with fewer spurious resonant points (probably due to fewer material interfaces), but the maximum sound pressure level was approximately the same as found in Design No. 1. The sound level meter was not available for precise sound measurements so comparison measurements between Design 1 and 2 using the oscilloscope and a high frequency microphone were made.

5.2.4 Cleaning Test Results

Because proper operation of the transducer was not realized, the cleaning tests performed are limited. The purpose of the cleaning tests is to show possible feasibility of the concept and not ultimate cleaning power. With a possible feasibility indicated the transducer design should be optimized and then tested for ultimate cleaning ability.

The preliminary cleaning tests reported herein were performed using the Design No. 2 transducer operating at 15.4 kHz with an approximate sound pressure level of 130+ dB. The

tests performed are:

1. Determination of optimum height of radiating plate off the mirror surface (prior to cleaning)
2. Cleaning test of unaged mirror specimen with and without ultrasonic radiation
3. Cleaning test of a 4-day aged mirror specimen with and without ultrasonic radiation

As indicated in Reference 10, the sound pressure level in front of the radiating plate varies with axial distance from the plate center. From the aluminum radiating plate test data of Reference 10 this variation may be as high as 20 dB (a factor of 10 times). Tests were performed on the Design No. 2 head assembly which indicated an optimum radiating plate to mirror surface distance of 41 mm for maximum incident power at the mirror surface. This height was used for both cleaning tests accomplished.

Figure 5-29 illustrates the test setup used. The dimensional values used are: h = 41 mm, d = 40 mm. The converging air nozzle of Concept No. 1 (Section 5.1.4) without water mist injection was used as the air blast source. The "unaged" mirror specimen was dust coated in the wind tunnel and allowed to sit in the lab environment for 1 day prior to cleaning tests. The "4-day aged" specimen was wind tunnel dust coated, aged for 4 days in an outdoors environment (protected from rain and wind but exposed to sun, humidity and temperature changes) and allowed to remain in the lab environment for 7 days prior to testing.

During testing, two spots on each mirror were cleaned. One consisted of air blast alone with radiating plate in position but not activated, and the second included air blast with the radiating plate turned on. After testing, reflectance profiles were measured along lines perpendicular to the air blast centerline and at various distances from the air jet impingement

point on the mirror surface. This allowed the creation of a complete reflectance map of the cleaned area. From the reflectance maps, and knowing the "clean" reflectance of the mirror, iso lines of constant reflectance recovery can be plotted for each cleaned area.

Figure 5-38 presents iso-recovery plots for the unaged mirror specimen. To illustrate the effect of the ultrasonic sound field, the tests with and without the ultrasound have been superimposed. As can be seen, the presence of ultrasound does have a beneficial effect.

Constant reflectance recovery plots for the 4-day aged mirror are shown in Figure 5-39. The cleaning enhancement of the ultrasonic sound field is more pronounced in this case.

5.2.5 Conclusions and Recommendations for Concept No. 2

From the tests performed, it appears that the presence of "medium" intensity ultrasound does appreciably increase the cleanability of a non-perpendicular air blast-only system. It is evident that dust particle to mirror bonding forces are somewhat reduced. However, the full quantitative effect of the ultrasound is not apparent from the limited testing undertaken here. Higher levels of sound pressure, 160 dB or greater, as obtained with the Reference 10 transducer would be desirable. Upon reaching the higher transducer output power levels further cleaning tests would be necessary.

It is recommended that further optimization of the transducer assembly be undertaken with cleaning tests to follow. In this regard, it would be desirable to contact the authors of the original transducer concept at the Institute de Acustica del CSIC in Madrid, Spain for suggestions. Due to the ground work which has been established to this point in the investigation, completion of more conclusive research is not expected to be costly.

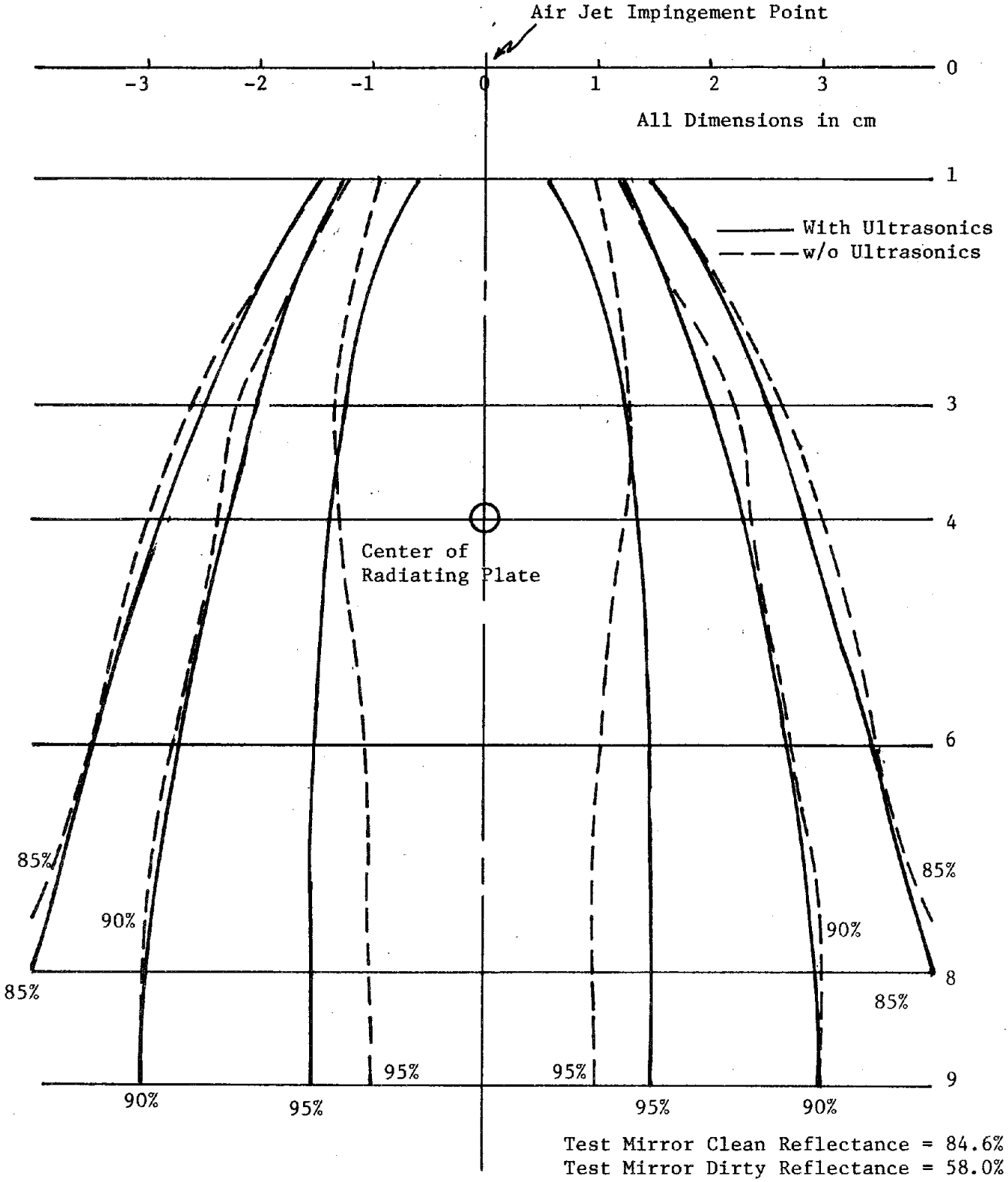

Figure 5-38. Ultrasonic Transducer Enhanced Air Blast, Iso-Reflectance Recovery Plot of Mirror Surface, Unaged Mirror Specimen

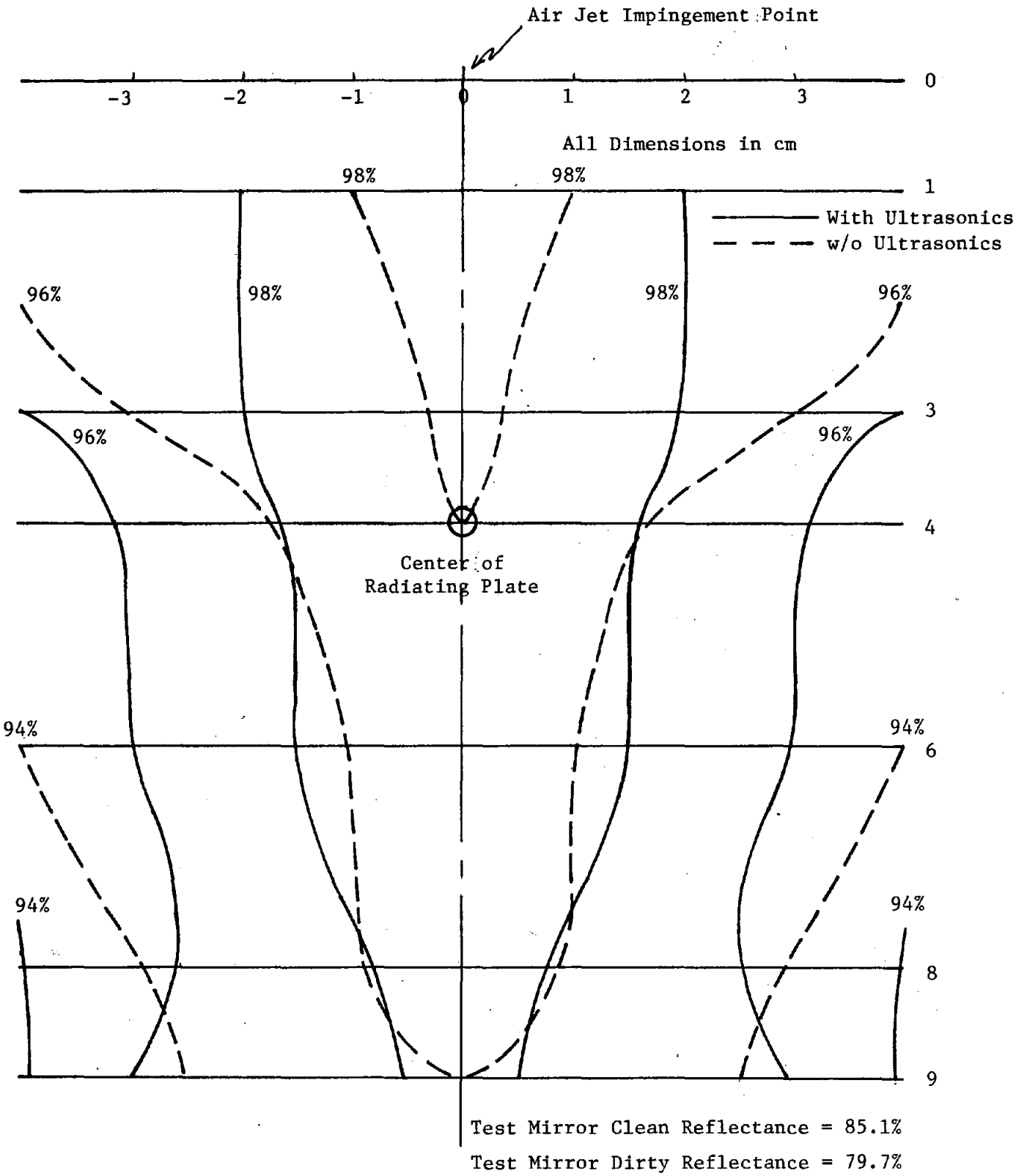

Figure 5-39. Ultrasonic Transducer Enhanced Air Blast, Iso-Reflectance Recovery Plot of Mirror Surface, 4-Day Aged Mirror Specimen

6.0 CONCEPTUAL DESIGN OF MANUFACTURING, INSTALLATION, DEPLOYMENT AND MAINTENANCE PROCESSES

The system proposed is comprised of components which are obtainable as off-the-shelf items or can easily be fabricated with standard manufacturing techniques. The only unique component being proposed is the all-electric transport vehicle, which is discussed in more detail in Section 7.0. Electric vehicles have existed for many years, but there has been a recent resurgence in interest and activity. One major development in this area is the "Electric and Hybrid Vehicle Research, Development, and Demonstration Act of 1976" (P.L. 94-413 as amended by P.L. 95-238.) Reference 29 has a brief overall description of the nature and scope of this effort. By the time the first 100 MW plant is complete, a suitable electric truck should be commercially available. If not, one can readily be designed and built.

Figure 6-1 illustrates, in a somewhat schematic way, the installation and deployment of the vortex scrubbing system. The system is entirely complete as shown with the manipulating boom, cleaning head, and supporting components permanently installed on, but easily removable from, the electric transport vehicle.

The cleaning head itself is a component which will not be off-the-shelf. It is, however, easily fabricated from metals and plastics in the form of tubing, sheet, and bar. Only standard manufacturing techniques such as turning, drilling, tapping, welding, and adhesive bonding are required. Early in the project, in order to have some basis for rough estimating the field system cost, the simplest possible extrapolation from test item to field system was envisioned. This configuration took a number of identical test heads and interconnected them with a common support plate and

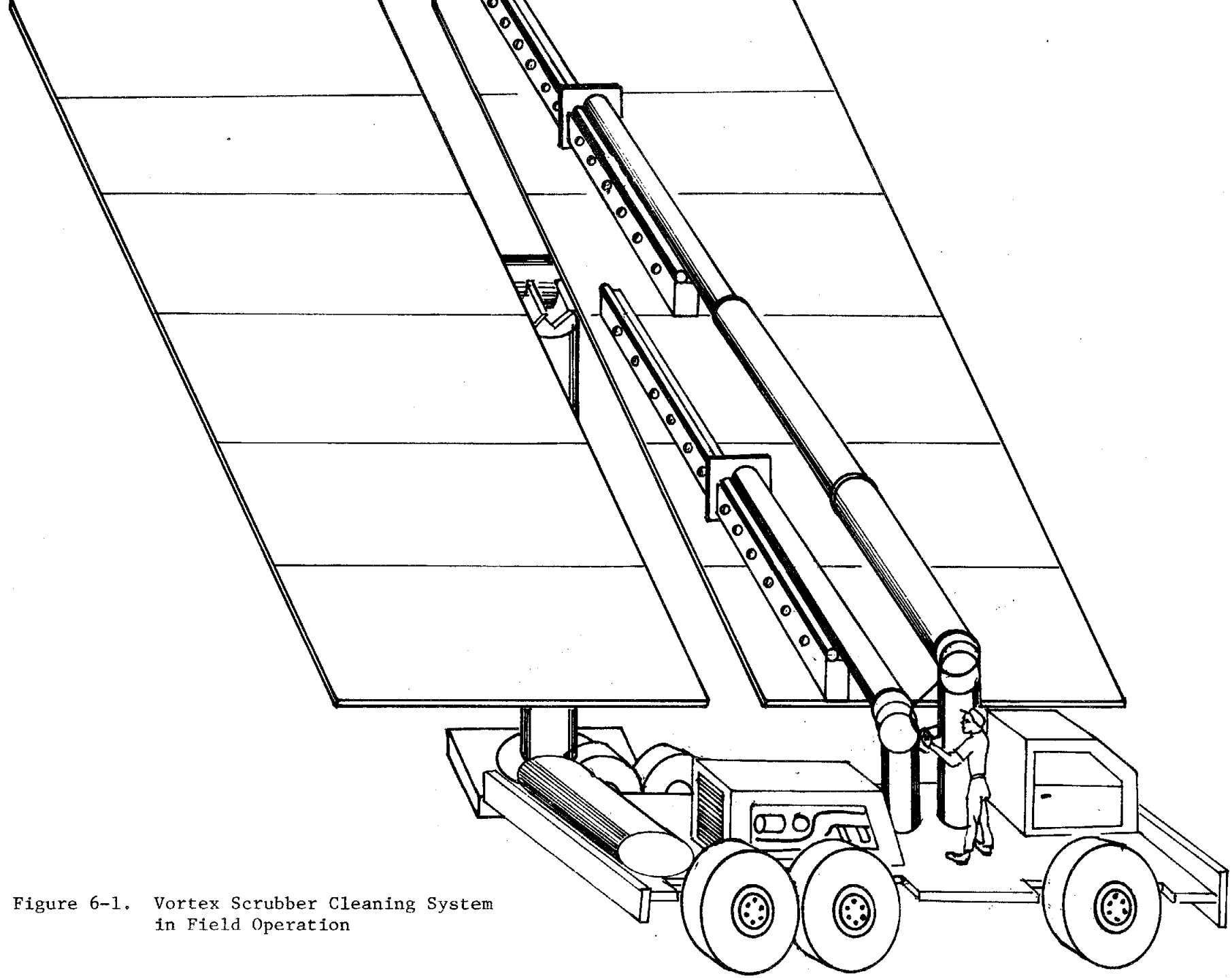

Figure 6-1. Vortex Scrubber Cleaning System in Field Operation

vacuum and compressed air manifolds as illustrated schematically in Figure 6-2. It soon became apparent, however, especially as more test results became available, that this would not be an efficient or economical system. A schematic of a more efficient concept is presented in Figure 6-3.

The cleaning head supporting components, i.e., those items which provide the medium and energy for freeing and capturing the dirt particles, are proposed to be the same as the corresponding items in the test system. These are the

- Air compressor with storage tank, pressure gauge, and solenoid control valve.
- Electronic filter with power pack (transformer to step the 110V line voltage up to several thousand volts).

These items will, of course, be increased in number and/or capacity by extrapolation from the work done in tests to that required in the field operation.

Among other reasons, in order for the supporting items to be available as off-the-shelf, electrically driven components it is proposed that the all-electric transport vehicle be powered directly from the heliostat field electricity rather than by batteries. If an above-the-ground trolley line system would be objectionable, receptacles with transformers to provide 220V could be provided at frequent intervals along the route.

The manipulating boom, which provides careful positioning and controlled traverse while cleaning, will not be commercially available in a 100 percent ready to use condition. A hinged, telescoping mechanism is envisioned, and there are many such "cherry-picker" type machines produced by the materials handling industries, both remote

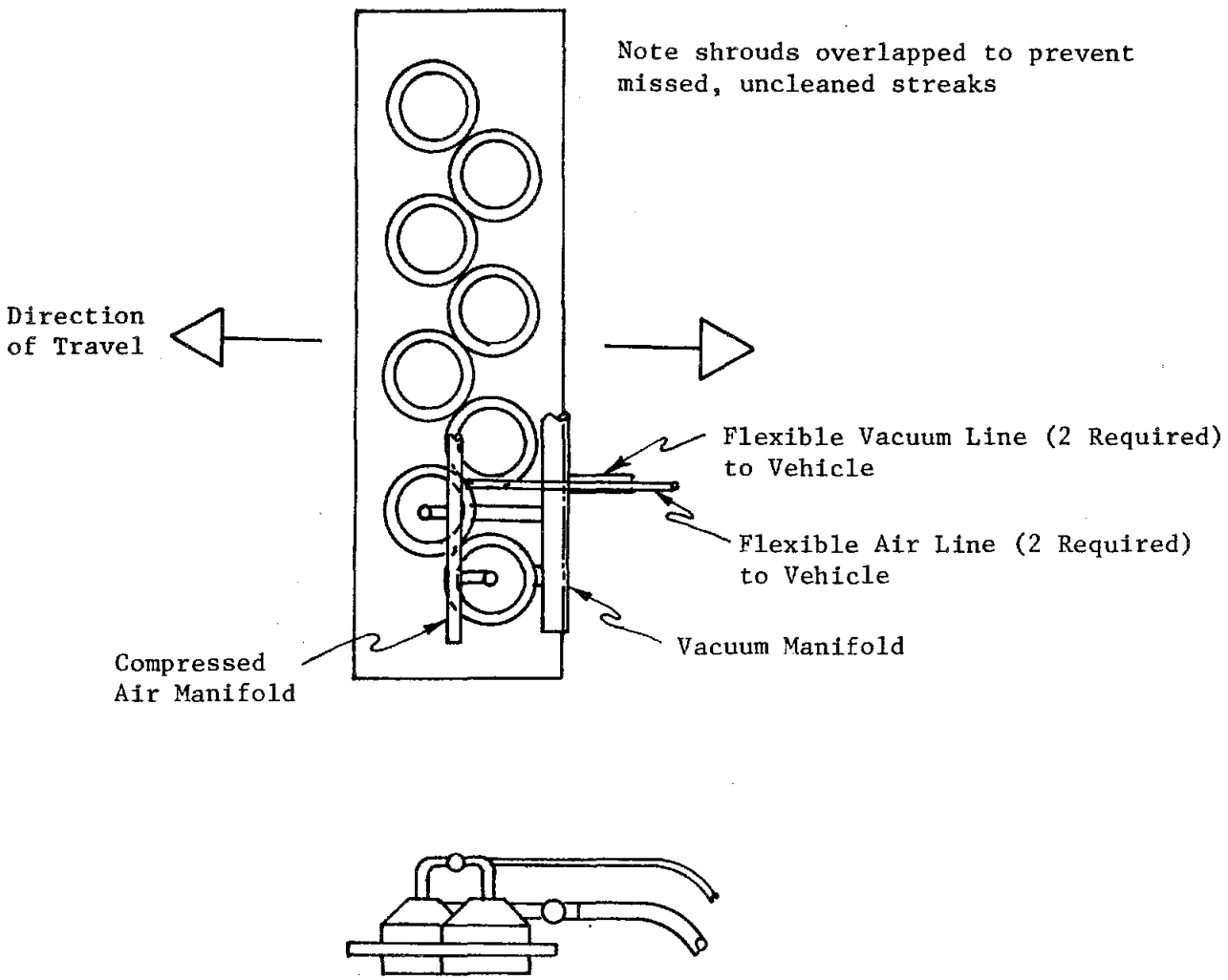

Figure 6-2. Schematic Illustration of Simple Extrapolation from Test to Field Operation

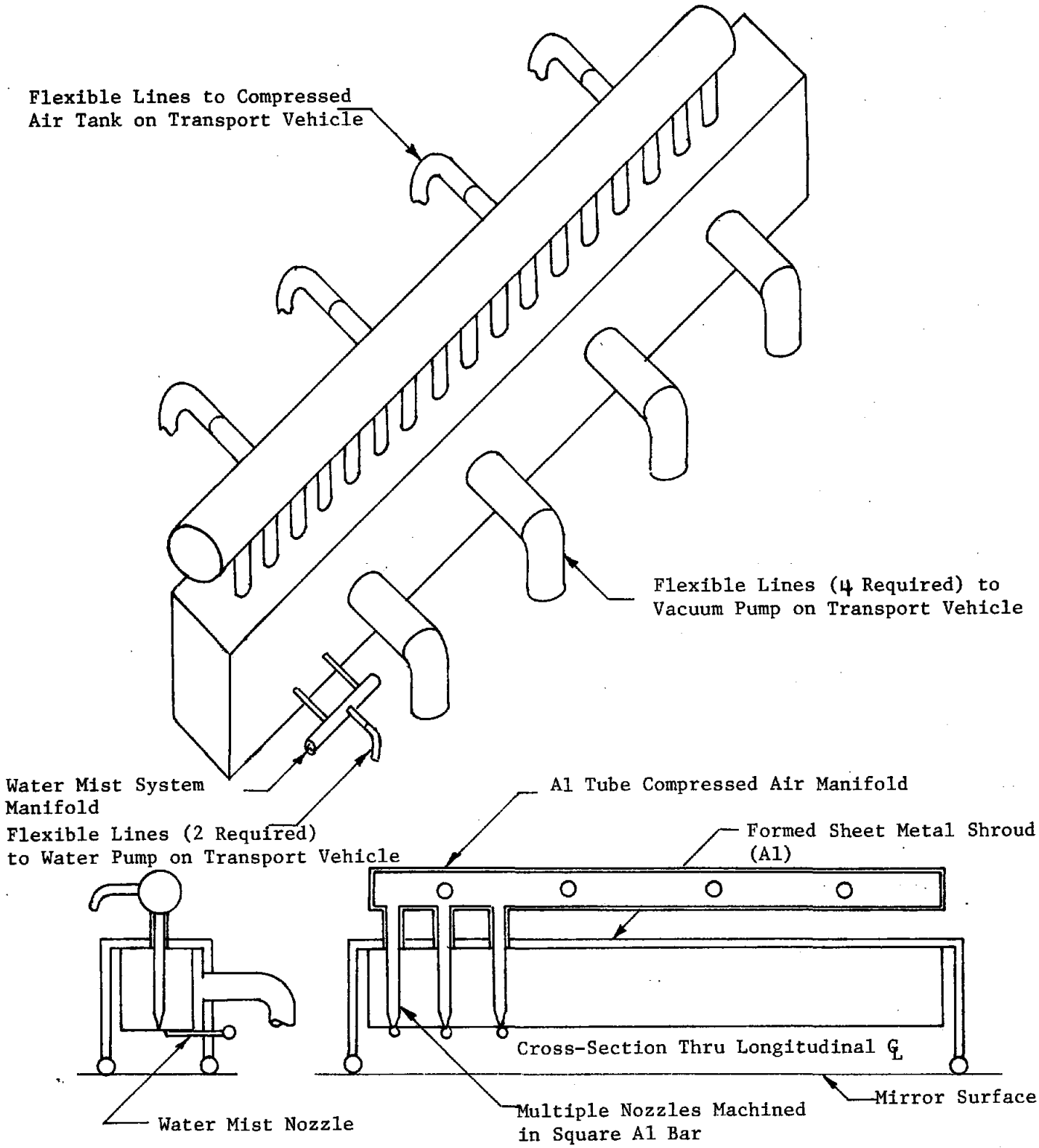

Figure 6-3. Schematic of Vortex Scrubber Cleaning System Head for Field Operations

and conventional. It is anticipated that one can be found which will require only the addition of a more sophisticated control system for proximity and traverse control. Various methods are available to achieve precise close proximity control including

- Infra-red L.E.D.'s, which are small and inexpensive,
- Ultrasonics, such as used in certain new cameras for automatic focusing,
- Touch sensors and micro-switches.

Of these, the latter would appear to be the better choice from the standpoint of simplicity, economy, and long-proven reliability. Soft, flexible reeds can be used coupled with a "window-type" micro-switch arrangement. A first switch signal would activate an indicator meaning the cleaning head had reached a specified proximity to the mirror surface, and the second switch signal would cause the motor controls to effect a stop at the desired final clearance from the surface. The required motor controls should be readily available since they have been in use for a long time for applications such as elevator positioning and stopping.

As mentioned earlier, a suitable electric truck will probably be commercially available by the time a first 100 MW plant construction is complete. One should be selected, or otherwise designed and built, which employs the ultimate in simplicity compatible with efficient operation for this very specialized application. There are a multitude of features on vehicles designed for street and highway travel which are not required here. This is anticipated to be a very significant area for cost savings potential over conventional washing techniques employing expensive commercial trucks.

The deployment of the system in the field is dictated to a large extent by the frequency and time of day of washing. It should be best to use only one work shift, the graveyard because of better atmospheric conditions for cleaning and because the mirrors are not reflecting over most of that period. On this basis and a frequency of 18 cleanings per year, it is shown in the following Section 7 that 11 systems are required for daily use year round.

No unusual or difficult maintenance items are anticipated. The most frequent item, and this might be considered more operational than maintenance, is the cleaning of the electronic filters. This is accomplished in the same way as with a domestic, metallic furnace filter, i.e., by water pressure spray wash. One potential problem area is constriction or plugging of the small diameter nozzles in the water mist system. For this reason, the water will be introduced downstream of the vortex nozzle, not inside as considered earlier. The water nozzle itself will be protected by use of demineralized water only. The amount of water used is so small that is not considered to be a major cost item.

All other potential repair or replace items are conventional mechanical and electrical components for which standard processes exist as well as much statistical data on frequency of failure. This data can be used to estimate the maintenance cost in following Section 7.0.

7.0 CAPITAL, OPERATION, AND MAINTENANCE COST ESTIMATES

7.1 Introduction

It is doubtful that a valid cost estimate can be made at this stage based only on theory and laboratory tests. At this point, however, this is the only type of data available except for some helpful information that might be derived from comparisons with other similar components, systems, and processes. The following calculations began with the perhaps somewhat optimistic assumption that the laboratory vortex scrubber cleaning head, if sufficiently multipled in an assembly, could be made to do the full scale heliostat cleaning job in no more than the three minutes presently quoted for water pressure spray washes. Eight of these heads of 6 inches I.D. in parallel would make a horizontal swath of 48 inches, just equal to the vertical dimension of one of the mirrors in the heliostat assembly. Six passes across the heliostat, therefore, three left and three right, would complete the job.* The following calculations are based on this procedure, where applicable.

7.2 Capital Costs

Capital Cost Component	($) Cost	Basis
Multiple Nozzle Vortex Scrubber Cleaning Head (Including air & vacuum hoses from head to vehicle)	346	Note (1)
Air Compressor	435	Note (1)
Air Storage Tank	58	Note (1)
Solenoid Air Control Valve	56	Note (1)
Vacuum Pump	63	Note (1)
Electronic Filter & Transformer	250	Note (1)
Manipulator Boom with Proximity and Traverse Controls	12,000	Note (2)
Electric Transport Vehicle	18,000	Note (3)
TOTAL	$31,208	= $1040/yr./system

* Note: This concept is no longer consistent with Figure 6-1, which has been modified to illustrate a more labor-effective arrangement.

Note (1) - One of the major items, i.e., the air compressor, was investigated for its price in the laboratory system as compared to the price of the larger unit required for field operations. The price of the ½hp laboratory unit was $251.38. The price of an 8 x ½ = 4 hp field unit from the same supplier would be $435.82. This ratio of $435.82/$251.38 = 1.73 was used to extrapolate the prices of all the components from lab to field.

Note (2) - In the next phase of this effort, materials handling system vendors would be contacted in hopes of finding a manipulator that would be suitable for, or at least adaptable to this application. For the present, we have limited our investigation to conversations with one local materials handling equipment supplier and the buyer of such equipment for local Pacific Telephone. It appears that a machine of roughly the size and performance required here would be in the vicinity of $10,000. For modification of the control system to provide the precise proximity and traverse control required, add $2,000.

Note (3) - Based on the experience of one of our staff working on this project who has actually built his own electric vehicle and discussions with electric vehicle vendors, a cost of $15,000 is estimated for the vehicle proper plus $3,000 more to semi-permanently install the boom and supporting components.

7.3 Labor Cost

Because of somewhat less removal of debris, as compared with washing after one-month exposure, consider 18 cleanings a year. Considering holidays, vacations, sick leave, etc., there are 1872 working hours per man per year.

- Time required per washing = 3 x 22,000/60 = 1100 hours
- Time required per year = 1100 x 18 = 19,800 hours
- No. men required = 19,800/1872 = 10.58 or 11 men, if a system could be operated by one man. However, two men are required per system for a total of 22 men. (It may be worthwhile to investigate whether the vehicle driver could also operate the boom efficiently).

- At a burdened labor rate of $15 per hour and 52 x 40 = 2080 hours pay per year, the total annual labor cost is 22 x 2080 x 15 = $686,400.

7.4 Energy Cost

The test component vortex scrubber cleaning head has 6 in. shroud I.D. In order to clean one of the six mirrors, of 48 in. vertical dimension, with a single swath, eight tangent (actually overlapping) cleaning heads would be required. To estimate field system energy cost take the energy consumption corresponding to the test system components' ratings times a factor of eight. This will be conservative since the eight heads will be manifolded to something less than eight supporting components (compressor, filter, etc.), each of which will be larger and more efficient than its corresponding counterpart in the test system.

Component	Test System Component Rating	Field System Component Energy Consumptions (KW)	
Air Compressor	½ hp	½(.7455) x 8 = 2.982	2.982
Vacuum	5.2A, 115 V	(5.2)(115)(.8)x 8/1000 =	3.827
Electronic Filter	.3A, 120 V	(.3)(120)(.8)x 8/1000 =	0.230
Solenoid	12 W	12 x 8/1000 = 0.096	0.096
Manipulator Boom	--	(See Note (1))	0.036
Transport Vehicle	--	(See Note (2))	0.36
			7.531

Energy Cost per Year =

$$\$(.04)\ \frac{3 \times 22{,}000 \times 18}{60}\ (7.531)(11) = \$65{,}610$$

Note (1) - Manipulator Boom Energy

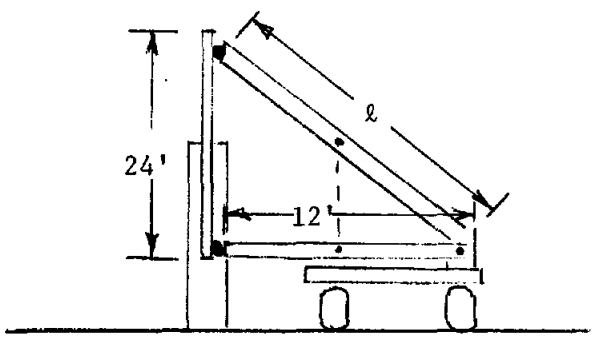

$$\ell = \sqrt{12^2 + 24^2} = 26.08 \text{ ft.}$$

Consider with telescoping, that boom is equivalent to 30 feet long Al pipe of 12" O.D. x ¼" wall.

$$Wt = \frac{\pi}{4}(12^2 - 11.5^2)(30 \times 12)(.1)$$

$$= 332 \text{ lbs.}$$

The weight of the test system cleaning head is about two pounds. Double this for weight of supporting structure and attached

hoses, and take times 8 to account for the multiple heads: 2 x 2 x 8 = 32 lbs. This weight is raised through 24 feet while the boom raises its own mass and C.G. through 12 feet. Work done on the alternate heliostats, starting at the top and working down, would be less. However, to compensate for uncalculated effects such as efficiency and acceleration, ignore this.

Work done per mirror = 32 x 24 + 332 x 12

$= 4752$ ft. lbs. $= \frac{4752}{2.656(10)^6}$ or .00178 $\frac{\text{kwh}}{\text{mirror}}$

For 20 mirrors per hours,

Consumption = .00178 x 20 = .036 kw

Note (2) - Transport Vehicle Energy

Assume that the traversing across the width of the heliostat is accomplished by forward and aft motion of the transport vehicle. (It would be more efficient to accomplish this with swivelling of the boom in a horizontal plane through its base. However, requiring the boom tip to go to every corner of the heliostat through 3-dimensional space results in a boom length, $l = \sqrt{12^2 + 24^2 + 24^2} = 36$ ft., which may prove too flexible).

For a cleaning rate of 3 min. per heliostat or 20 heliostats per hour, six 24 ft. long traverses per heliostat, 12 ft. (est.) between heliostats, and an 8 hour working day, the total distance traversed,

$$S = (20 \times 8)\ (6 \times 24 + 12) = 24{,}960 \text{ ft. or } 4.73 \text{ mi.}$$

Except for acceleration and deceleration at the beginning and end, respectively, of each traverse, the above total distance would represent an almost insignificant consumption of energy. For purposes of completing this calculation, estimate the average rate per hour for the vehicle as ten times that of the boom.

7.5 Maintenance

As discussed in Section 6.0, no special maintenance problems are anticipated. In fact, the system is comprised of components that are all so standard that the maintenance is not expected to be any more of a problem than with conventional water wash systems. On this basis, consider the maintenance cost to be the same percentage of operator labor cost as it was in the Reference 30 study, i.e., approximately 8.5%.

(.085)$686,400 = $58,344 per year.

7.6 Summary

Due to the inherent simplicity and the ruggedness that can be built into the type of vehicle proposed here, replacement every 10 years as assumed in the Reference study is not considered here.* It is assumed that maintenance with only appropriate repair/replacement of parts as required will keep the complete system going for the 30 year life of the plant. The total annual cost breakdown is then as follows.

Item	Annual Cost
Capital Equipment	$ 11,443 = 31,208 x 11/30
Operator Labor	686,400
Operating Energy	65,610
Maintenance	62,735
TOTAL	$826,188

A comparison follows with costs as established in the Reference 30 study. The comparison in made only with the CAL CHEM method since it is believed that it is the only one reported for which the labor costs are reasonable. In fact, our labor costs are unconservative from the standpoing of not having allowed any work time for

* Plus the fact that the vehicle is driven less than five miles during an 8 hour shift at an average speed less than 1 mph.

travelling to the work start location, for coffee break, for malfunctions, etc. On this basis, no labor estimate should be less than ours, and a second CAL CHEM column is shown with their labor cost adjusted to ours for a fairer comparison.

Table 7-1

Total Annual Cleaning Costs:

	CAL CHEM	S & A	CAL CHEM Adjusted
Vehicle Investment	$48,000	11,443	48,000
Diesel Fuel	189,540	--	189,540
Electricity	--	65,610	--
Deionized H_2O	8,019	Negl.	8,019
Active Cleaner	41,310	--	41,310
Operator Labor	508,860	686,400	686,400
Maintenance	43,740	62,735	62,735
Total	$839,469	$826,188	$1,036,004

8.0 RECOMMENDED FUTURE WORK

Based upon the results obtained in this phase of the heliostat cleaning study, a number of recommendations can be made regarding the future direction to be taken in cleaning methods and instrumentation as well as auxiliary research into dust adhesion. These recommendations are itemized below:

(1) Cleaning Concept

It is believed that the use of an ultrasonic air transducer in conjunction with a high velocity air flow system holds the best promise for the detachment of dust from heliostat mirrors without washing. This concept may or may not include a water particle mist injector. The recommended further development work on this system may be outlined as follows:

a. Optimization of ultrasonic transducer output
b. Slight redesign of air nozzle head to allow for multiple jets.
c. Testing of the ultrasonic-air blast system with regard to cleanability for mirror specimens possessing varying degrees of environmental aging. Enough tests would be performed to provide more statistical backup for the conclusions to be drawn.

If the above tests prove feasibility,

d. Detailed design of a prototype cleaning system would be undertaken.
e. Analysis of the system in (d) for manufacturing, deployment and operational processes as well as full cost and performance estimates.

(2) Reflectometer

Experience with the design, fabrication and use of the laboratory reflectometer developed during this program indicates that a very useful field instrument can be produced at low cost. A suggested design specification for such an instrument is as follows:

a. Low unit manufacturing cost - less than $3000 in quantities greater than 100 and approximately $5000 for quantities of 20 or less.

b. Complete portability - light weight

c. General field instrument with less precision than found in current lab units. For example, reflectance capability to nearest .5% or greater

d. Display to be analog meter movement or digital readout

e. Self-calibrating, thereby eliminating a reflectance standard

f. Unaffected by outdoors ambient light levels

g. Fixed filter installation (not changeable in the field, but convertible by partial disassembly)

(3) Dust Adhesion

It is recommended that research into adhesion mechanisms and adhesion forces be conducted using representative heliostat glass surfaces and characterized dust particles. Adhesion forces should be determined as a function of dust particle size over a realistic range of heliostat environmental conditions and cleaning cycle times.

9.0 REFERENCES

1. SANDIA RFP MDH/83-0035, "New Ideas, Collector Subsystem for Solar Central Receiver," August 21, 1978.

2. Schumacher and Associates, Inc. Proposal No. 78-011-SAN, October 5, 1978, "New Ideas for Heliostat Reflector Cleaning Systems," October 5, 1978.

3. SANDIA Contract 83-0035K, March 12, 1979.

4. E.D. Eason, "The Cost and Value of Washing Heliostats," SAND78-8813, June 1979.

5. A.D. Zimon, "Adhesion of Dust and Powder, Plenum Press, 1969.

6. Raymond S. Berg, "Heliostat Dust Buildup and Cleaning Studies," SAND78-0510, March 1978.

7. Julian R. Frederick, "Ultrasonic Engineering," John Wiley and Sons, Inc., 1965.

8. L.D. Rozenberg, "Physical Principles of Ultrasonic Technology, Volume 1," Plenum Press, 1973.

9. J.A. Gallego-Juarez and G. Rodriguez-Corral, "Piezoelectric Transducer for Air-Borne Ultrasound," Acustica, Vol. 29, 1973, p. 234-239.

10. J.A. Gallego-Juarez , G. Rodriguez-Corral and L. Gaete-Garreton, "An Ultrasonic Transducer for High Power Applications in Gases," Ultrasonics, November 1978.

11. R.B. Pettit, J.M. Freese, D.E. Arvizu, "Specular Reflectance Loss of Solar Mirrors Due to Dust Accumulation", Presented at the Institute of Environmental Sciences Seminar on Testing Solar Energy Materials and Systems, NBS, Washington, DC, May 22-24, 1978.

12. J.M. Freese, "The Development of a Portable Specular Reflectometer for Field Measurements of Solar Mirror Materials," Report SAND78-1918, October 1978, Sandia Laboratories, Albuquerque, N.M.

13. R.B. Pettit, "Characterization of the Reflected Beam Profile of Solar Mirror Materials," Solar Energy, Vol. 19, pp. 733-741.

14. Reflectometer Optical Performance Requirements, Section 2.0 of Sandia Document No. MDH/83-0385, August 1978.

15. A.M. Zarem and D.D. Erway, "Introduction to the Utilization of Solar Energy," McGraw-Hill Book Company, 1963.

16. G. Kortum, "Reflectance Spectroscopy, Principles, Methods, Applications," Springer-Verlag, Berlin, 1969.

17. E.P. Lavin, "Monographs on Applied Optics, No. 2, Specular Reflection," American Elsevier Publishing Co., Inc., 1971.

18. Leo Levi, "Applied Optics: A Guide to Modern Optical System Design," John Wiley and Sons, Inc., 1968.

19. Sample Reflectance vs. Wavelength Data for PPG low iron glass used in MDAC Heliostat (3/15/79) - supplied to Schumacher and Associates, Inc. by R.B. Pettit.

20. D.W. Peterson, R.H. Croll, R.E. Luna and A.J. Russo, "Sandia Laboratories Low-Speed Wind Tunnel for Research in Atmospheric Flows and Incompressible Fluid Mechanics," Sandia Laboratories Report SAND75-0124, April 1975,

21. REPCON Rain Repellent and Surface Conditioner, Technical Data and Specifications Guide, Unelko Corporation, 727 East 110th Street, Chicago, Ill. 60628

22. J.M. Freese, "Effects of Outdoor Exposure on the Solar Reflectance Properties of Silvered Glass Mirrors," Sandia Laboratories, Report No. SAND78-1649, September 1978, presented at International Solar Energy Society Conference, Atlanta, May 1979.

23. T.F. Hueter, R.H. Bolt, "Sonics', John Wiley and Sons, Inc., 1955.

24. B. Carlin, "Ultrasonics", McGraw Hill, 1960.

25 A. Barone and J.A. Gallego-Juarez, Acustica, "On a Modification of Vibrating Flat Plates in Order to Obtain Phase-Coherent Radiation", Volume 22, 1969-71

26. A. Barone and J. A. Gallego-Juarez, "Flexural Vibrating Free-Edge Plates with Stepped Thicknesses for Generating High Directional Ultrasonic Radiation", Journal of the Acoustical Society of America, 5 April 1971

27. J.A. Gallego-Juarez,"Axisymmetric Vibrations of Circular Plates with Stepped Thickness", Journal of Sound and Vibration, 1973, 26(3), 411-416

28. Fred P. Blissmer, Robert W. Kirby, Fred E. Peterson, "EASE2-Elastic Analysis for Structural Engineering, Engineering Analysis Corporation, 1979

29. "Electric Vehicle Outlook," Mechanical Engineering, June 1978

30. McDonnell Douglas Report MDC G7399, "Solar Central Receiver Prototype Heliostat, CDRL Item B.d, Final Technical Report, Volume I", by C.R. Easton, August 1978.

DISTRIBUTION:

Foster-Miller Associates
135 Second Avenue
Waltham, MA 02154
Attn: Paul Tremblay

General Electric Company
P. O. Box 8661 - Room 7310
Philadelphia, PA 19101
Attn: R. Hobbs

Booz, Allen & Hamilton, Inc.
8801 E. Pleasant Valley Road
Cleveland, OH 44131
Attn: C. G. Howard

Solaramics, Inc.
1301 El Segundo Boulevard
El Segundo, CA 90245
Attn: H. E. Felix

General Electric
1 River Road
Schenectady, NY 12345
Attn: Richard Horton
John Garate
R. N. Griffin

Busche Energy Systems
7288 Murdy Circle
Huntington Beach, CA 92647
Attn: Ken Busche

Brookhaven National Laboratory
Upton, NY 11973
Attn: G. Cottingham

Aerospace Corporation
El Segundo Boulevard
El Segundo, CA 90274
Attn: Philip de Rienzo

McDonnell Douglas Astronautics
5301 Bolsa Avenue
Huntington Beach, CA 92647
Attn: R. L. Gervais
D. A. Steinmeyer

Martin Marietta Corporation
P. O. Box 179
Denver, CO 80201
Attn: T. R. Heaton
Lloyd Oldham

Northrup, Inc., Blake Laboratory
Suite 306
7061 S. University Boulevard
Littleton, CO 80122
Attn: Floyd Blake

Boeing Engineering & Construction
P. O. Box 3707
Seattle, WA 98124
Attn: Roger Gillette

Westinghouse Electric Corporation
Box 10864
Pittsburgh, PA 15236
Attn: J. J. Buggy

Northrup, Incorporated
302 Nichols Drive
Hutchins, TX 75141
Attn: J. A. Pietsch

Schumacher & Associates
2550 Fair Oaks Blvd., Suite 120
Sacramento, CA 95825
Attn: John C. Schumacher

Bechtel National Inc.
M/S 50/16
P. O. Box 3965
San Francisco, CA 94119
Attn: Ernie Lam

Ford Aerospace
3939 Fabian Way, T33
Palo Alto, CA 94303
Attn: Howard Sund

Veda, Inc.
400 N. Mobil, Bldg. D
Camarillo, CA 93010
Attn: Walter Moore

Pittsburgh Corning
800 Presque Isle Drive
Pittsburgh, PA 15239
Attn: David Rostoker

Springborn Laboratories
Water Street
Enfield, CT 06082
Attn: R. E. Cambron

Solar Energy Research Institute
1536 Cole Boulevard
Golden, CO 80401
Attn: Barry Butler
Dennis Horgan
John Thornton

Electric Power Research Institute
P. O. Box 10412
Palo Alto, CA 93403
Attn: John Bigger

Aerospace Corporation
Solar Thermal Projects
Energy Systems Group
P. O. Box 92957
Los Angeles, CA 90009
Attn: Elliott L. Katz

M. U. Gutstein, DOE/HQ
G. M. Kaplan, DOE/HQ
L. Melamed, DOE/HQ
J. E. Rannels, DOE/HQ
S. D. Elliott, DOE/SAN
R. N. Schweinberg, DOE/STMPO

Sandia Albuquerque:
C. N. Vittitoe, 4231
G. E. Brandvold, 4713
T. A. Dellin, 4723
J. A. Leonard, 4725
L. H. Harrah, 5811
R. B. Pettit, 5842
F. P. Gerstle, 5844

Sandia Livermore:
T. S. Gold, 8320
P. J. Eicker, 8326
P. L. Mattern, 8342
H. R. Sheppard, 8424
R. C. Wayne, 8450
W. G. Wilson, 8451 (10)
T. D. Brumleve, 8451
W. R. Delameter, 8451
C. L. Mavis, 8451
H. F. Norris, Jr., 8451
S. G. Peglow, 8451
C. J. Pignolet, 8451
A. C. Skinrood, 8452
J. D. Gilson, 8453

Technical Publications and Art Division, 8265 for TIC (27)
F. J. Cupps, 8265/Technical Library Processes Division, 3141
Technical Library Processes Division, 3141 (2)
Library and Security Classification Division, 8266-2 (3)